EXPERIMENTAL AND THEORETICAL STUDIES OF ION-MOLECULE REACTIONS

A thesis presented in partial fulfilment of the requirements for the degree of

Doctor of Philosophy in Chemistry

at the

University of Canterbury,
Christchurch, New Zealand

by

Sean Campbell Smith

February 1989

The three years encompassing my PhD have included more satisfaction, pain, achievement and pleasure than I could possibly have hoped for. Which, of course, is just the way life should be.

So here's to life (long may it!)

ACKNOWLEDGEMENTS

I wish to thank my supervisors, Drs Murray McEwan and Colin Freeman, and my associate supervisor, Associate Professor Robert Gilbert, for accepting the supervision of my PhD project.

The support of the Department of Chemistry at the University of Canterbury, the New Zealand University Grants Committee (for the award of a Post-graduate Scholarship 1985-1988, and a Shirtcliffe Fellowship 1988), the Department of Theoretical Chemistry at the University of Sydney and the Australian Research Grants Committee are gratefully acknowledged. Financial assistance from the Royal Society of New Zealand (Canterbury Branch), the New Zealand Institute of Chemistry (Canterbury Branch), and the Evans Fund (University of Canterbury) are also greatly appreciated.

On a more personal note, I am grateful to Murray McEwan and Colin Freeman for the confidence they have shown in allowing me a "long rope" in the pursuit of the objectives of the project and for their support throughout the period of my PhD Many thanks are also owed to Bob Gilbert: his teaching, encouragement, friendship and lively arguments are an enduring inspiration for me.

I am grateful to Professor David Smith and Dr Nigel Adams for the chance to spend a week in their laboratory in the Department of Space Research, University of Birmingham, pursuing experimental work. Their contribution, along with that of Mr Kevin Giles, was fundamental to the development of Chapter 5. Thanks are also owed to Mr Paul Wilson for help with the modelling of the CH_3^+/CH_3CN reaction (Chapter 4), and Mr Michael James for help in preparation of the diagrams and references.

A number of people, aside from those already mentioned, have made significant contributions to the science contained herein through discussions, for which I am grateful: Dr Andrew Whyte, Dr John Harrison, Dr David Golden, Professor Sture Nordholm, Dr

George Bacskay, Professor Leon Phillips, Dr Michael Meot-Ner, and Dr Peter Harland.

For all the things one would like to thank friends for but seldom has the chance, my thanks to Andy Whyte, John Harrison, Jane Ayrey, Stephen Robertson, Michael Robertson, Pascal Roussel, Alison Downard, Ian Maxwell, Jolanta Sztaba, Bob Gilbert, Judy Furby, and, of course, many others.

Finally, my love and thanks to Mark, Cathy, Marie and David who have been friends, family and safety net.

CONTENTS

CHAPTER 3 cont.

PUBLICATIONS

Parts of the work presented herein may be found in the following articles:

S.C. Smith and R.G. Gilbert, "Angular Momentum Conservation in Unimolecular and Recombination Reactions",
Int. J. Chem. Kinet. 20, 307-329 (1988).

S.C. Smith and R.G. Gilbert, "Angular Momentum Conservation in Multichannel Unimolecular Reactions",
Int. J. Chem. Kinet. 20, 979-990 (1988).

S.C. Smith, M.J. McEwan and R.G. Gilbert, "The Pressure Dependence of Ion-Molecule Association Rate Coefficients",
J. Chem. Phys. 90, 1630-1640, (1989).

S.C. Smith and R.G. Gilbert, "Program 'Falloff': Calculation of fall-off curves for unimolecular and recombination reactions through solution of the master equation",
Quantum Chemistry Program Exchange 8, 168, (1988).

S.C. Smith, M.J. McEwan and R.G. Gilbert, "The Relationship Between Recombination, Chemical Activation and Unimolecular Dissociation Rate Coefficients",
J. Chem. Phys. 90, 4265-4273, (1989).

S.C. Smith, M.J. McEwan, and R.G. Gilbert, "Microscopic Reaction Rates in Ion-Molecule Reactions: Effects of Uncoupled Modes",
J. Phys. Chem., in press.

S.C. Smith, P.F. Wilson, M.J. McEwan, P. Sudkeaw, R.G.A.R. Maclagan, W.T. Huntress, and V.G. Anicich, "A Model for Competitive Binary and Ternary Reactions in the CH_3^+/CH_3CN System",

J. Phys. Chem., to be submitted.

S.C. Smith, M.J. McEwan, K. Giles, N.G. Adams and D. Smith, "Unimolecular Decomposition of a Polyatomic Ion in a Variable-Temperature Selected-Ion-Flow-Drift Tube: Experiment and Theoretical Interpretation", in preparation.

ABSTRACT

The present work deals with the development of a coherent and accurate means of modelling unimolecular decomposition, association and chemical activation reactions, particularly those involving ions, by the use of RRKM theory in conjunction with solution of the master equation.

A new solution of the chemical activation master equation (which includes association as a special case) is derived which reveals a very simple relationship between the non–equilibrium rate coefficient for association and that for the reverse unimolecular dissociation. It is shown that the non–equilibrium association rate coefficient is related to the reverse non–equilibrium unimolecular dissociation rate coefficient by the equilibrium constant and a non–equilibrium factor that is calculated from solution of the unimolecular master equation. Hence separate solution of the chemical activation or association master equations to obtain the stabilisation rate coefficient is not necessary: both solutions are implicit in the solution of the single or multichannel unimolecular master equation.

Solutions to the two–dimensional unimolecular master equation are developed which allow full incorporation of the constraint of angular momentum conservation into single– and multi–channel unimolecular master equation calculations at any pressure for the first time. In conjunction with the solution to the chemical activation and association master equations, this allows ion/molecule association and chemical activation reactions, predictions for which are very sensitive to the effects of angular momentum conservation, to be modelled by accurate master equation calculations for the first time.

Two extensions to RRKM theory, necessary for the accurate prediction of microscopic rate coefficients $k(\epsilon,J)$ in ion/molecule reactions, are identified. (1) Correct incorporation of the hindrance to dipole rotation, produced by the non–central ion/dipole potential, into the determination of the density of states in the loose transition state. An exact semiclassical means of incorporating this effect is derived and implemented. (2) Adiabatic

effects, i.e., the absence of coupling of many degrees of freedom with the reaction coordinate at large separation of an ion/dipole pair, are shown to significantly reduce the predicted capture rate from that obtained by normal microcanonical variational implementation of RRKM theory. A variant of the normal RRKM expression for $k(\epsilon,J)$ is derived which enables exact accounting for this non-coupling.

The theory is applied to three well-studied ion/molecule reactions: (1) the association of CH_3^+ and HCN in a helium bath gas, (2) the chemical activation reaction between CH_3^+ and NH_3 in helium, and (3) the chemical activation reaction between CH_3^+ and CH_3CN in both helium and CH_3CN bath gases. In the case of the reaction between CH_3^+ and HCN, RRKM parameters are sufficiently well known to allow the average downward transfer of internal and (external) rotational energies in collisions to be estimated as $150cm^{-1} \pm 50\%$. The results of modelling of the other reactions are consistent with similar sized average energy transfer parameters. Illustrative calculations for two neutral reactions, the recombination of methyl radicals and the two-channel dissociation of 1-iodopropane, are also presented.

An experimental study involving unimolecular dissociation of the $CH_3CH_2OH_2^+$ ion, induced in the drift field of a Variable-Temperature, Selected-Ion-Flow-Drift Tube, is presented. The theoretical interpretation of this experiment is discussed. It is found that (1) the induction time for approach to steady state of the vibrational and rotational degrees of freedom of the $CH_3CH_2OH_2^+$ ion in the helium carrier gas is negligible on the experimental timescale for motion of the ions through the drift region, and (2) the unimolecular dissociation rate coefficients do *not* correspond directly to thermal data at an elevated temperature with mean energy equal to the ion centre-of-mass energy. This implies that the steady-state ion translational-energy distribution is not sufficiently close to a Maxwellian distribution to enable simple interpretation of the results as pseudo-thermal data. The form of interpolation to zero field required to obtain thermal data is not yet clear. A simple extension to the Langevin capture model is derived which allows an improved estimate of the total non-reactive ion/induced-dipole collision frequency

(necessary for master equation modelling of ion/molecule reactions) by including steric effects due to the finite size of the species involved.

INTRODUCTION

In a very general sense, there are two questions central to reaction chemistry: can a chemical process occur? If so, then at what rate does it proceed? The former question is related to the potential surface in the vicinity of a minimum, whereas the latter is related to the potential surface in the dynamically unstable region between minima. In the last sixty years, theoretical chemistry has developed and come of age with the realisation that the potential surface provides the key to answering these fundamental questions; the development of increasingly powerful computers, which provide the wherewithal to calculate quantitative details of the potential surface by solution of the Schrödinger equation; and the development of increasingly powerful kinetic theory which, given the potential surface, allows one to predict and model rates of chemical processes.

This thesis deals with the rate at which chemical processes occur and the development of kinetic theory for predicting and modelling rates. In particular, the chemical processes of interest are unimolecular and recombination reactions in the gas phase.

Unimolecular and recombination reactions are ubiquitous in gas phase chemistry. They constitute a major part of, for instance, combustion chemistry, atmospheric chemistry, ionospheric chemistry and interstellar chemistry. There are a number of variations on the fundamental unimolecular process: (1) In a unimolecular decomposition, a stable molecule becomes energetically excited and decomposes through one or more dissociative channels; (2) In a recombination process (also called association), two reactant moieties combine to form a single excited collision complex, which may then be stabilised to form a molecule[†]; (3) In a chemical activation process, reactant moieties combine to form a single excited collision complex, which may be stabilised or, in addition, dissociate through one or more product channels; 4) Isomerisation, where a molecule attains sufficient

[†]In ion–molecule chemistry, the term *association* is preferred because the term *recombination* usually refers to the process of an ion combining with an electron. Since in this work we do not deal with the latter process, the two terms will be used interchangeably with the understanding that they refer to the reaction of type 2).

excitation to undergo rearrangement of its internal structure, thereby forming a different chemical species.

In most areas of interest the thermal reactions occur at gas densities such that collisions are the main activation/deactivation mechanism. For this reason, the present work deals with the calculation of rate coefficients for such systems.

There are two main aims in the development of theory for the calculation of rate coefficients. The first is to make possible the reliable extrapolation of experimental data over a wide range of different conditions. This is necessary because any one experimental technique tends to be restricted by the limitations of the apparatus to a limited range of pressure or temperature. Nature does not feel bound by the same conditions (e.g., the conditions of interstellar chemistry are not easily achieved in the laboratory because of the very long timescale and extremes of temperatures). The optimal conditions for a reaction in an industrial process, or the conditions under which a reaction occurs in the atmosphere, are often not those under which the isolated reaction rate has been measured. It is therefore very important to develop a reliable theoretical means of extrapolating existing data.

The second aim is to develop an understanding of the fundamental processes which dictate the rate of reactions with a view to *a priori* prediction of rate coefficients. This goal, being more virtuous, is more difficult. If one has *some* experimental data to fit it will be possible, on a good day, to determine the unknowns in the theoretical model through the fitting procedure. One can then extrapolate the data reliably. However, the ability to fit existing experimental data is not *per se* a criterion for acceptability of a theory. Furthermore, what if there are no data to fit? In order to make an *a priori* prediction, we have to eliminate the unknowns. Thus an understanding of the fundamental processes determining the rate, *viz.* the collisional activation/deactivation and the dissociation/recombination steps, is important not only because seeking it is fun but because it will provide a means of quickly and reliably determining rates of reactions which may

never have been studied experimentally. Of course, one does not suggest that kinetic theory will make kinetic experiments unnecessary! Rather, reliable predictive theory will allow experimental resources to be used on other challenging and pressing problems.

An important characteristic of unimolecular reactions is the variation of the rate coefficient with pressure. The reactant (or, in the case of recombination, reactants) usually constitutes only a small part of the total gas density. The remaining gas, which is not chemically involved in the reaction but makes up the bulk of the mixture and hence determines the pressure, is often called the "bath gas". By changing the pressure of the bath gas, the pressure of the system can be altered without affecting the reactant concentration. It is found that at high pressures the rate of reaction depends solely on the reactant concentration, and is independent of the pressure. At lower pressures, however, the observed rate coefficient begins to decrease as the pressure decreases. As the pressure is lowered further, the rate coefficient eventually becomes directly proportional to the pressure and hence the bath gas concentration. This qualitative behaviour, commonly called "fall–off", is quite independent of the chemical identity of the bath gas.

The fall–off behaviour of such reactions as the pressure is reduced is due to the fact that a molecule has to be energetically excited, with sufficient energy to break the appropriate bond, before reaction can occur. In thermal systems, collisions with the bath gas are the mechanism of activation. At high pressures, collisions are so frequent that the unimolecular dissociation itself is the rate determining step. As the pressure decreases, both collision and reaction play a part in determining the rate. At low pressures collisional activation is the rate determining step and hence the rate becomes directly proportional to the bath gas concentration.

This fall–off behaviour was first understood qualitatively by Lindemann (1922). His postulate involved a single step collisional activation to some excited state which might, if sufficiently energetic, dissociate. Later this concept was generalised to include many excited states of the molecule, each having its own intrinsic reactivity, most successfully in RRKM

(Rice, Ramsperger, Kassel, Marcus) theory. It was later recognised that the collisional activation/deactivation process is not a one–step process, but rather involves multiple weak collisions. These developments, along with some of the useful background theory of unimolecular reactions, will be summarised in more detail in Chapter 1.

It has long been recognised that recombination reactions bear an intimate relationship to unimolecular dissociation reactions, since the two processes are the reverse of each other. One might expect a comparitively direct relationship to exist between the rate coefficients for a single channel unimolecular dissociation and the reverse recombination reaction. Indeed, a common practice has been to assume that they are always related by the equilibrium constant (see, e.g., Keck and Carrier 1965, Troe 1977, Gilbert and McEwan, 1985). A rigorous derivation of the exact relationship between the non–equilibrium rate coefficients for the two types of reaction, however, does not appear to have been presented previously. This problem is discussed in Chapter 2, where relevant earlier work is summarised and an exact solution to the recombination/chemical activation problem is presented. This is through the master equation, which relates the microscopic rates for reaction and collision to the overall thermal rate coefficient.

A large class of unimolecular reactions show sensitivity to angular momentum effects. These reactions include decomposition which occurs by a simple fission transition state, radical–radical recombination and ion–molecule reactions. In such reactions there is a large change in the moment of inertia of the molecule as it proceeds to the transition state (or vice–versa). Application of master equation solutions to the calculation of fall–off behaviour for these reactions has foundered in the past, however, due to inadequate account of angular momentum effects. Only limited means of accounting for this effect have been available previously (Waage and Rabinovitch, 1970; Troe, 1977,1987; Penner and Forst, 1975,1976). In Chapter 3 the general problem of angular momentum (J) conservation is discussed. A general method of solving the master equation with J conservation is derived and compared with previous, more restricted, solutions. This allows ion–molecule fall–off behaviour to be reliably modelled using an accurate weak–collision master equation solution

for the first time.

Calculation of rate coefficients requires not only an accurate method of solution of the master equation (which accounts for the effect of collisional activation and deactivation on the rate), but also an accurate means of determining the intrinsic reactivity of excited molecules: specifically, the microscopic rate coefficient for dissociation, $k(\epsilon,J)$. This is done most conveniently using RRKM theory (see Chapter 1). However, RRKM theory in its traditional form requires some modification in order to be applicable to ion–molecule reactions: in Chapter 4 the required extensions are discussed and appropriate formulae for implementing these extensions derived. In particular, the problems dealt with are the microcanonical variational selection of transition states and the effect on the rate coefficient of a neutral reactant molecule with a permanent dipole.

Theory is rarely developed in a vacuum: the inadequacy of existing theory for modelling certain well–studied ion–molecule reactions stimulated much of the current work. One such example is the reaction of methyl cation with methyl cyanide. This reaction is of the chemical activation type, and has been studied over a wide range of pressures to yield the complete fall–off behaviour at room temperature. A modelling study which compares theory with the experimental results and illustrates in particular the importance of correct treatment of the dipole, is included in Chapter 4.

An important aspect of modern transition state theory is the realisation that the rate coefficient obtained is an upper bound to the true rate coefficient, and hence the best choice of transition state is that which gives the minimum rate (see Chapter 1). Practically, one finds that at room temperature the transition state tends to lie at large separations of the reactants (or products), where the potential of interaction is electrostatic. This makes calculation of rate coefficients simpler (!) because the electrostatic potential is well–defined. Such is not the case at high temperatures, however, since as one raises the temperature the best choice of transition state moves in to smaller separations where the chemical forces are important. This change in character of the transition state with

increasing temperature has important ramifications for the calculation of ion–molecule rate coefficients in high–temperature applications, e.g., plasma etching, laser processes and "hot" interstellar chemistry.

In Chapter 5 an experiment is presented which was designed with the aim of determining high temperature ion–molecule thermal rate coefficients. The study involves observing unimolecular dissociation of a polyatomic ion (protonated ethanol) in a Selected Ion Flow Drift Tube (SIFDT) and was carried out at the University of Birmingham. This is a novel use of the SIFDT which utilises the effect of the electric field gradient to raise the internal temperature of the ion by collisional activation.

One of the central aims of the current work has been to produce computer programmes employing a high level of theory which are nevertheless economical and easily used by workers wishing to model their experimental data or estimate rates of reaction under various conditions. All of the calculations presented herein (except those from other theories which are used for comparative purposes) were carried out using the programmes which have been so developed. The presentation of these programmes is not considered to be appropriate for the present work. However, full documentation and FORTRAN code is separately available (Smith and Gilbert 1989).

CHAPTER 1

THEORY OF UNIMOLECULAR DISSOCIATION: A SUMMARY

A summary of the theory of unimolecular reactions is presented in this chapter as a background to the work of the following chapters. There are two main aspects to the calculation of unimolecular dissociation rate coefficients: 1) The calculation of a microscopic rate coefficient k(E) for dissociation of an excited molecule AB^* with energy E, and 2) The calculation of the non-equilibrium molecular population distribution over energies, g(E), appropriate to the conditions. The thermally observed rate coefficient k_{uni} will be an average of k(E) over g(E). In this chapter the basic theory for solving for g(E) will be summarised first. Following this a brief description of the RRKM theory for k(E) and some refinements thereof will be given.

The first model for describing the interplay between reaction and collision steps in a unimolecular dissociation reaction was that proposed by Lindemann (1922). Lindemann's postulate involved a single step activation of the molecule AB to an excited state AB^*, occuring with a rate coefficient k^a as a result of collisions with a third body M. The energetically excited molecule AB^* may then dissociate with rate coefficient k^r or be stabilised, by further collisions with the third body M, with rate coefficient k^s. This is represented schematically in Eq. (1.1):

$$\begin{aligned} AB + M &\underset{k^s}{\overset{k^a}{\rightleftharpoons}} AB^* + M \\ AB^* &\xrightarrow{k^r} A + B \end{aligned} \qquad (1.1)$$

After solving for the steady state concentration of AB^*, one obtains for the rate coefficient k_{uni}:

$$k_{uni} = k^r k^a [M] / \{[M]k^s + k^r\} \qquad (1.2)$$

At high pressures, k_{uni} becomes independent of the third body concentration, [M], attaining the value $k^r k^a/k^s$. At low pressures k_{uni} becomes proportional to [M]. Hence the Lindemann postulate qualitatively predicts the characteristic fall-off behaviour of dissociation reactions. The model is not quantitatively accurate, however, and a significant improvement was obtained through the recognition that a molecule can be excited with varying amounts of energy, and that the rate coefficient is sensitive to the amount of excitation above the threshold energy for dissociation (Kassel 1928; Rice and Ramsperger 1927). Hence it is necessary to allow for many excited states AB_i^*, each with its own specific rate coefficient for dissociation, k^r_i. The reaction scheme is then as indicated in Eq. (1.3):

$$\begin{aligned} AB + M &\underset{k^s_i}{\overset{k^a_i}{\rightleftharpoons}} AB^*_i + M \\ AB^*_i &\xrightarrow{k^r_i} A + B \end{aligned} \qquad (1.3)$$

Molecules with more than about four atoms will generally have a very dense state distribution at the excitation energies required for reaction, and so it is convenient to treat the state manifold as continuous, writing $AB^*(E)$ and $k(E)$ rather than AB^*_i and k_i.

Various approaches to the calculation of the *microscopic* rate coefficient k(E) have been tried. The most successful has been RRKM (Rice, Ramsperger, Kassel, Marcus) theory, which arose from an important extension by Marcus (1952) of the earlier work of Rice, Ramsperger (e.g., 1927) and Kassel (e.g., 1928). RRKM theory provides a simple and (today) easily evaluated expression for k(E) which is the basis of most practical calculation procedures.

The activation and stabilisation rate coefficients k^a_i and k^s_i were originally evaluated using the assumption, called the *strong collision* assumption, that a *single* collision is sufficient to relax a molecule into an equilibrium probability distribution (Hinshelwood 1927). One writes k^a_i as the product of the rate coefficient for collisions between AB and

M, denoted Z, and a probability P(E',E) for collisional energy transfer from energy E to energy E'. The strong collision assumption will set P(E',E) to the equilibrium (Boltzmann) distribution function $f(E') = \rho(E')\exp(-E'/k_BT)$, where $\rho(E')$ is the molecular density of states and k_B is Boltzmann's constant. k^a_i in Eq. (1.3) then becomes $Zf(E_i)$.

The strong collision assumption generally leads to an overestimate of the dissociation rate coefficient, primarily because it overestimates the amount of energy transfer in collisions. The recognition that *multiple* ("weak") collisions are required for such activation/deactivation processes leads to a further modification of the basic reaction scheme:

$$\begin{aligned} AB(E) + M \quad &\underset{ZP(E,E')}{\overset{ZP(E',E)}{\rightleftharpoons}} \quad AB^*(E') + M \\ AB^*(E') \quad &\xrightarrow{k(E)} \quad A + B \end{aligned} \tag{1.4}$$

In order to determine the population distribution for molecules AB(E), one formulates and solves a *master equation* (Zwolinski and Eyring 1947). The master equation describes the rate of collisional transitions between and reactive loss from the individual energy levels with populations g(E,t):

$$\begin{aligned} \partial g(E,t)/\partial t = \omega \int [P(E,E')g(E',t) - P(E',E)g(E,t)]dE' \\ - k(E)g(E,t) \end{aligned} \tag{1.5}$$

where $\omega = Z[M]$ is the average collision frequency [$\omega P(E',E)$ then gives the rate of energy transfer from state E to state E']. Eq. (1.5) describes: a) the rate of collisional influx to state E from other states, b) the rate of collisional loss from state E to other states, and c) the rate of dissociative loss from state E. If there is more than one dissociative channel then $k(E) = \Sigma_i\, k^i(E)$, where $k^i(E)$ is the microscopic rate coefficient

for dissociation through channel i. Eq. (1.5) represents a series of simultaneous equations, since there is a separate equation of this form for each energy of the molecule,

The general solution of Eq. (1.5) will be outlined in the next section, followed by a treatment of the special case of strong collisions, wherein the solution of the master equation becomes particularly simple. The technique of solving the master equation for the latter case will be used in Chapter 3 in the development of a more general solution of the two dimensional master equation (in energy E and angular momentum J).

I. Solution of the Master Equation in the Fall-off Regime

It is convenient to write Eq. (1.5) in matrix form (Montroll and Schuler 1958):

$$dg(t)/dt = Jg(t) \tag{1.6}$$

where J is a matrix containing the collisional and reactive terms of the master equation:

$$J_{ij} = \omega\, P(E_i,E_j)$$

$$J_{ii} = -[\omega + k(E_i)] \tag{1.7}$$

Eq. (1.6) is entirely equivalent to the set of equations (1.5): **g**(t) is the population vector whose elements are the individual populations g(E,t).

The probability function for energy transfer P(E',E) is not well known in general, though it must obey the constraints of microscopic reversibility [Eq. (1.9) below] and normalisation, i.e., $\int P(E',E)dE' = 1$. It has been demonstrated (see, e.g., Tardy and Rabinovitch 1977) that the fall-off behaviour of a reaction is essentially dependent only on the first moment of P(E',E). Reliable means of determining this first moment at modest computational expense have recently been developed (Whyte *et al.* 1988), and a

well-founded model for the shape of P(E',E) has been presented (Gilbert 1984, Lim and Gilbert 1986).

In solving Eq. (1.6), one first transforms to an equation involving an Hermitian matrix B (Montroll and Shuler 1958) by making the substitution $\mathbf{g}(t) = \mathbf{S}\mathbf{c}(t)$, where S is a diagonal matrix whose i^{th} diagonal element is the square root of the equilibrium population $b(E) = \rho(E)\exp(-E/k_BT)$ [$\rho(E)$ being the density of states of the molecule]:

$$\mathbf{dc}(t)/dt = \mathbf{B}\mathbf{c}(t) \tag{1.8}$$

Here $\mathbf{B} = \mathbf{S}^{-1}\mathbf{J}\mathbf{S}$ is a symmetric matrix. This symmetrisation takes advantage of the fact that the probability function for energy transfer, P(E',E), must obey microscopic reversibility (see,e.g., Messiah 1964):

$$P(E',E)b(E) = P(E,E')b(E') \tag{1.9}$$

Eq. (1.9) is often also referred to as the detailed balance constraint (Tardy and Rabinovitch 1977). Eq. (1.8) has the formal solution (see, e.g. Ritger and Rose 1968):

$$\mathbf{c}(t) = \exp(\mathbf{B}t)\mathbf{c}(t=0) \tag{1.10}$$

Since B is Hermitian, its eigenvectors $\{\psi_i\}$ form a complete set and may be chosen to be orthogonal. We may therefore express the initial population vector $\mathbf{c}(t=0)$ as a linear combination of the set $\{\psi_i\}$:

$$\mathbf{c}(t=0) = \Sigma_i\, a_i\psi_i \tag{1.11}$$

Substituting into Eq. (1.10) yields:

$$\mathbf{c}(t) = \Sigma_i\, a_i\psi_i \exp(\lambda_i t) \tag{1.12}$$

where λ_i is the eigenvalue corresponding to the eigenvector ψ_i. Now since the population c(t) clearly must decrease with time, all λ_i are negative. Furthermore, it may be shown (Nikitin 1966, Pritchard 1984) that one eigenvalue is generally significantly larger (less negative) than the others. Therefore, after a brief induction period Eq. (1.12) reduces to:

$$\mathbf{c}(t) = a_1\psi_1\exp(\lambda_1 t) \tag{1.13}$$

where it is assumed that the largest eigenvalue is labelled λ_1. Hence

$$\mathbf{g}(t) = a_1\mathbf{x}_1\exp(\lambda_1 t) \tag{1.14}$$

where $\mathbf{x}_1$ is the eigenvector of J corresponding to λ_1. From Eq. (1.14) it can be seen that after the brief induction period:

$$d\mathbf{g}(t)/dt = \lambda_1\mathbf{g}(t) = J\mathbf{g}(t) \tag{1.15}$$

That is, the system has attained a pseudo–steady state such that all populations obey single exponential unimolecular decay with rate coefficient $k_{uni} = -\lambda_1$, where λ_1 is the largest (least negative) eigenvalue of the collisional/reactive matrix J. The *relative* non–equilibrium population distribution becomes time–independent (since all populations are decaying with the same rate coefficient) and is determined by the eigenvector of J corresponding to the largest eigenvalue λ_1:

$$\hat{\mathbf{g}}(E) = \mathbf{g}(E,t)/\int\mathbf{g}(E,t)dt = \mathbf{x}_1(E)/\int\mathbf{x}_1(E)dE \tag{1.16}$$

Since most experimental applications involve time–scales much greater than the induction period, the time–independent, relative distribution $\hat{\mathbf{g}}(E)$, determined as the eigenvector of J corresponding to the largest eigenvalue, is the relevant distribution. The master equation is therefore often formulated as a time–independent eigenvalue problem:

$$-k_{uni}g(E) = \omega\int[P(E,E')g(E') - P(E',E)g(E)]dE' - k(E)g(E) \quad (1.17)$$

where $\hat{g}(E)$ is written as g(E) for notational convenience.

Calculation of the rate coefficient k_{uni} can therefore be seen to amount to finding the largest eigenvalue of a matrix. To define the dimensions of the matrix, one selects an appropriate energy grainsize and chooses a "ceiling" energy high enough to ensure convergence of the rate. Very efficient methods of calculating k_{uni} in this way have been developed (see, e.g., Gaynor *et al.* 1978, Schranz and Nordholm 1983). It is easily shown by summing Eq. (1.15) over all energies that k_{uni} (or, $-\lambda_1$) is indeed an average of the microscopic rate coefficients k(E) over the non-equilibrium population distribution g(E):

$$k_{uni} = \Sigma_i\ k(E_i)g(E_i) \ /\ \Sigma_i\ g(E_i) \quad (1.18)$$

The general behaviour of the unimolecular rate coefficient as a function of pressure and temperature has been discussed in great detail (see, e.g., Forst 1973). The pressure dependence of the rate coefficient falls into three regimes: a) The pressure saturated regime. At high pressures the rate coefficient is independent of pressure. This is because above a certain pressure collisions are so rapid that reaction is a minor perturbation and a Boltzmann distribution of populations is always maintained. b) The fall-off regime. At intermediate pressures the reaction competes with collisions to produce depleted populations at energies above the threshold for reaction, E_o. This produces a generally complex monotonic "fall-off" in the rate coefficient with decreasing pressure. c) The low pressure limiting regime. At low pressures reaction dominates to produce a complete depletion of the molecular population above E_o. The rate determining step is collisional activation from energies below E_o to energies above E_o. The rate coefficient is therefore directly proportional to the bath gas population and shows bimolecular behaviour.

This pressure dependent behaviour is represented schematically in Figure 1.1. The pressure range in going from the low-pressure to the pressure-saturated regimes is

typically several orders of magnitude.

II. Solution of the Master Equation at Low Pressures

At low pressures, where the rate of collisional activation becomes rate determining, the population of molecules with excitation above the reaction threshold E_o becomes almost entirely depleted. The master equation therefore simplifies to one which deals only with molecules with energies *below* the reaction threshold E_o, i.e., collisional transitions between energies below E_o and collisional activation from beneath E_o into excited states whence reaction occurs rapidly. Firstly, one notes that at low pressures where $\omega \ll k(E)$ the collisional terms in Eq. (1.17) are a small perturbation to the k(E) terms for energies above E_o. Treating the collisional terms, which are proportional to ω, as a perturbation on the reaction terms, which are independent of ω, shows (Gilbert and Ross 1971) that as $\omega \to 0$, $g(E)=0$ for $E>E_o$. Then g(E) for $E<E_o$ and the low-pressure rate coefficient are

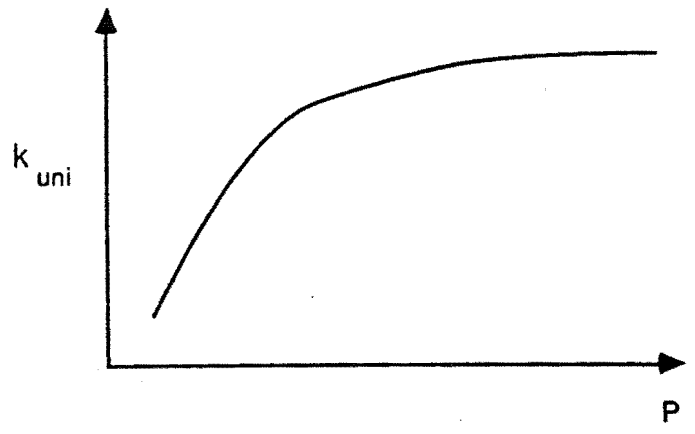

Figure 1.1. Schematic representation of the pressure-dependent "fall-off" behaviour that is characteristic of unimolecular reaction rate coefficients.

determined by the eigenvalue equation:

$$-k_{uni}g(E) = -\omega k_0 g(E) = \omega\int_0^{E_0}[P(E,E')g(E')-P(E',E)g(E)]dE' - \omega g(E)\int_{E_0}^{\infty}P(E',E)dE'$$

$$= \omega\int_0^{E_0}P(E,E')g(E')dE' - \omega g(E) \qquad (1.19)$$

where k_0 is the low-pressure rate coefficient expressed as a dimensionless quantity. Note that Eq. (1.19) has an equivalent form to Eq. (1.17), the difference being that one only deals with levels *below* E_0 and the "k(E)" term is simply the total rate of collisional activation from the population g(E) to excited levels. Hence a consistency check for any numerical solution to the master equation is that k_{uni} calculated at low pressures by solving Eq. (1.17) should be consistent with ωk_0 calculated by solving Eq. (1.19).

An important shortcoming of master equation solutions to date has been the lack of a practical means of incorporating angular momentum conservation effects. Many reactions are sensitive to these effects and so one has to deal with k(E,J) rather than k(E), P(E',J',E,J) rather than P(E',E), etc. This problem is dealt with in Chapter 3.

III. The Case of Strong Collisions

As described above, the strong collision assumption involves setting the probability distribution for collisional energy transfer from an initial level E, P(E',E), to the equilibrium distribution f(E'). Substituting this into Eq. (1.17) and noting that f(E') is normalised, Eq. (1.17) becomes:

$$-k_{uni}g(E) = \omega\, f(E) \int g(E')dE' - [\omega + k(E)]g(E) \qquad (1.20)$$

Rearranging to obtain g(E) and noting that $k_{uni} \ll \omega + k(E)$, one has:

$$g(E) = \omega\, f(E) / [\omega + k(E)] \qquad (1.21)$$

where we made the approximation that $\int g(E)dE \approx 1$. The thermal dissociation rate coefficient is then the average of the microscopic rate coefficients k(E) over the population g(E):

$$k_{uni} = \omega \int dE\; k(E)f(E) / [\omega + k(E)] \qquad (1.22)$$

At low pressures the strong collision result for k_{uni} reduces to:

$$k_{uni} = \omega \int_{E_0}^{\infty} f(E)dE \qquad (1.23)$$

The strong collision assumption in most cases overestimates the amount of energy transfer in collisions. This causes g(E) to be overestimated for a given pressure in the fall–off regime, and so rate coefficients calculated in the fall–off regime are too large. A commonly used means of rectifying this error is to include a "collision efficiency" factor β which multiplies ω in order to decrease the activation/deactivation rate coefficients (β is a fraction between zero and one). The physical interpretation of such an efficiency is that a portion β of the collisions are "strong" whilst the remaining $(1-\beta)$ are elastic. Inclusion of β is a pragmatic means of mimicking weak collision effects within the simple strong collision formalism. Such a modification will generally allow a moderately good fit of experimental data within a limited range of pressure or temperature. However, a strong collision curve fitted to data in this way tends to be unreliable for extrapolating over a wide range of conditions, such as when making comparisons between results of experimental techniques that operate in different pressure regimes. A strong collision curve extrapolated in this way can lead to rate coefficients in error by a factor of two or three

(Gilbert *et al.* 1983). However, the strong collision formalism is easily adjusted to include angular momentum effects (see Chapter 3). Because of earlier difficulties in treating angular momentum conservation, workers in the ion–molecule field have generally persevered with the strong collision method, as master equation methods have hitherto been inadequate for application to ion–molecule reactions which are very sensitive to angular momentum effects.

IV. RRKM Theory for k(E)

The RRKM theory is a statistical theory for calculating microscopic rate coefficients. It incorporates the dynamics of the excited molecule in a statistical fashion, and was developed by Marcus (1952) from earlier work by Rice and Ramsperger (e.g., 1927) and Kassel (e.g., 1928). The derivations of Marcus succeeded in placing the earlier work on a theoretically rigorous statistical mechanical footing.

One notes first that the timescale for a collision event, being of the order of picoseconds or less, is much shorter than that for unimolecular dissociation of an excited molecule (typically nanoseconds to microseconds). Hence the bath gas need not be included in considering the dynamics of dissociation of an excited molecule: it will have "been and gone" before the real action happens.

There are two fundamental assumptions made in determining the RRKM result for k(E): the ergodicity, or "strong coupling", assumption and the transition state assumption. Consider an excited molecule AB^* with energy E deposited primarily in some local mode of excitation after a collision. The ergodicity assumption considers all possible states of the molecule with energy E to be accessible on the timescale of dissociation, and so takes as an ensemble all such states. The microscopic rate coefficient k(E) is calculated as the proportional dissociation per second of this hypothetical ensemble. This rate of dissociation is evaluated by applying transition state theory: one assumes that a dividing surface exists

on the potential surface between the reactant potential well and the product region across which trajectories leaving the reactant region cross only once. Evaluation of the total flux of trajectories across the "transition state", $\Phi(E)$, divided by the ensemble population, $\rho(E)$, then gives the RRKM approximation to the microscopic rate coefficient k(E). The classical expression for the rate coefficient is (Garrett and Truhlar 1979):

$$k(E) = \frac{\int \ldots \int d\Gamma \, \frac{p_r}{m} \, \delta(r-s) S(p_r) \chi(\Gamma) \delta(E-H)}{\int \ldots \int d\Gamma \delta(E-H)} \qquad (1.24)$$

The numerator is a surface integral which counts classical states, determined by coordinates Γ which represent all degrees of freedom of the molecule, excluding those degrees of freedom which due to conservation laws do not participate in the randomisation of internal energy (e.g., external translational degrees of freedom). The $\delta(r-s)$ function specifies the dividing surface by restricting the integral to a surface where the reaction coordinate r has a fixed value s. The $\delta(E-H)$ function specifies that the integral count only those states on this surface that have the prescribed total energy E. Now, since each of these states corresponds to a trajectory passing *through* the dividing surface (neglecting the special case of periodic orbits), the flux of trajectories from the reactant region of the potential surface to the product region is obtained simply by counting only those trajectories with positive momentum p_r along the reaction coordinate: hence the inclusion of the step function $S(p_r)$, which is zero if $p_r<0$ and unity if $p_r>0$. The quantity p_r/m is the speed of trajectories along the direction of the reaction coordinate: this counts the *rate* of passage of trajectories across the surface. The characteristic function $\chi(\Gamma)$ selects only those trajectories which do not recross the dividing surface: $\chi=1$ in such cases and $\chi=0$ otherwise. The transition state assumption, that *all* trajectories crossing the surface do not recross therefore sets $\chi\equiv1$. The denominator of Eq. (1.24) is simply the population of the hypothetical ensemble: the total number of classical states of the molecule consistent with the energy E, obtained by integration over all the coordinates Γ.

Counting trajectories crossing through the dividing surface and counting the population

of the ensemble both reduce to an exercise in counting classical states. It may be shown (see, e.g., Messiah 1964) that the denominator in Eq. (1.24) corresponds to $h^n\rho(E)$, where h is Planck's constant and $\rho(E)$ is the quantum mechanical *density* of states. It may also be shown (see, for e.g., Garrett and Truhlar 1979) that, to an excellent approximation, the numerator in Eq. (1.24) may be written as $h^{n-1}W^\dagger(E-E_0)$, where $W^\dagger(E-E_0)$ is the quantum mechanical *sum* of states evaluated at the transition state [E_0, the "critical energy", being the potential V(r=s)]. The RRKM expression for k(E) therefore reduces to:

$$k(E) = W^\dagger(E-E_0)/h\rho(E) \tag{1.25}$$

where

$$W^\dagger(E-E_0) = \int_0^{E-E_0} \rho^\dagger(E_+)dE_+ \tag{1.26}$$

In order to implement Eq. (1.25), one requires the vibrational frequencies and rotational constants of the molecule and transition state, since these determine the density of states of these species. Also required is a knowledge of the critical energy for dissociation, E_0.

Eq. (1.25) is applicable to reactions involving a transition state at a maximum in the potential surface, indicated schematically in Figure 1.2. There is a large class of reactions for which there is no maximum in the potential surface along the reaction coordinate, as indicated in Figure 1.3. Such reactions include radical–radical recombinations, dissociations proceeding via a "simple-fission" transition state, and ion–molecule associations. These cases require further refinement of the basic result of Eq. (1.25) to include angular momentum effects and incorporate a variational selection of the transition state. The effect of angular momentum conservation may be simply incorporated into Eq. (1.25) (Marcus 1965). This will be summarised in Chapter 3.

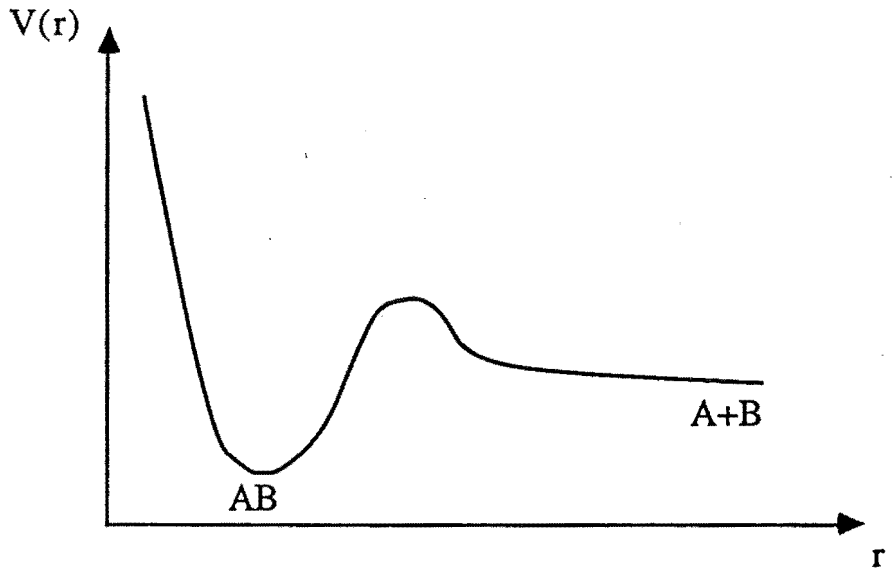

Figure 1.2. Schematic representation of the potential along the reaction coordinate for a chemical reaction with a pronounced barrier. Eqs. (1.25) and (1.26) typically apply to such systems.

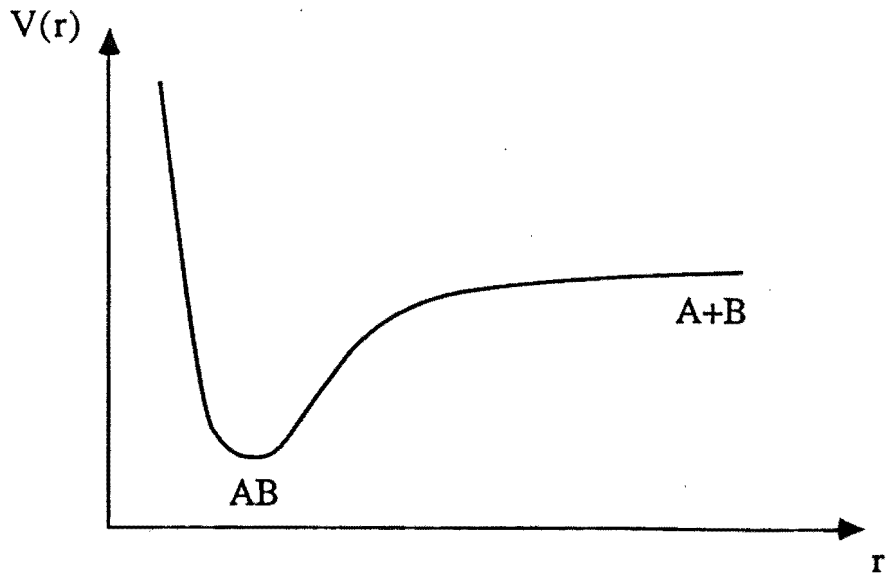

Figure 1.3. Schematic representation of the potential along the reaction coordinate for a chemical reaction with no pronounced barrier. Eqs. (1.25) and (1.26) require modification to include the effect of angular momentum conservation before application to such systems.

V. Variational Selection of the Transition State

The RRKM expression for k(E) provides an upper bound to the true microscopic rate coefficient. This is because the transition state assumption assumes that *every* trajectory crossing the dividing surface in the direction of products will indeed go on to products and will not recross the dividing surface. Hence *all* states of the transition state with energy $E_+ \leqslant E-E_0$ are counted in evaluating the sum of states, $W^\dagger(E-E_0)$. This must clearly overestimate the true rate coefficient, since at least some of the states counted will correspond to trajectories which do not go on to products, but recross the transition state surface. The optimum position for the transition state surface along the reaction coordinate is that which minimises this over-counting of states, i.e., transition state theory may be used *variationally* by trying a range of dividing surfaces and selecting as the transition state the one which gives the minimum sum of states $W^\dagger[E-V(s)]$ (see, e.g., Bunker and Patengill 1968, Hase 1976, Quack and Troe 1977).

For a reaction with a potential along the reaction coordinate such as that illustrated in Figure 1.2, the assumption that the minimum sum of states lies at the top of the barrier will be an excellent one. There is therefore no need for a variational treatment. For reactions with a potential such as that in Figure 1.3, however, the position of the transition state is not well defined due to the absence of any pronounced barrier along the reaction coordinate. It would seem initially that since the potential V(r) decreases as r decreases, the sum of states $W^\dagger(E-V(r))$ must correspondingly increase as one moves in along the reaction coordinate: enthalpic effects tend to push the position of minimum "reactive flux" out to large values of r. However, as r decreases, the density of states on the dividing surface decreases due to free rotations of the separate moieties becoming hindered and eventually becoming vibrations in the molecule. This entropic effect tends to push the position of the transition state inwards to smaller values of r. It is the interplay of these enthalpic and entropic effects which produces a minimum of the sum of states at some particular value r=s along the reaction coordinate.

The optimum method of calculating microscopic rates is therefore to select the transition state variationally for each separate energy E and (since angular momentum effects are important for these types of reaction) angular momentum J. This technique is called Micro-canonical Variational Transition State Theory (MVTST).

An alternative method (which is not as accurate as MVTST but which gives reasonable results and is much more easily implemented) is Canonical Variational Transition State Theory (CVTST) (see, e.g., Garrett and Truhlar 1979). This method involves choosing a single position r=s for the transition states for *all* E and J, and simply varying this position to obtain the best *average* transition state.

CHAPTER 2

THE RELATIONSHIP BETWEEN CHEMICAL ACTIVATION, RECOMBINATION, AND UNIMOLECULAR DECOMPOSITION RATE COEFFICIENTS

Recombination and unimolecular decomposition reactions are the reverse of each other. One might therefore expect a comparatively direct relationship to exist between the rate coefficients for the two types of reaction. In this chapter the relationship between these processes, and the preferred method for calculating their respective rate coefficients, are discussed.

It is easily shown, from thermodynamics or statistical mechanics, that when a system is in equilibrium the forward and reverse rate coefficients are related by the equilibrium constant. Experimentally, reaction rates are usually measured under conditions far from equilibrium so that the analysis is not complicated by having to allow for the reverse reaction. Under such non-equilibrium conditions the rate coefficients may be substantially depressed from their equilibrium values (e.g., if the conditions place the rate coefficient in the fall-off regime). There is an accumulated tradition which holds that the forward and reverse *non-equilibrium* rate coefficients are also related by the equilibrium constant (e.g., Troe 1977a; Gilbert and McEwan 1985). This relates to early work which examined the relationship between the non-equilibrium rate coefficients for recombination and dissociation of diatomics (e.g., Snider 1965; Keck and Carrier 1965). However, a proof of the relationship for the more general case of polyatomic species does not appear to have been published.

The way to approach the problem is to write down the master equation for the recombination/chemical activation process, solve it, and then examine the solution and see if it is indeed related to the equilibrium constant and the reverse unimolecular rate coefficient. Before attacking this problem in earnest, the general reaction scheme is

described and the methods which have been used previously to calculate recombination/chemical activation rate coefficients are summarised.

The reaction scheme for recombination and chemical activation reactions is as follows:

$$\begin{array}{ccccc} A + B & \underset{k^{1}(E,J)}{\overset{k^{-1}(E-\Delta H_1,J)}{\rightleftharpoons}} & AB^{*}(E,J) & \xrightarrow{k^{2}(E,J)} & C + D \\ & & \downarrow\uparrow & & \\ & & \downarrow\uparrow\ M & & \\ & & \downarrow\uparrow & & \\ & & AB & & \end{array} \qquad (2.1)$$

Two reactant moieties A and B, which have concentrations A(t) and B(t) and are assumed to be thermalised, collide to form an excited collision complex $AB^{*}(E,J)$ with total energy E and total angular momentum J. AB^{*} is excited because the binding energy ΔH_1 is released into the reaction coordinate as the reactant moieties come together. This energy does not remain in the reaction coordinate (otherwise the collision complex would dissociate again within a vibrational period), but is rapidly randomised throughout the internal degrees of freedom of the complex†. This randomisation process leads to a finite lifetime (in the absence of any collisions) for the excited complex prior to dissociation. Note that, since the system is assumed to be far from equilibrium, the population of products C and D will be so small as to enable neglect of the recombination of C and D; hence there is no reverse arrow for this channel. In a recombination reaction, the only channel through which dissociation can occur is that leading back to reactants (i.e., there are no alternative products C and D). Recombination may therefore be seen as a special case of the more general chemical activation scheme.

† The term *complex* will always be used in the present work to refer to the metastable collision complex which occurs on collision between reactant moieties in a recombination or chemical activation reaction. In the older literature the term "activated complex" was used to designate the transition state for a reaction: we will use the term *transition state* in this context.

The excited collision complex $AB^*(E,J)$ has a specific (or microscopic) rate coefficient for dissociation (or possibly rearrangement) $k^i(E,J)$, where i denotes the i^{th} channel. This is most conveniently calculated from RRKM theory (Chapter 3). There are, of course, a number of refinements to the usual RRKM algorithm required for the calculation of k(E,J) in ion–molecule systems: these will be considered in Chapter 4.

In addition to dissociation, an excited collision complex may also undergo collisions with another gas molecule. Such collisions will in general remove a certain amount of energy from the excited complex. If a sufficient number of collisions occurs, the complex will become stabilised with respect to dissociation to form the molecular product.

For simplicity the following discussion will deal with one–dimensional master equations, in energy alone. The conclusions drawn are valid for the more general case where angular momentum must also be considered, but there is little extra physical insight to be gained in the present context by treating the two dimensional case in detail. Angular momentum does, however, have an important influence on the absolute magnitude of the rate coefficients involved. This effect is dealt with in the following chapter.

The traditional method of solving the chemical activation problem (of which recombination is a special case) has been to solve for the excited collision complex population distribution by a steady state method, and then to calculate from this distribution the rates of decomposition to products and stabilisation to molecular product. This can be done with varying degrees of sophistication. For example, Kohlmaier and Rabinovitch (1963) have solved a steady state master equation with a weak collisional description for the energy transfer in collisions, while Herbst (1985) used an empirical rate coefficient for stabilisation which decreases as the energy of the complex increases above the reaction threshold (the lowest threshold for dissociation).

The simplest, and most commonly employed, steady state method is the strong

collision model: one uses a rate coefficient for stabilisation which is simply the collision rate (between the complex and the bath gas) multiplied by an "efficiency factor", β (see, e.g., Bass *et al.* 1981, Larson *et al.* 1988). The strong collision model is easy to apply and will always reproduce experimental data over a *limited* range of pressure, but can often be inaccurate when used to extrapolate data outside the experimental range (see, e.g., Gilbert *et al.* 1983).

There is one feature common to all the steady state methods: only those populations of the molecule which have energies *above* the threshold for dissociation are considered. This amounts to assuming that once the energy of a molecule drops below the dissociation threshold it may be considered to be irreversibly stabilised and can be forgotten thereafter. Such an approximation can lead to a significant error, particularly at high temperatures and low pressures (Schranz and Nordholm 1984). *Activation* of molecules from levels just below the threshold can have an important effect in reducing the rate of association under these conditions. A proper weak collision treatment which includes *all* energy levels of the molecule, including those below the dissociation threshold, is necessary.

There is an additional reason for dealing with a master equation which includes *all* the states of the molecule, aside from the fact that it enables one to allow for activation originating beneath the threshold in chemical activation systems. Whilst this approach might seem at first to increase the complexity of the problem, it has the conceptual advantage of setting the problem on the same footing as the unimolecular master equation, which also considers all states of the molecule. The direct comparison of the solutions to the two master equations, which is the overall aim of this analysis, is then possible.

The basic method of solution of the chemical activation/recombination master equation is well known. Schranz and Nordholm (1984) in a pioneering study have presented a solution to the master equation for chemical activation reactions and illustrated some of the limitations of the steady state approach. In the following section the basic, time-independent solution as presented by Schranz and Nordholm is extended to the case

of chemical activation reactions with a time-dependent reactant concentration (which will normally be the case). It is shown that, by explicit invocation of microscopic reversibility for activating and deactivating collisions and for forward and reverse *microscopic* rate coefficients, the non-equilibrium association rate coefficient may be exactly expressed in terms of the reverse decomposition rate coefficient, the equilibrium constant and a non-equilibrium factor which is trivially evaluated.

I. Solution of the Chemical Activation Master Equation

The master equation for a chemical activation reaction, describing the rate of formation and loss of molecules in a given state of energy E and population g(E,t), is written:

$$\partial g(E,t)/\partial t = \omega \int [P(E,E')g(E',t) - P(E',E)g(E,t)]dE' - k(E)g(E,t) + k^{-1}(E-\Delta H_1)f_r(E-\Delta H_1)A(t)B(t) \qquad (2.2)$$

where $k^{-1}(E-\Delta H_1)$ is the (bimolecular) microscopic rate coefficient for recombination of the reactants A and B, $k(E)=\sum_i k^i(E)$, and $f_r(E-\Delta H_1)$ is the thermal (Maxwell-Boltzmann) distribution of energies for reactants:

$$f_r(E-\Delta H_1) = \rho_r(E-\Delta H_1)\exp[-(E-\Delta H_1)/k_BT] \;/\; Q_AQ_B \qquad (2.3)$$

where Q_A and Q_B are the partition functions for reactants A and B respectively [$Q=\int\rho(E)\exp(-E/k_BT)$]. The last term in Eq.(2.2) describes the influx into a given state due to reactants combining. The other terms have the same significance as in the previous chapter. In addition, the initial condition that g(E,t=0) = 0 must be satisfied, i.e., one starts with reactants A + B and no product AB.

The first step in solution of Eq.(2.2) is to note that $k^{-1}(E-\Delta H_1)$ is related to $k^1(E)$

by microscopic reversibility (see, e.g., Messiah 1964):

$$k^{-1}(E-\Delta H_1)\rho_r(E-\Delta H_1) = k^1(E)\rho(E) \tag{2.4}$$

This enables Eq.(2.2) to be re-expressed as:

$$\partial g(E,t)/\partial t = \omega\int[P(E,E')g(E',t) - P(E',E)g(E,t)]dE' - k(E)g(E,t) + K_{eq}A(t)B(t)k^1(E)b(E) \,/\, Q \tag{2.5}$$

where Q is the partition function for AB, b(E) is the (unnormalised) equilibrium population for AB, $b(E)=\rho(E)\exp(-E/k_BT)$, and K_{eq} is the equilibrium constant between the reactants A + B and molecular product AB:

$$K_{eq} = [Q/Q_AQ_B]\exp(-\Delta H_o/k_BT) \tag{2.6}$$

If for convenience one discretises the energy, Eq.(2.5) is represented in matrix form as:

$$dg(t)/dt = Jg(t) + K_{eq}A(t)B(t)\mathbf{r} \,/\, Q \tag{2.7}$$

where J is the unimolecular collisional/reactive matrix as defined above, and **r** is an "equilibrium flux" vector: $r_i = k^1(E_i)b(E_i)$. As in the unimolecular case, this equation is transformed to one involving an Hermitian matrix operator B with the substitution **g** = Sc. Appropriate rearrangement then yields:

$$dc(t)/dt = Bc(t) + K_{eq}A(t)B(t)\mathbf{u} \,/\, Q \tag{2.8}$$

where $\mathbf{u} = S^{-1}\mathbf{r}$ and $B = S^{-1}JS$. Eq.(2.8) has the formal solution (see, e.g., Ritger and Rose 1968):

$$c(t) = \frac{K_{eq}}{Q} \int_0^t ds\ e^{B(t-s)}\ \mathbf{u}\ A(s)B(s) \tag{2.9}$$

where the initial condition that $\mathbf{g}(t=0) = \underline{0}$ has been invoked. The vector $\mathbf{u}$ may be expanded in terms of the complete set of orthogonal eigenvectors $\{\psi_i\}$ of the Hermitian matrix B:

$$\mathbf{u} = \Sigma_i\ a_i\psi_i \tag{2.10}$$

Substituting into Eq.(2.9) yields:

$$c(t) = \frac{K_{eq}}{Q} \sum_i a_i\psi_i \int_0^t ds\ e^{\lambda_i(t-s)} A(s)B(s) \tag{2.11}$$

where λ_i is the eigenvalue of B corresponding to the eigenvector ψ_i. Now, due to the separation of eigenvalues (one, denoted λ_1, being significantly larger than the others), the terms involving higher eigenvalues relax very quickly on an experimental timescale (Nikitin 1966; Pritchard 1984). After this induction period, the terms involving higher eigenvalues reduce as follows:

$$\int_0^t ds\ e^{\lambda_i(t-s)} A(s)B(s) \quad \approx \quad \frac{A(t)B(t)}{|\lambda_i|}\ ,\ i > 1 \tag{2.12}$$

This is because the exponential term relaxes very rapidly compared with the reactant populations A(s)B(s) (all λ are negative, with λ_1 being the least negative), and so the integrand only contributes significantly when $A(s)B(s) \approx A(t)B(t)$. Eq.(2.11) therefore reduces to:

$$c(t) = \frac{K_{eq}}{Q} \left\{ a_1\psi_1 \int_0^t ds\, e^{-k_{uni}(t-s)} A(s)B(s) + \left[\sum_i \frac{a_i}{|\lambda_i|}\psi_i - \frac{a_1}{k_{uni}}\psi_1 \right] A(t)B(t) \right\} \quad (2.13)$$

where $-\lambda_1$ has been identified as k_{uni}, the total rate coefficient for unimolecular dissociation through all channels. Multiplying through by S to obtain the population g(t) gives:

$$g(t) = \frac{K_{eq}}{Q} \left\{ a_1x_1 \int_0^t ds\, e^{-k_{uni}(t-s)} A(s)B(s) + \left[\eta - \frac{a_1}{k_{uni}}x_1 \right] A(t)B(t) \right\} \quad (2.14)$$

In Eq.(2.14) η is defined as:

$$\eta = \Sigma_i\, a_i\mathbf{x}_i \,/\, |\lambda_i| = \mathbf{J}^{-1}\mathbf{r} \quad (2.15)$$

From Eq.(2.14) it is apparent that the population g(t) is composed of two terms. We examine each in turn.

The first term of Eq.(2.14) is a population which builds up gradually over time. It is governed by the eigenvector $\mathbf{x}_1$. Recall that $\mathbf{x}_1$ is also the population distribution attained in unimolecular dissociation: it has significant magnitude chiefly below the threshold and is Boltzmann in nature at lower energies, though it may be depleted at higher energies. This first term may be identified as corresponding to the population of stabilised molecules which builds up over the period of the experiment, $g^s(t)$:

$$g^s(t) = \frac{K_{eq}}{Q} a_1 x_1 \int_0^t ds\, e^{-k_{uni}(t-s)} A(s)B(s) \qquad (2.16)$$

The second term of Eq.(2.14) is at steady state with the reactant population A(t)B(t). It comprises the difference between the vectors η and $\mathbf{x}_1$. Now, the population distribution $K_{eq}A(t)B(t)\eta/Q$ can be seen from Eq.(2.15) to be the solution of a steady state equation, obtained by setting $dg(t)/dt = \underline{0}$ in Eq.(2.7). Hence η corresponds to a steady state distribution where all the molecular states have "filled up" so that the net rate of formation of molecule is zero. Such a distribution will again be Boltzmann in nature at lower energies (below the thresholds for dissociation) but may deviate from equilibrium at higher energies. It is clear, however, that both η and $\mathbf{x}_1$ are "Boltzmann-like" distributions that have significant magnitude primarily below the dissociation thresholds, and moreover only deviate from each other at higher energies. The second term of Eq. (2.14), being the difference between these two vectors, will therefore only have significant value at energies above and slightly below the dissociation thresholds. When summed over energies, it is small in magnitude compared with the "stable population" obtained by summing the first term over energies (since $|\lambda_1|^{-1} \gg |\lambda_2|^{-1}, |\lambda_3|^{-1}, \ldots$), and it is at steady state with the reactant populations. The second term therefore may be regarded as the mathematical equivalent of the "steady-state collision complex population", $g^*(t)$, which is used in the steady state models (see, e.g., Kohlmaier and Rabinovitch 1963, Hoare 1963, Herbst 1985, Bass *et al.* 1981):

$$g^*(t) = \frac{K_{eq}}{Q}\left[\eta - \frac{a_1}{k_{uni}} x_1\right] A(t)B(t) \qquad (2.17)$$

Note that the long time limit of the molecular population in Eq.(2.14) is indeed the steady-state distribution $K_{eq}A(t)B(t)\eta/Q$. It is convenient now to evaluate the expansion coefficient a_1. Taking advantage of the fact that the eigenvectors $\{\psi_i\}$ of the Hermitian matrix B may be chosen as an orthogonal set, a_1 may be evaluated as:

$$a_1 = \psi_1 \cdot u \;/\; \psi_1 \cdot \psi_1 = x_1 \cdot S^{-2} r \;/\; x_1 \cdot S^{-2} x_1$$

$$= \frac{\sum_i x_1(E_i) k^1(E_i)}{\sum_i x_1(E_i)^2 \;/\; b(E_i)}$$

$$= \frac{k_{uni}{}^1 \sum_i x_1(Ei)}{\sum_i x_1(E_i)^2 \;/\; b(E_i)} \qquad (2.18)$$

The expression for the total population, G(t), is found by summing Eq.(2.14) over energies:

$$G(t) = \left[K_{eq}\, k_{uni}{}^1\, f_{ne} \int_0^t ds\; e^{-k_{uni}(t-s)}\, A(s)B(s) \right]$$

$$+ K_{eq} \left[\frac{\sum_i \eta(E_i)}{Q} - \frac{k_{uni}{}^1}{k_{uni}} f_{ne} \right] A(t)B(t)$$

$$= G^s(t) + G^*(t) \qquad (2.19)$$

where $G^s(t)$ and $G^*(t)$ are the total populations of stabilised molecule and collision complex respectively, and the non-equilibrium factor f_{ne} is defined as:

$$f_{ne} = \frac{\left[\sum_i x_1(E_i) \right]^2}{Q \sum_i \left[x_1(E_i)^2 / b(E_i) \right]} \qquad (2.20)$$

The total rate of formation of the molecule is therefore given by:

$$dG(t)/dt = K_{eq}\, k_{uni}{}^1\, f_{ne}\, A(t)B(t) - k_{uni}\, G^s(t) + dG^*(t)/dt \qquad (2.21)$$

Through Eq.(2.21) the relationship between the rate coefficient k_s for stabilisation and k_{uni} can be established. Firstly, one notes that the collision complex population $G^*(t)$ is small

and varies only slowly compared with the total flux of reacting molecules. The final term in Eq.(2.21) may therefore be neglected. The second term in Eq.(2.21) corresponds to the reverse reaction. Since the reaction is assumed to be far from equilibrium, this term will also be negligible. Thus Eq.(2.21) may be accurately approximated as:

$$dG(t) = K_{eq}\ k_{uni}^{1}\ f_{ne}\ A(t)B(t) \tag{2.22}$$

and hence

$$k_s = K_{eq}\ k_{uni}^{1}\ f_{ne} \tag{2.23}$$

where k_s is the stabilisation rate coefficient. This is the desired relationship between the forward and backward *non-equilibrium* rate coefficients.

Note that, once that k_{uni}^{1} has been calculated by solving the unimolecular master equation, f_{ne} is easily calculated from the non-equilibrium population eigenvector $\mathbf{x}_1$ via Eq.(2.20). The solution of the unimolecular master equation therefore also provides the solution to the reverse process in an association or chemical activation reaction.

In the case of an association reaction, the stable molecule is the only product observed, hence k_{ass} (or k_{rec}) = k_s.

Further information is required in order to characterise completely the chemical activation reaction since, in addition to stabilisation or dissociation back to reactant moieties, dissociation to produce other products is an alternative fate of the collision complex. Indeed, at low pressures where stabilising collisions are infrequent, the dissociation processes are dominant (this limiting case will be discussed in Section II).

The rate of dissociation for an energy E will be given by the product of the microscopic rate coefficient $k^i(E)$ (where i denotes the i^{th} dissociative channel) and the

collision complex population $g^*(E)$. The total rate of dissociation through channel i, k_d^i, will be the integral of this quantity over all energies E:

$$k_d^i A(t)B(t) = \frac{K_{eq}\, A(t)B(t)}{Q} \left\{ \sum_j k^i(E_j)\eta(E_j) - \left[\frac{k_{uni}^{\,i} \sum_j x_1(E_j)}{k_{uni} \sum_j [\, x_1(E_j)^2 / b(E_j)\,]} \right] \sum_j k^1(E_j)x_1(E_j) \right\}$$

$$= k_{ss}^i A(t)B(t) - [\, k_s k_{uni}^i / k_{uni}\,] A(t)B(t) \qquad (2.24)$$

where k_{ss}^i is the steady state rate coefficient for dissociation into the product channels. Some further explanation of this quantity may be required: it is not to be confused with k_d^i. k_{ss}^i is determined from $\eta(E)$ which, from Eq.(2.15), is the solution of the steady state master equation:

$$-k^1(E)b(E) = \omega \int [\, P(E,E')\eta(E') - P(E',E)\eta(E)\,] dE' - k(E)\eta(E) \qquad (2.25)$$

(recall that the term on the left-hand side is proportional to the reactive influx). Eq.(2.25) is the continuous version of the matrix equation, (2.15). It determines the distribution which occurs if the molecular state populations are completely filled up and the nett rate of formation of molecule is zero (i.e., all of the capture flux goes into dissociation). k_{ss}^i is then determined as:

$$k_{ss}^i = (K_{eq}/Q) \int k^i(E)\eta(E)dE \qquad (2.26)$$

With this understanding, the non-equilibrium dissociative rate coefficient k_d^i is given, from Eq.(2.24), by:

$$k_d^i = k_{ss}^i - (k_{uni}^i / k_{uni})k_s \qquad (2.27)$$

k_d^i approaches zero at high pressures, where stabilisation dominates because of the high frequency of collisions. At low pressures k_d^i rises to a constant value which may be calculated independently of ω (see, e.g., Forst 1973), since the collisions produce a negligible perturbation on the steady state population as determined by the microscopic rate coefficients (Section II).

The relationships between non–equilibrium rate coefficients for association, chemical activation and the reverse unimolecular dissociation reactions are now established for any temperature or pressure by Eq.(2.23). The rate coefficients for the additional product channels in a chemical activation reaction are defined by Eq.(2.27).

As has been mentioned earlier, the procedure of approximately relating the reverse rate coefficients by the equilibrium constant is by no means new (see, e.g., Keck and Carrier 1965). The exact relationship presented here indicates that an additional non–equilibrium factor f_{ne}, defined by Eq.(2.20) is involved. A question concerning the conditions under which this factor might deviate from unity then arises. As can be seen from Eq.(2.20), f_{ne} depends essentially on the extent to which the non–equilibrium population $x_1(E)$ is depressed from the equilibrium population b(E): in particular $\sum_i x_1(E_i)$ as compared with the partition function Q. In general $f_{ne} \approx 1$, since $\sum_i x_1(E_i) \approx Q$. This will be the case for strongly bound molecules at moderate to low temperatures. However, if $\sum_i x_1(E_i)$ is significantly less than Q, then f_{ne} will be significantly less than unity. This will be the case for weakly bound molecules at higher temperatures and should be borne in mind when dealing with high temperature applications such as combustion modelling.

II. Chemical Activation Reactions in the Low Density Limit.

Calculation of the dissociation rate coefficients for chemical activation reactions requires in general the solution of the system of coupled steady state equations represented by Eq. (2.25). However, under low pressure conditions the solution of Eq. (2.25) for energies above the dissociation threshold becomes considerably simpler. This limiting case is

now discussed, since it has application in several areas.

A number of ion–molecule reactions for which association is the major pathway at *ca.* 1 Torr pressure show quite different behaviour when studied at much lower pressures, *ca.* 10^{-5} Torr, using an Ion Cyclotron Resonance (ICR) spectrometer. At the lower pressures association is often found to be a minor or even negligible product, and the products of the reaction are produced by dissociation of the excited collision complex (see, e.g., Bass *et al.* 1983). This behaviour is characteristic of chemical activation reactions, since at low pressures stabilising collisions are infrequent and so dissociation is the major fate of the collision complex. The stabilisation rate coefficient becomes termolecular; it is still related to the reverse unimolecular rate coefficient through Eq.(2.23), but is so small in magnitude that stabilisation is a negligible perturbation on the dynamics of the reaction.

This "low–density" regime encompasses a wider range of pressures as temperature increases. A characteristic of the temperature dependence of unimolecular processes is that as the temperature is raised at a fixed pressure, the rate coefficient moves further down in the fall–off regime. Therefore at higher temperatures the low–density regime for a chemical activation reaction extends to increasingly higher pressures.

The form of the dissociation rate coefficient becomes particularly simple in the low–density limit, since the small magnitude of collisional terms compared with reactive terms in the master equation enables them to be neglected in determining the collision complex population distribution. Consider Eq.(2.5) for energies E above the lowest dissociation threshold of the molecule: when $\omega \ll k(E)$ and $\omega \ll K_{eq}k^1(E)b(E)A(t)B(t)/Q$ (ie., the collision frequency is much less than the the reactive loss and reactive influx terms respectively), the collisional terms may be neglected. Eq.(2.5) then becomes:

$$dg^*(E,t)/dt = -k(E)g(E,t) + K_{eq}A(t)B(t)k^1(E)b(E)/Q \quad , E > E_o^{min} \qquad (2.28)$$

where E_o^{min} represents the lowest dissociation threshold. Recall that $k(E) = \Sigma_i k^i(E)$. Eq.(2.28) has solution:

$$g^*(E,t) = \frac{K_{eq}\, k^1(E)b(E)}{Q} \int_0^t e^{-k(E)(t-s)} A(s)B(s)\, ds \qquad (2.29)$$

However, since A(t) and B(t) vary only very slowly compared with $1/k(E)$, the integral simplifies analogously to Eq.(2.12) to become:

$$g^*(E,t) = K_{eq}A(t)B(t)k^1(E)b(E) \,/\, Qk(E) \qquad (2.30)$$

which is the steady state result (see, e.g., Forst 1973). Note that this is only non-zero for energies above the threshold E_o^1 for the reactant channel. Having determined the population of the collision complex in the low density limit, the dissociative rate coefficient may be written as (see, e.g., Olmstead and Brauman 1977):

$$k_d^i = (K_{eq}A(t)B(t)/Q) \int dE\; k^i(E)k^1(E)b(E)/k(E) \qquad (2.31)$$

Another quantity which is of interest is the average lifetime, τ, of the collision complex. The lifetime at a given energy E is $1/k(E)$. Therefore, the overall lifetime of AB^* with respect to unimolecular dissociation will be an average of this quantity over the steady state distribution of the collision complex, Eq. (2.30) (e.g., Forst 1973):

$$\tau = \int\{[1/k(E)]\,[k^1(E)b(E)/k(E)]\}dE \,/\, \int dE\; k^1(E)b(E)/k(E) \qquad (2.32)$$

The basic formulae of this section are not new. It has been found, however, that a number of refinements are required in order to predict accurately k_d^i and τ in the low-density limit for ion-molecule reactions, and these will be dealt with in Chapters 3 and 4.

III. Application: the CH_3^+ / NH_3 Chemical Activation Reaction.

To illustrate the use of the equations derived in the current chapter, kinetic data for the chemical activation reaction between CH_3^+ and NH_3 is modelled.

The reaction between CH_3^+ and NH_3, as with most ion–molecule reactions, is very sensitive to the effects of angular momentum conservation, weak collisions, and the dipole on the neutral molecule. The power of the relationships derived in this section is that, once these effects have been incorporated into the solution of the unimolecular master equation, the reverse chemical activation problem can also be solved exactly using the same computer programme. The precise means of including these effects into solution of the unimolecular dissociation master equation will be dealt with in the next two chapters. However, the results of the modelling study for the CH_3^+/NH_3 reaction are presented here to give a taste for the results which can be obtained.

The reaction between CH_3^+ and NH_3 has been studied over a range of pressures. At pressures of *ca.* 0.4 Torr using a Selected Ion Flow Tube (SIFT) apparatus, Smith and Adams (1977,1978) observed two bimolecular product channels and the association product:

$$CH_3^+ + NH_3 \rightleftarrows [CH_3NH_3^+]^* \qquad (2.33a)$$

$$[CH_3NH_3^+]^* \longrightarrow CH_2NH_2^+ + H_2 \qquad (2.33b)$$

$$[CH_3NH_3^+]^* \longrightarrow NH_4^+ + CH_2 \qquad (2.33c)$$

$$[CH_3NH_3^+]^* + M \rightleftarrows \cdots \rightleftarrows CH_3NH_3^+ + M \qquad (2.33d)$$

The association product accounted for about 20% of the observed reaction rate, indicating that the reaction is somewhat into the fall–off regime at SIFT pressures. However, no

pressure dependence of the association rate was observed in the range 0.2–0.7 Torr. The major product channel was that producing $CH_2NH_2^+$ [Eq.(2.33b)], Eq.(2.33c) contributing only *ca.* 5% of the products. A later study by Saxer *et al.* (1987) covered a wider range of pressures (0.2–1.3 Torr) and revealed pressure dependence typical of a reaction in the fall–off regime. The experimental data of Saxer *et al.* are shown in Figure 2.1 with the results of calculations to be discussed below. The reaction has also been studied at low pressures by the Ion Cyclotron Resonance (ICR) technique (Huntress *et al.* 1973). At low pressures ($\sim 10^{-5}$ Torr) only the bimolecular product channels are observed. The bath gas in these studies was helium.

The reaction has also been the subject of theoretical study. Nobes and Radom (1983) determined the structure, energy and vibrational frequencies of the association product and the transition state for the major product channel [Eq.(2.33b)]. Herbst (1985), using the results of Nobes and Radom, carried out a theoretical analysis of the kinetic data. His study reproduced the kinetic data for the association rate and illustrated the effect of angular momentum conservation, the dipole moment of ammonia, and the barrier height of the major exit channel on the predicted results.

The model used by Herbst involved calculating the steady state population of the excited collision complex with a given total energy E and angular momentum J, and thereafter evaluating the rates of dissociation and stabilisation from this population distribution. Microscopic rate coefficients for the reactive influx and its reverse dissociation were calculated using the Phase Space theory of Chesnavich and Bowers (1976,1977). In this approach, the two moieties in the transition state are treated as free rotors acting under the influence of a central potential. The microscopic rate coefficients for the major dissociation channel, Eq. (2.33b), were calculated using RRKM theory. Collisional stabilisation was modelled using a particular form of "relaxation rate coefficient" k_{rel}, which is a function of the excess internal energy of the complex above the lowest dissociation threshold.

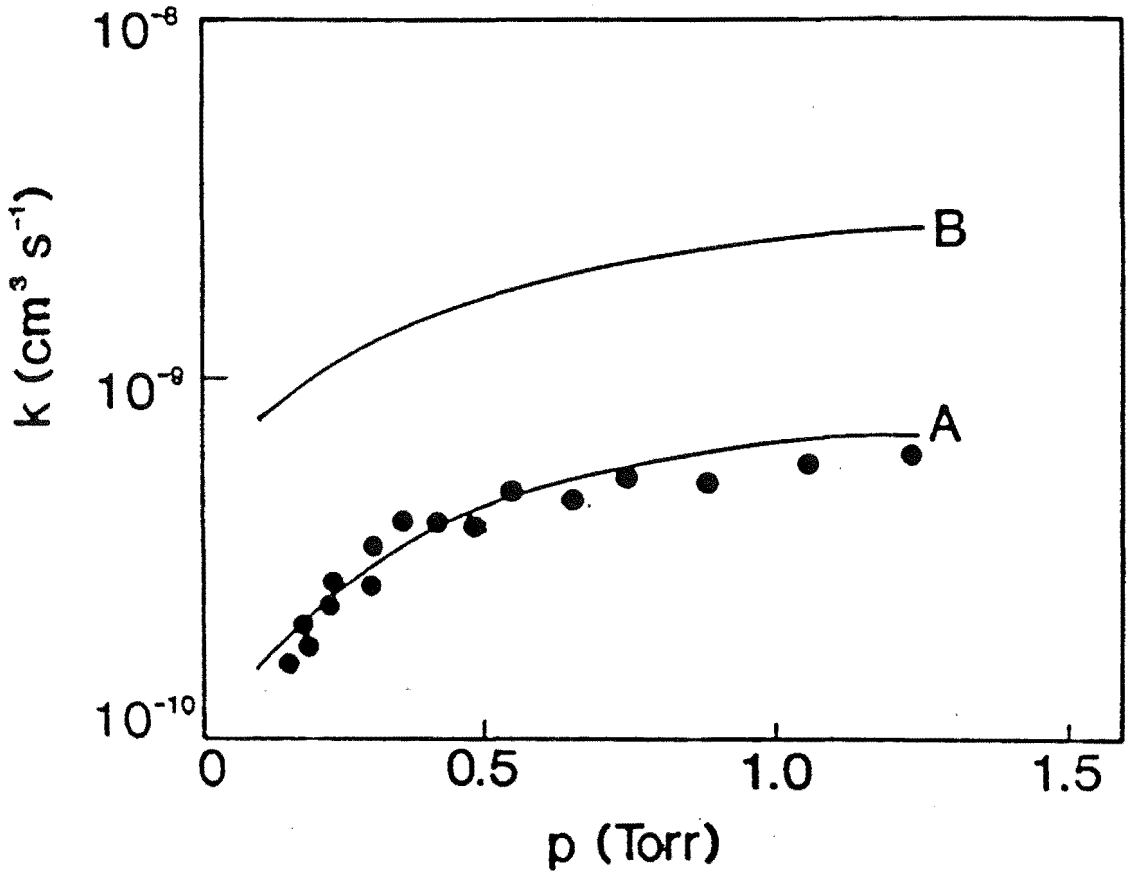

Figure 2.1. Calculated pressure dependence of stabilisation rate coefficient k_s (as ratio to high-pressure limiting value) for CH_3^+/NH_3 chemical activation reaction at 298K. Parameters for the calculation are as in the text and Appendix A. For conversion from unimolecular rate coefficients, $K_{eq} = 2.93 \times 10^{51}$ cm^3. Filled circles are representative experimental data of Saxer *et al.* (1987). Curve A is calculated by solution of the master equation with angular momentum conservation. Curve B is the strong collision stabilisation rate, again with J-conservation included.

What does the approach outlined above have to add to this? The Herbst model has two important deficiencies: 1) The effect of the dipole moment of ammonia is identified as being primarily to increase the range of angular momenta which can lead to reaction because of the long range ion–dipole potential. However, the fact that the long range ion–dipole potential is non–central is neglected in applying the phase space approach. As has been discussed previously by several authors (Chesnavich *et al.* 1980; Troe 1985,1988) the ensuing hindrance of the dipole rotation causes the density of states at the transition state to be substantially reduced, thus reducing the predicted reactive influx. In order to compensate for this deficiency, Herbst was forced to use an "effective dipole moment" of 0.3 Debye, which is much smaller than the actual dipole moment of 1.47 Debye. A correct accounting for this dipole effect is necessary: the method used to do this will be elucidated in Chapter 4. 2) The second deficiency, which relates much more to the improvements developed in the present chapter, is in the treatment of collisional effects. The correct way to incorporate weak collision effects is by the solution of the master equation [Eq.(2.2), or its two–dimensional equivalent in E and J]. The model used by Herbst assumed that collisional stabilisation below the threshold is irreversible, thus neglecting activating collisions. In addition, he used an energy–dependent stabilisation rate coefficient (which decreases as the excess energy increases) to mimic weak collision effects. This may be a sensible thing to do, but its accuracy can only be tested by accurate solutions of the full master equation. The relationship derived in the present chapter enables such a master equation solution to be obtained from the solution of the reverse unimolecular dissociation problem. This can now be done (as will be illustrated in the present work) with only a moderate investment of computer time and storage.

Figure 2.2 gives a schematic representation of the relative stabilities of the species involved in the reaction and the barrier height for the major exit channel (to be discussed further below). The parameters for the calculation are included in Appendix A. In Figure 2.1 is illustrated the result of the calculations: the curve which fits the experimental data of Saxer *et al.* (1987) is that derived by solution of the two–dimensional unimolecular master equation and subsequent conversion to the reverse stabilisation rate coefficients via

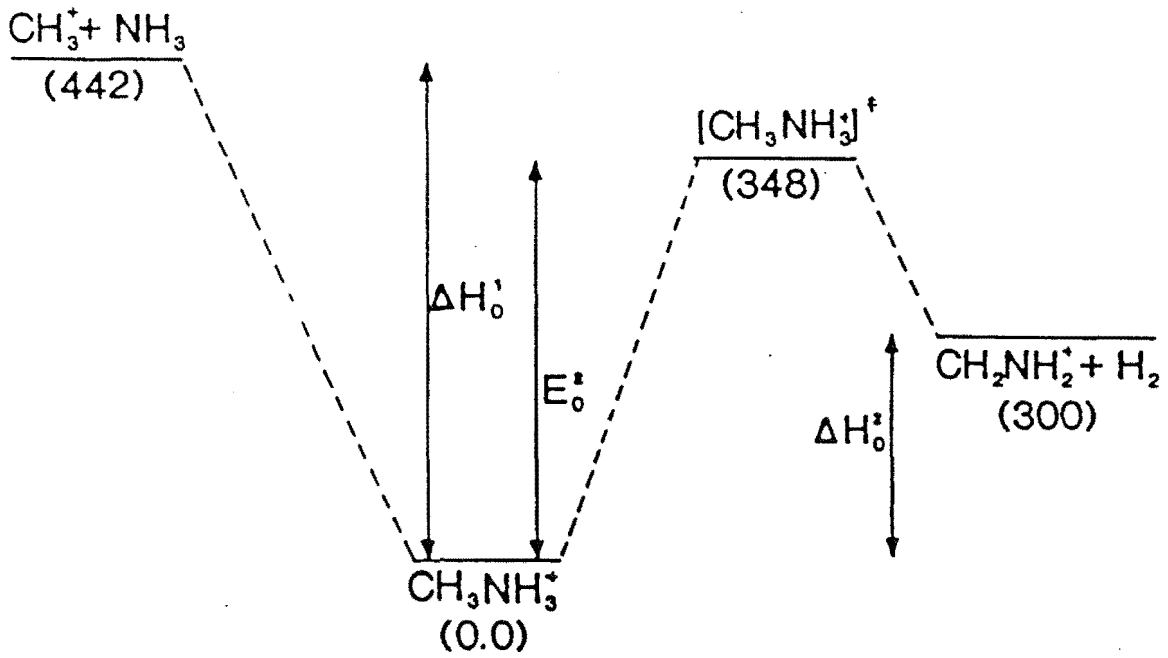

Figure 2.2. Schematic representation of potential along the reaction coordinate for CH_3^+/NH_3 reaction, relative to $CH_3NH_3^+$ having an energy of 0.0 kJ mol^{-1}.

Eq.(2.23) (the f_{ne} contained therein was found to be unity to within 1% for the present reaction). The upper curve is the result of a strong collision calculation (the same RRKM microscopic rate coefficients are used, but one simply substitutes ω, the total collision frequency, for the stabilisation rate coefficient).

The structural data used in the calculation were either those of the separated reactants (for the loose, "orbiting" transition states in the reactant channel) or those calculated by Nobes and Radom (1983). The minor exit channel, Eq.(2.33c) was neglected under the assumption that it presents a negligible perturbation to the population distributions occuring in the reaction. Microscopic rate coefficients for the major exit channel were calculated in the traditional RRKM fashion. Microscopic rate coefficients for the reaction channel, where the transition states occur at long range, were determined variationally using canonical variational transition state theory (CVTST). Recall that this involves using a single separation $r^{\dagger}$ for the transition states for all E and J: $r^{\dagger}$ is determined as that which gives the minimum high pressure thermal association rate. The high pressure association rate so calculated is 4.65×10^{-9} cm^3s^{-1}. To find the pressure dependence of the association rate, one solves the master equation. This requires the specification of the average internal and average rotational energy transfers, $<\Delta E_{down}>$ and $<\Delta R_{down}>$ respectively, on collision with the bath gas. A typical range of values for these quantities at room temperature is about $100-300cm^{-1}$ ($0.5-1.5k_BT$). The results indicated in Figure 2.1 were obtained using values of $156cm^{-1}$ ($0.75k_BT$). The barrier height for the exit channel was adjusted downward from the value predicted by Nobes and Radom, 367kJ mol^{-1}, to 348kJ mol^{-1}. This was neccesary in order to reduce the predicted association rate to fit the data with values of the energy transfer within the range mentioned above. Such an adjustment is not unreasonable as quantum chemical predictions of barrier heights are not as reliable as predictions of well depths, and tend to overestimate the former. Because of this uncertainty, it is not possible to gain a reliable estimate for the energy transfer parameters describing the collisions between the collision complex $[CH_3NH_3^+]^*$ and the bath gas helium.

It will be apparent that the current method does not have a monopoly in fitting the experimental results of Figure 2.1! Indeed, it would be possible to fit the data with a strong collision calculation if one used a collision efficiency β to modify the stabilisation rate coefficient (set to the collision frequency ω in the strong collision model). However, it should be noted that the pressure range of the data constitutes only a small part of the total fall–off regime: in order to extrapolate data over a wide range of pressures it is necessary to use an accurate (and, ideally, computationally convenient) theoretical approach. For example: a β value (or "collision efficiency") of 0.13 is required to fit the data of Saxer *et al.* in Figure 2.1; however, extrapolating the strong collision calculation to low pressures with this value for β causes the stabilisation rate at low pressures to be overestimated by a factor of 2. Unfortunately, Herbst did not provide the results of his calculation over the entire fall–off regime. A comparison of the results of the two theories over the full fall–off range, and over a range of temperatures, would clearly be very useful.

Aside from fitting and reliably extrapolating experimental data, the calculation of the association rate by solution of the master equation is advantageous because reasonable bounds for the average energy transfer parameters are known. In cases where another factor, such as the barrier height to further dissociation, is uncertain, the requirement that these energy transfer parameters lie within reasonable bounds enables an approximate estimate to be made for these quantities. Calculations at the level of Canonical Variational Transition State Theory (CVTST) imply that the theoretically predicted barrier height (Nobes and Radom 1983) is of the order of 20kJ mol^{-1} too large. To carry such conclusions any further is unjustified at this stage, however, since it is possible to tidy our own house further by calculating microscopic rate coefficients using microcanonical variational transition state theory (μVTST): this will provide improved values for these quantities, and may therefore affect any ensuing conclusions regarding barrier heights or energy transfer. The calculation of microscopic rate coefficients for ion/molecule reactions using μVTST will be discussed in Chapter 4.

CHAPTER 3

ANGULAR MOMENTUM CONSERVATION IN UNIMOLECULAR AND RECOMBINATION REACTIONS

The theory for microscopic rate coefficients in unimolecular reactions involves consideration of the dynamics of an isolated molecule with sufficient excitation to dissociate. The dynamics of the dissociation process will be subject to the conservation laws for an isolated system, *viz.* conservation of energy and angular momentum (in cases of very high symmetry, other "good quantum" numbers may also exist). Conservation of energy requires that the total energy, less the external translational energy, be conserved throughout the dissociation process (the overall translational energy of the system is separately conserved). Conservation of angular momentum requires that the total angular momentum remain constant as the molecule dissociates into separate fragments. Inclusion of this conservation requirement has a large effect on the predicted rate coefficient for reactions without a pronounced barrier to recombination such as ion–molecule reactions. The reason for this will be discussed below.

The RRKM theory summarised in chapter 1 incorporated energy conservation only. A simple and accurate method of incorporating angular momentum conservation into the RRKM expression for the microscopic rate coefficient was developed by Marcus (1965,1970). This allows the gross effects of angular momentum conservation to be incorporated into the *microscopic* rate coefficient, which is then written as a function of E and J, k(E,J) (given below in section I). Calculation of the thermal rate coefficient, k_{uni}, requires also the non–equilibrium population distribution g(E,J), which in principle requires the solution of a two–dimensional master equation. A general method of solving the two–dimensional master equation has not hitherto been available. The present chapter addresses this problem. A method is developed which enables the two–dimensional master equation in E and J to be reduced to a one dimensional problem in terms of the active "internal" energy, ϵ, alone, which may then be solved rapidly using existing techniques.

The outline of the chapter is as follows. In Section I, the physical basis of the angular momentum effect is described, and the incorporation of this effect into the RRKM formula for the microscopic rate coefficient discussed. Section II deals with the solution of the two-dimensional master equation. Three different categories for solution of the master equation are identified: (1) The relaxation of both the energy and the angular momentum are modelled with strong collisions; (2) The relaxation of the vibrational energy is modelled with weak collisions and the rotational relaxation is modelled with strong collisions; and (3) Both the energy and the angular momentum relaxation are modelled with weak collisions. The solution for category (1) is well known (e.g., Marcus 1965; Waage and Rabinovitch 1970), but conditions for its validity rarely apply. Solutions for the latter two categories that are applicable throughout the fall-off regime are developed. The criteria for choosing the method of solution for any given reaction system are discussed, and application to typical reactions (the methyl radical recombination, and the association of CH_3^+ with HCN) presented. In Section III, the solutions developed are compared with previous approaches to the problem of incorporating J-conservation into the low-pressure-limiting solution of the master equation (Troe 1977a,1987a; Penner and Forst 1975,1976). In Section IV the extension of the solutions developed to multichannel reactions is presented. This enables both multichannel dissociations and chemical activation reactions (see Chapter 2, Chapter 4) to be modelled. Illustrative calculations for the two-channel dissociation of 1-iodopropane are presented. Brief concluding remarks are made in Section V.

I.The Effect of Angular Momentum Conservation: Microscopic Rates

The effect of angular momentum conservation is most easily seen by comparison with a two-body collision. Conservation of the angular momentum of the two particle system causes a term $L^2/2\mu r^2$, where μ is the reduced mass, L the angular momentum and r the separation, to appear in the radial part of the Hamiltonian when one changes from cartesian to polar coordinates. This is the energy tied up in rotation at any given separation of the two bodies, and because this rotational energy is gained at the expense

of motion in the r coordinate, it acts as a component in the effective radial potential. This term is often added to the potential V(r) to construct an "effective potential" $V_{eff}(r)$. Since the (positive) repulsive term $L^2/2\mu r^2$ generally takes effect at longer range than the (negative) attractive terms in the potential, the effective potential rises at long range, and passes through a maximum as the attractive part of the potential starts to dominate. This is illustrated schematically in Figure 3.1.

In a polyatomic system, the situation is considerably more complex, since the rotations of the separate moieties also contribute to the total angular momentum. These individual rotations will be affected in a complex manner when the moieties approach close enough to interact with each other. However, the gross effect of angular momentum conservation can be incorporated into the polyatomic system by treating it as a "pseudo-diatomic" and treating the orbital rotation as adiabatic (see, e.g., Forst 1973). Thus the orbital angular momentum is approximated as a conserved quantity (L≈J) and

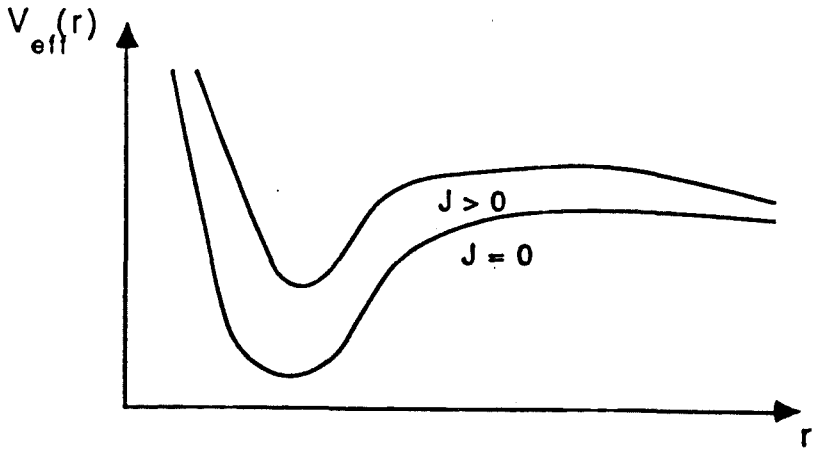

Figure 3.1. Schematic representation of the effective potential for a reaction with no pronounced barrier to recombination.

the individual rotational motions of the moieties in the dissociating molecule are treated as active internal modes. In this context, the term "active" refers to a degree of freedom which is assumed to be able to exchange energy with the reaction coordinate (and, incidentally, all other active degrees of freedom) in a statistical fashion.

Now consider the picture from the reverse direction: a single molecule dissociating so that the two moieties fly apart rather than towards each other. The molecule initially has a certain amount of external ("orbital") rotational energy, R, which under the adiabatic assumption stated above will not be available for internal motion along the reaction coordinate. However, as the moieties move apart the external moment of inertia, I(r), becomes larger. The external rotational energy, $L^2/2I(r)$, therefore decreases as it is converted into motion along the reaction coordinate.

If the active internal energy of the molecule is denoted ϵ, we have under the above approximation ($L \approx J$):

$$\epsilon + R = E \tag{3.1}$$

where E is the total energy. Since the external rotational energy R is considered unavailable for randomisation within the molecule, the external rotational degrees of freedom are not treated as active modes and so are not included in the density of states $\rho(\epsilon)$ that appears in the RRKM expression. Note that the one-dimensional external rotational degree of freedom (which does not correlate with an orbital rotational degree of freedom of the transition state, but rather to one of the internal rotational degrees of freedom of the separating moieties) is treated as an active degree of freedom (see, e.g., Forst 1973; Troe 1977a,1977b).

With the above considerations, the energy available for motion along the reaction coordinate at some separation of the moieties $r^\dagger$ is:

$$\epsilon + [R - L^2/2I(r^\dagger)] - V(r^\dagger) = E - R^\dagger - V(r^\dagger) \qquad (3.2)$$

The required extension to the RRKM expression for the microscopic rate coefficient is therefore (Marcus 1965):

$$k(E,J) = W^\dagger[E-R^\dagger-V(r^\dagger)]/h\rho(E-R) \qquad (3.3)$$

This may be equivalently written in terms of the internal energy ϵ:

$$k(\epsilon,J) = W^\dagger[E-R^\dagger-V(r^\dagger)]/h\rho(\epsilon) \qquad (3.4)$$

II. The Two-Dimensional Master Equation

Because of the distinction between the active internal energy ϵ and the external rotational energy R of the molecule, it is convenient to choose ϵ and J as independent variables in the master equation. The molecular population relaxes on a very short timescale to a pseudo-steady state (see Chapter 1 and references therein), where the population of each state decays in a single exponential fashion governed by k_{uni}, the largest eigenvalue of the collisional / reactive operator J (chapter 1 and references therein). Hence the master equation may be written:

$$-k_{uni}g(\epsilon,J) = - k(\epsilon,J)g(\epsilon,J) + \omega\int\int[\hat{P}(\epsilon,J,\epsilon',J')g(\epsilon',J') - \hat{P}(\epsilon',J',\epsilon,J)g(\epsilon,J)]\, d\epsilon' dJ' \qquad (3.5)$$

where $g(\epsilon,J)$ is the time-independent non-equilibrium population distribution (equivalent to $\hat{g}(E)$ in chapter 1), $\hat{P}(\epsilon',J',\epsilon,J)$ is the probability of transfer from a state with internal energy ϵ and angular momentum J to a state with energy ϵ' and angular momentum J'.

In examining the solution of the master equation, one notes firstly that at high pressures where $\omega \gg k(\epsilon,J)$ the reaction term is a negligible perturbation on the collisional terms. Under these conditions perturbation theory shows (Gilbert and Ross 1971)

that the resulting population distribution is the equilibrium (Boltzmann) distribution, and the high-pressure-limiting rate coefficient, k_{uni}^{∞}, is given by:

$$k_{uni}^{\infty} = \int\int d\epsilon dJ \; k(\epsilon,J)f(\epsilon,J) \tag{3.6}$$

where $f(\epsilon,J)$ is the normalised Boltzmann distribution:

$$f(\epsilon,J) = \rho(\epsilon)\exp[-(\epsilon+R)/k_BT]/k_BTQ \tag{3.7}$$

$Q=\int\rho(\epsilon)\exp(-\epsilon/k_BT)d\epsilon$ is the partition function for the active degrees of freedom of the molecule.

The method of solution of Eq.(3.5) in the fall-off regime depends on the nature of collisional activation and relaxation in the reaction under study, as determined by $\hat{P}(\epsilon,J,\epsilon',J')$. Three categories may be identified: (1) Fast collisional relaxation of both the internal energy and the angular momentum; (2) Fast collisional relaxation of the angular momentum and slow collisional relaxation of the internal energy; and (3) Slow collisional relaxation of both the internal energy and the angular momentum. The first category is very easily solved via the strong collision approximation (see, e.g., Robinson and Holbrook 1972). Unfortunately, this assumption is almost always a poor one, since for most systems at least the internal energy relaxation is slow and requires a weak collisional treatment (see, e.g., Tardy and Rabinovitch 1977). A number of reactions fall into the second category where the angular momentum transfer probability may be treated by a strong collision model (the reasons for this will be discussed later). These include most neutral dissociation/recombination reactions and also ion-molecule reactions with a polyatomic bath gas. Reactions in a monatomic bath gas where reacting molecules have a high average angular momentum (by virtue of $k(\epsilon,J)$ increasing rapidly with J) appear generally to exhibit slow relaxation of both the internal energy and the angular momentum. These reactions require a solution of Eq.(3.5) which applies a weak collisional approach to both the internal energy and the angular momentum transfer. Ion-molecule

reactions with monatomic bath gases generally fall into this category.

The three categories of solution are detailed below, with illustrative applications to typical reactions.

II.1a *Fast Relaxation for both ϵ and J: the Fall-Off Regime.*

A system in which molecules are relaxed to the equilibrium probability distribution in a single (or a very few) collisions may be modelled by use of the strong collision assumption for both ϵ and J. This involves setting the probability function for energy and angular momentum transfer equal to an equilibrium (Boltzmann) distribution of final states, with the assumption that a single collision is sufficient to relax a molecule into an equilibrium probability distribution (see, e.g., Marcus 1965; Waage and Rabinovitch 1970):

$$\hat{P}(\epsilon,J,\epsilon',J') = f(\epsilon,J) \tag{3.8}$$

Substituting Eq.(3.8) into Eq.(3.5) and carrying out the integrals over J' and ϵ' gives:

$$-k_{uni}g(\epsilon,J) = \omega f(\epsilon,J)G - [\omega + k(\epsilon,J)]g(\epsilon,J) \tag{3.9}$$

where $G = \int\int g(\epsilon',J')d\epsilon'dJ'$. Rearranging to obtain $g(\epsilon,J)$ and noting that $k_{uni} \ll \omega + k(\epsilon,J)$, the strong collision result for $g(\epsilon,J)$ is obtained (see, e.g., Forst 1973):

$$g(\epsilon,J) = \omega\ G\ f(\epsilon,J)/[\omega + k(\epsilon,J)] \tag{3.10}$$

The normalisation constant G is often left out here, since it cancels out on evaluation of k_{uni}:

$$k_{uni} = \int\int k(\epsilon,J)g(\epsilon,J)d\epsilon dJ \ /\ \int\int g(\epsilon,J)d\epsilon dJ \tag{3.11}$$

II.1b *Fast Relaxation for ϵ and J: the Low-Pressure Limit.*

The result for $g(\epsilon,J)$ and k_{uni} simplifies at low pressures when $\omega \ll k(\epsilon,J)$ (see, e.g., Forst 1973):

$$\begin{aligned} g(\epsilon,J) &= Gf(\epsilon,J) \qquad , \epsilon \ll \epsilon_o(J) \\ &= \omega Gf(\epsilon,J)/k(\epsilon,J) \qquad , \epsilon > \epsilon_o(J) \end{aligned} \tag{3.12}$$

where $\epsilon_o(J)$ is the internal energy threshold for the given angular momentum J. Thence:

$$k_{uni} = (\omega/Q)\int\int f(\epsilon,J)d\epsilon dJ \tag{3.13}$$

where the approximation that $\int\int g(\epsilon,J)d\epsilon dJ \approx Q$ has been made.

As has been stated earlier, the strong collision approximation generally overestimates the amount of energy transfer in collisions, and so overestimates the rate coefficient. However, it has the benefit of including angular momentum conservation in a relatively simple fashion. Dimensionless angular momentum correction factors such as the Waage-Rabinovitch factor (1970) derive from the J-dependent strong collision treatment. However, such corrections are applicable only within the strong collision formalism: an accurate method of including angular momentum effects into the master equation solution is required.

II.2a *Slow Relaxation of ϵ, Fast Relaxation of J: the Fall-Off Regime.*

In order to simplify the solution of the two-dimensional master equation, and to study the average behaviour of internal and rotational energy transfer in collisions, it is useful to make the approximate separation (see, e.g., Troe 1977a,1987a; Penner and Forst 1975,1976):

$$\hat{P}(\epsilon,J,\epsilon',J') \approx P(\epsilon,\epsilon')P(J,J') \tag{3.14}$$

It is now generally recognised (see, e.g., Tardy and Rabinovitch 1977) that collisional relaxation of the internal (vibrational) energy is slow and requires a weak collisional description for the function describing the probability of energy transfer, $P(\epsilon,\epsilon')$. The probability of energy transfer in a weak collision form of $P(\epsilon,\epsilon')$ decreases as the difference between the final and initial energies, $(\epsilon-\epsilon')$, becomes sufficiently large. Figure 3.2 shows schematically the difference between weak and strong collision forms for $P(\epsilon,\epsilon')$. The strong collision form, it will be noted, is independent of the starting energy.

The form of P(J,J') is less well understood. One of the complicating factors is that the level of excitation of J is such that the requirement that the angular momentum be always nonnegative has an important affect on the functional form of P(J,J') when J' is not too large. In order to represent the physics of the reacting system in the optimum way, it is necessary to choose a functional form for P(J,J') [or, in terms of the rotational

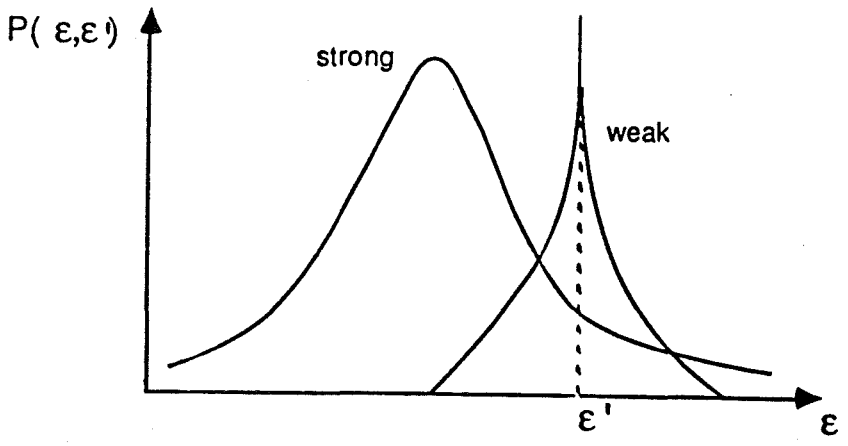

Figure 3.2. Schematic representation of the probability distribution function for collisional transition from energy ϵ' to energy ϵ, $P(\epsilon,\epsilon')$: the weak collisional form depends on the energy difference $(\epsilon-\epsilon')$, whereas the strong collisional form depends *only* on the final energy ϵ, irrespective of the starting energy ϵ'.

energy, P(R,R')] which is appropriate to the average excitation of *reacting* molecules. One might use a functional form which is independent of the initial value of J, such as the strong collision form, or a weak collisional form which depends on the difference between the initial and final angular momenta.

There are certain factors which should be borne in mind when choosing the functional form appropriate to a given reaction. The probability function for energy and angular momentum transfer must always satisfy detailed balance [chapter 1, Eq.(1.9), or its equivalent for P(J,J')]. The form of the probability function should correctly describe the behaviour of energy and angular momentum transfer *at the level of excitation where most reaction occurs*. For the internal energy ϵ this excitation is generally very high (i.e., many times k_BT) and a weak collision model seems to encompass a proper physical description of the energy transfer, since the average downward internal energy transfer $<\Delta\epsilon_{down}>$ is very small in comparison to the average excitation of reacting molecules.

A weak collisional form is, however, not always appropriate for P(J,J'). The average excitation of angular momentum in reacting molecules corresponds to rotational energies (of the order of a few k_BT) much lower than the average internal excitation. This is because the large density of states of internally active modes makes thermal excitation to high internal energies much more probable than corresponding excitation of the external rotational energy. Trajectory studies indicate that the average downward internal energy transfer, $<\Delta\epsilon_{down}>$, and the average downward rotational energy transfer, $<\Delta R_{down}>$ are approximately the same size (Date *et al.* 1984; Whyte and Gilbert 1989). Therefore, whilst $<\Delta\epsilon_{down}>$ is very small compared with the excitation of internal energy involved in reactions, $<\Delta R_{down}>$ can often be a significant fraction of the corresponding rotational excitation. The choice of a strong or weak collisional form for P(J,J') will depend on the reaction in question and on the bath gas involved. If the average rotational excitation of reacting molecules is much greater than $<\Delta R_{down}>$, then a weak collision form will be required. As will be seen below, this is necessary in the case of ion–dipole reactions in a monatomic bath gas, since for such reactions $<\Delta R_{down}>$ is small and the average angular

momentum of reacting molecules is large [since $I^{\dagger} \gg I$ ($I^{\dagger}$ being the moment of inertia of the transition state and I that of the molecule) and so $k(\epsilon,J)$ increases rapidly with J]. For reactions where $\langle \Delta\epsilon_{down} \rangle$ and $\langle \Delta R_{down} \rangle$ are larger *or* the average rotational excitation is less, a strong collision form for P(J,J') will be more appropriate (Smith and Gilbert 1988, this proof developed by RGG). Most neutral reactions (having less average rotational excitation) and ion-molecule reactions with polyatomic bath gases (where $\langle \Delta R_{down} \rangle$ will be markedly larger than for a monatomic bath gas) will fall into this category.

With the foregoing considerations in mind, an exact solution to the two-dimensional master equation for the case where P(J,J') may be represented by a functional form which is independent of the initial angular momentum is developed. In the derivations which follow the strong collisional form, which is the established means of modelling fast relaxation, is used (though the solution is not limited to this form).

Assuming separability of $P(\epsilon,J,\epsilon',J')$ [Eq.(3.14)] and strong collisions for J, one has:

$$P(\epsilon,J,\epsilon',J') = P(\epsilon,\epsilon')f(J) \tag{3.15}$$

Substituting Eq.(3.15) into Eq.(3.5) and invoking normalisation of $P(\epsilon,\epsilon')$ and P(J,J'), Eq.(3.5) becomes:

$$-k_{uni}g(\epsilon,J) = \omega\, f(J) \int [P(\epsilon,\epsilon') \int g(\epsilon',J')dJ' \,]d\epsilon' - \omega g(\epsilon,J) - k(\epsilon,J)g(\epsilon,J) \tag{3.16}$$

Integrating over J produces:

$$-k_{uni}\bar{g}(\epsilon) = \omega\int [P(\epsilon,\epsilon')\bar{g}(\epsilon') - P(\epsilon',\epsilon)\bar{g}(\epsilon)]d\epsilon' - \bar{k}(\epsilon)\bar{g}(\epsilon) \tag{3.17}$$

where the J-averaged quantities $\bar{g}(\epsilon)$ and $\bar{k}(\epsilon)$ are defined by:

$$\bar{g}(\epsilon) = \int g(\epsilon,J)\, dJ \tag{3.18}$$

$$\bar{k}(\epsilon) = \int k(\epsilon,J)\, g(\epsilon,J)\, dJ \;/\; \int g(\epsilon,J)\, dJ \tag{3.19}$$

Eq.(3.17) shows that the two-dimensional master equation may be exactly reduced to a one dimensional master equation provided a J-averaged microscopic rate coefficent $\bar{k}(\epsilon)$ as defined in Eq.(3.19) is used. Note, however, that evaluating $\bar{k}(\epsilon)$ in principle requires a knowledge of $g(\epsilon,J)$. The resolution of this problem is achieved as follows. Rearranging Eq.(3.16), one obtains for $g(\epsilon,J)$:

$$g(\epsilon,J) = \omega f(J)\, \Xi(\epsilon) \;/\; [\omega + k(\epsilon,J) - k_{uni}] \tag{3.20}$$

where $\Xi(\epsilon) = \int P(\epsilon,\epsilon')\bar{g}(\epsilon')d\epsilon'$. Substituting Eq.(3.20) into Eq.(3.19) yields:

$$\bar{k}(\epsilon) = \int k(\epsilon,J)\, f(J)\, [\omega+k(\epsilon,J)-k_{uni}]^{-1}\, dJ \;/\; \int f(J)\, [\omega+k(\epsilon,J)-k_{uni}]^{-1}\, dJ \tag{3.21}$$

The threshold energy for reaction is denoted $\epsilon_o(J)$ and will in general be a function of the angular momentum, since the angular momentum affects the energy which will be available for barrier crossing through Eq.(3.3). Figure 3.3 illustrates schematically the threshold energy $\epsilon_o(R)$, expressed as a function of the rotational energy, for two different types of transition state: one with $I^\dagger<I$ and the other with $I^\dagger>I$ ($I^\dagger$ and I being the moments of inertia of the transition state and the molecule respectively). One can equivalently define the threshold behaviour in terms of the minimum angular momentum, $J_o(\epsilon)$, [or rotational energy $R_o(\epsilon)$] required for reaction. The threshold energy in the absence of angular momentum, i.e., $\epsilon_o(J=0)$, will be denoted E_o. For simple-fission dissociation and recombination reactions, $I^\dagger>I$ and so for $\epsilon>E_o$, $J_o(\epsilon)=0$ whilst for $\epsilon<E_o$, $J_o(\epsilon)>0$. Eq.(3.21) may therefore be written:

$$\bar{k}(\epsilon) = \frac{\int_{J_0}^{\infty} dJ\ [\omega+k(\epsilon,J)-k_{uni}]^{-1}\ f(J)\ k(\epsilon,J)}{\int_{0}^{J_0} dJ\ f(J)\ [\omega-k_{uni}]^{-1} + \int_{J_0}^{\infty} dJ\ f(J)[\omega+k(\epsilon,J)-k_{uni}]^{-1}} \tag{3.22}$$

where $J_o = J_o(\epsilon)$. Since $k_{uni} \ll \omega+k(\epsilon,J)$, one has to an excellent approximation:

$$\bar{k}(\epsilon) = \frac{\int_{J_0}^{\infty} dJ\ [\omega+k(\epsilon,J)]^{-1}\ f(J)\ k(\epsilon,J)}{\int_{0}^{J_0} dJ\ f(J)\omega^{-1} + \int_{J_0}^{\infty} dJ\ f(J)[\omega+k(\epsilon,J)]^{-1}} \tag{3.23}$$

Eqs.(3.17) and (3.23) enable the reduction of the two-dimensional master equation, Eq.(3.5), to a one-dimensional master equation for the case of rapid collisional relaxation

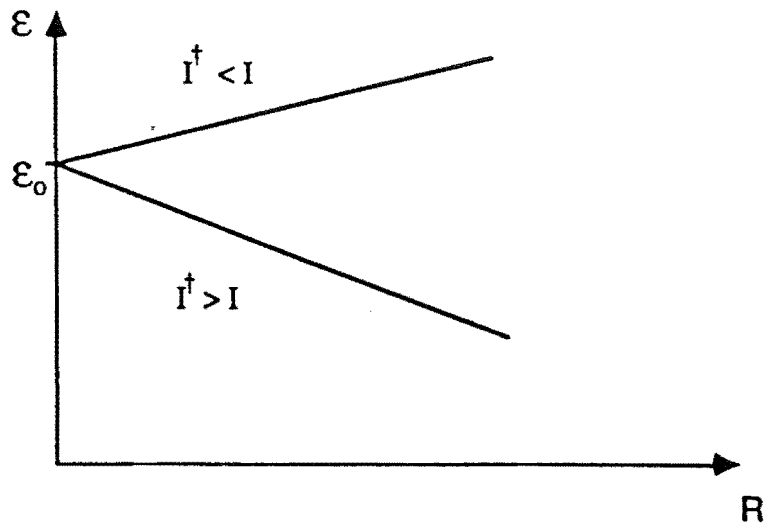

Figure 3.3. Schematic representation of the dependence of the reaction threshold energy, $\epsilon_o(R)$, on the external rotational energy R for cases where the external moment of inertia $I^\dagger$ of the transition state is greater than and less than the moment of inertia of the molecule, I.

of the angular momentum and slow relaxation of the internal energy. Eq.(3.17) can be solved by standard means (see, e.g., Tardy and Rabinovitch 1977; Gaynor *et al.* 1978a). In practice it is convenient to transform first to the independent variables ϵ and R [R=BJ(J+1)] before evaluating $\bar{k}(\epsilon)$.

Application to Methyl Radical Recombination

As an illustration of the effect of J–conservation on the predicted fall–off behaviour of a typical radical recombination reaction, Figure 3.4 shows the results of sample calculations on the pressure dependence of the methyl radical recombination to form ethane in a helium bath gas at 300K. The RRKM parameters used in the calculations are detailed in Appendix B. Curve A is that obtained by using the strong collision approximation for both ϵ and J. Curve B is that obtained by solution of Eq.(3.17) with the $\bar{k}(\epsilon)$ therein evaluated from Eq.(3.23). The value of $<\Delta\epsilon_{down}>$ used to obtain curve B was 500cm^{-1}. A value of $<\Delta R_{down}>$ need not be specified in this case since the functional form assigned to P(J,J') is independent of the difference between the final and initial angular momenta. Conversely, when fitting experimental data for reactions where the rotational relaxation is best approximated by a strong collision form for P(J,J'), no information is obtained as to the average transfer of angular momentum in collisions.

A method of incorporating angular momentum effects into the master equation which has been used previously (see, e.g., Robinson and Holbrook 1972; Gilbert and McEwan 1985) is to multiply the microscopic rate coefficient calculated with neglect of angular momentum, $k(\epsilon,J=0)$, by the ratio $I^{\dagger}/I$:

$$k(\epsilon) = (I^{\dagger}/I)\ W^{\dagger}[\epsilon-V(r^{\dagger})]/\ h\rho(\epsilon) \qquad (3.24)$$

It may be shown (Robinson and Holbrook 1972) that when $k(\epsilon)$ as defined in Eq.(3.24) is averaged over an equilibrium distribution $f(\epsilon)$, the resulting high pressure rate coefficient, k_{uni}^{∞}, is equivalent to that which would be obtained from Eq.(3.6). Curve C is that

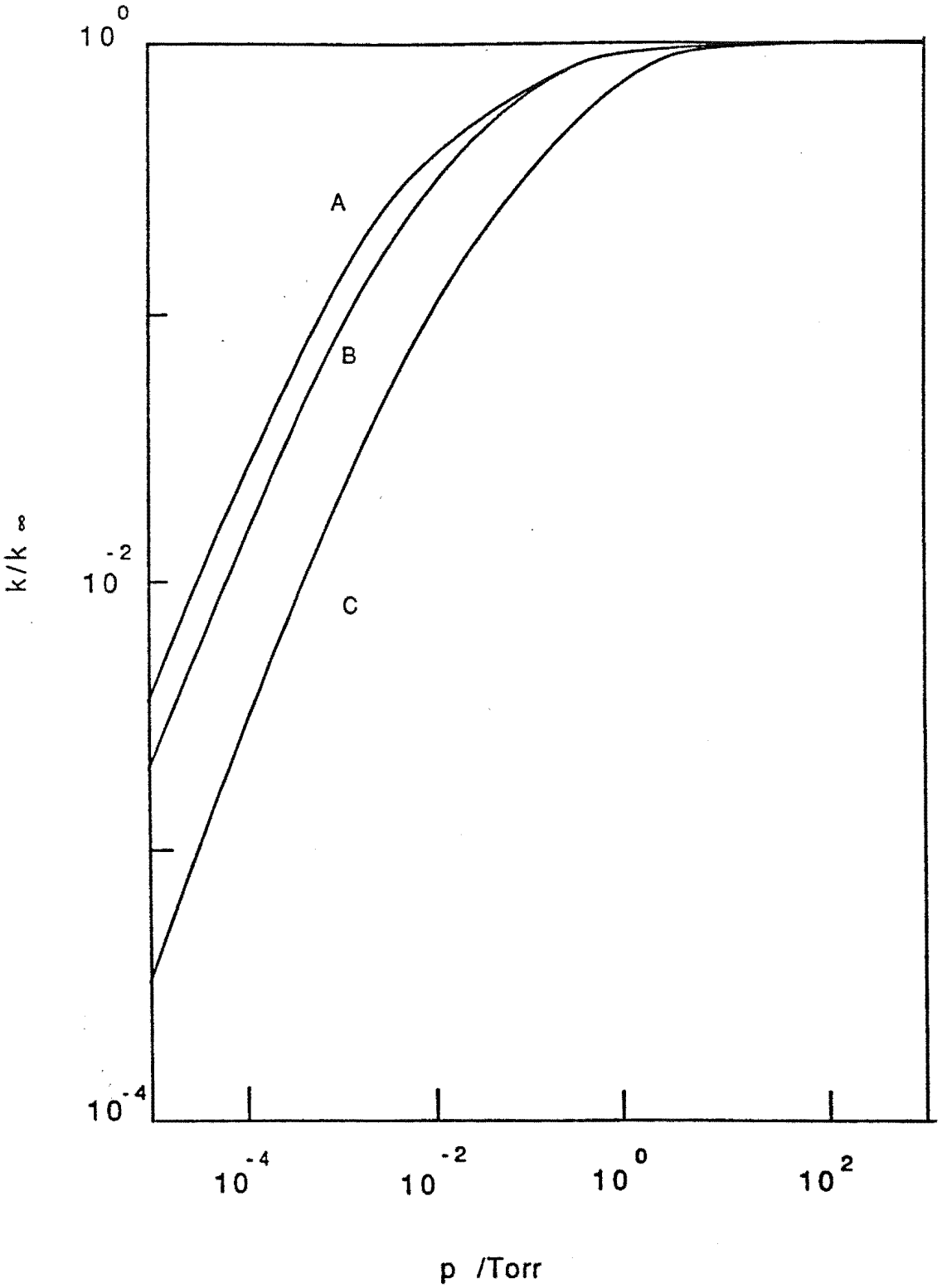

Figure 3.4. Plot of calculated pressure dependence of methyl/methyl recombination rate coefficient, plotted as the ratio k_{rec}/k_{rec}^{∞}, in helium at 300K. Curve A is the strong collision result. Curve B is obtained by solution of the master equation with with full J–conservation: $<\Delta\epsilon_{down}>$=500cm^{-1} and the rotational relaxation is treated as strong. Curve C is that obtained by solution of the one–dimensional master equation with a multiplicative factor for k(E) that accounts for angular momentum conservation approximately only in the high–pressure limit ($<\Delta\epsilon_{down}>$ is again 500cm^{-1}).

resulting from use of Eq.(3.24) throughout the fall-off regime.

The comparison of results illustrated in Figure 3.4 indicates that: (1) The strong collision approximation is a poor one because it overestimates the amount of internal energy transfer in collisions with the bath gas; hence the calculated k_{uni} in Figure 3.4 is significantly larger than that of curve B (which was calculated using a value of $<\Delta\epsilon_{down}>$ which is typical of such systems). (2) Eq.(3.24) accounts for angular momentum conservation only in the high-pressure limit and can cause rate coefficients calculated in the fall-off regime to be grossly in error. This is because as the pressure of the bath gas decreases, collisional activation gradually becomes rate determining and so at low pressures the factor $(I^{\dagger}/I)$ has no influence on the rate of reaction as determined by solution of the low-pressure master equation, Eq.(1.19) in Chapter 1. Curve C therefore substantially underestimates rate coefficients at lower pressures.

II.2b *Slow Relaxation of ϵ, Fast Relaxation of J: the Low-Pressure Limit.*

The low pressure limiting two-dimensional master equation may be formulated by generalisation of the perturbative treatment for the J-independent case (Gilbert and Ross 1971) described in chapter 1:

$$-g(\epsilon,J)k_0 = \int_0^{E_0} d\epsilon' \int_0^{J_0(\epsilon')} dJ'\ \hat{P}(\epsilon,J,\epsilon',J')g(\epsilon',J') - g(\epsilon,J) \qquad (3.25)$$

where ω has been cancelled from each side to produce a master equation for the dimensionless quantity k_0. Substituting Eq.(3.15) into Eq.(3.25) and integrating over J between the limits 0 and $J_0(\epsilon)$, one obtains:

$$-k_0\ \bar{g}(\epsilon) = Z(\epsilon) \int_0^{E_0} P(\epsilon,\epsilon')\bar{g}(\epsilon')\ d\epsilon' - \bar{g}(\epsilon) \qquad (3.26)$$

where:

$$Z(\epsilon) = \int_0^{J_0(\epsilon)} f(J)\, dJ \tag{3.27}$$

and

$$\bar{g}(\epsilon) = \int_0^{J_0(\epsilon)} g(\epsilon,J)\, dJ \tag{3.28}$$

Eq.(3.26) is the one-dimensional J-averaged low-pressure master equation, analogous to Eq.(3.17) which applies throughout the fall-off regime. It will be seen that Eq.(3.26) is equivalent in form to the J-independent low-pressure master equation of chapter 1 [Eq.(1.19)] except for the presence of $Z(\epsilon)$. $Z(\epsilon)$ modifies the collisional input to an energy level to take into account the proportion of collisions which will produce an unstable molecule with energy ϵ and angular momentum $J>J_0(\epsilon)$, i.e., it accounts for the additional possibility of *rotational* activation.

k_0, the eigenvalue solution of Eq.(3.26), may be explicitly written as the total rate of collisional activation from the non-equilibrium population $\bar{g}(\epsilon)$ to states with excitation above the reaction threshold (since at low pressures all molecules attaining such excitation are assumed to react):

$$k_0 = \int_0^{E_0} \bar{g}(\epsilon) \left[\int_0^{\infty} [1-Z(\epsilon')]P(\epsilon',\epsilon)\, d\epsilon' \right] d\epsilon \Big/ \int_0^{E_0} \bar{g}(\epsilon)\, d\epsilon \tag{3.29}$$

Eqs. (3.17) and (3.22) may be shown to reduce to Eq.(3.26) as $\omega \to 0$ by noting that at low pressures the $\bar{k}(\epsilon)$ have different behaviour, depending whether ϵ is greater than or less than E_0. Setting k_{uni} in Eq.(3.22) equal to ωk_0 and letting ω approach zero, one obtains:

$$\lim_{\omega \to 0} \bar{k}[\epsilon<E_0] = \omega[1-Z(\epsilon)](1-k_0)/Z(\epsilon) \tag{3.30}$$

i.e., below the critical energy, $\bar{k}(\epsilon)$ is proportional to ω. On the other hand, for $\epsilon>E_0$,

one finds from Eq. (3.22):

$$\lim_{\omega\to 0} \bar{k}[\epsilon>E_0] = 1/\int_0^\infty dJ\ [f(J)/k(\epsilon,J)] \tag{3.31}$$

Eqs. (3.30) and (3.31) show that, in the limit as $\omega\to 0$, $\bar{k}(\epsilon)$ separates into values below E_o, which are proportional to ω, and those above E_o, which are independent of ω. If we now insert this result directly into Eq. (3.17), and make the same perturbation treatment on this J-averaged equation, those elements of $\bar{k}(\epsilon)$ proportional to ω (i.e., below E_o) must be retained. We thus obtain:

$$-k_0\bar{g}(\epsilon) = \int_0^{E_0} P(\epsilon,\epsilon')\bar{g}(\epsilon')d\epsilon' - \bar{g}(\epsilon) - \frac{[1-Z(\epsilon)](1-k_0)}{Z(\epsilon)}\, g(\epsilon) \tag{3.32}$$

Re-arrangement of Eq. (3.32) yields the result obtained directly from the full (J,ϵ) low-pressure master equation, *viz.*, Eq. (3.26).

The general solution of the two-dimensional master equation for the case of strong collisional rotational relaxation and weak collisional relaxation of the internal energy has now been developed. However, as mentioned above, a number of ion-molecule reactions occuring in monatomic bath gases exhibit weak collisional relaxation (i.e., a transition probability which depends on both the initial and final states) for both the internal energy and the angular momentum. This third general category for solution of the master equation will now be considered.

II.3a *Slow Relaxation of ϵ and J: the Fall-Off Regime.*

The solution developed above for fast rotational relaxation relied for its simplicity on the probability function for rotational energy transfer (or angular momentum transfer, depending on the choice of independent variable) being independent of the initial state.

When a weak collisional form for P(J,J') is required, the master equation becomes more difficult to solve. Returning to Eq.(3.5), and invoking separability of $P(\epsilon,J,\epsilon',J')$ [Eq.(3.14)] and normalisation, one has:

$$-k_{uni}g(\epsilon,J) = \omega\int[P(\epsilon,\epsilon')\int P(J,J')g(\epsilon',J')dJ']d\epsilon' - [\omega+k(\epsilon,J)]g(\epsilon,J) \qquad (3.33)$$

By introducing the J-averaged quantities:

$$H(\epsilon',J) = \int P(J,J')g(\epsilon',J')dJ' \;/\; \int g(\epsilon',J')dJ' \qquad (3.34)$$

and $\bar{g}(\epsilon)$ [Eq.(3.18)], Eq.(3.33) may be written:

$$-k_{uni}g(\epsilon,J) = \omega\int P(\epsilon,\epsilon')H(\epsilon',J)\bar{g}(\epsilon')d\epsilon' - \omega g(\epsilon,J) - k(\epsilon,J)g(\epsilon,J) \qquad (3.35)$$

The quantity $P(\epsilon,\epsilon')H(\epsilon',J)$ represents the average probability that a molecule with energy ϵ' which undergoes a collision will be left in an (ϵ,J) state. Note that $H(\epsilon',J)$ is normalised with respect to J, i.e., $\int H(\epsilon',J)dJ = 1$. Integrating Eq.(3.35) over J therefore produces the J-averaged one-dimensional master equation, Eq.(3.17), with a J-averaged $\bar{k}(\epsilon)$ as defined in Eq.(3.19).

The crucial point is once again to find a way of evaluating $\bar{k}(\epsilon)$. This requires a knowledge of the way in which $g(\epsilon,J)$ varies with J, since $\bar{k}(\epsilon)$ is an average over the J distribution. Rearranging Eq.(3.35), one obtains for $g(\epsilon,J)$:

$$g(\epsilon,J) = [\omega\int P(\epsilon,\epsilon')H(\epsilon',J)\bar{g}(\epsilon')d\epsilon'][\omega + k(\epsilon,J)]^{-1} \qquad (3.36)$$

where k_{uni} has been neglected from the denominator since $k_{uni} \ll \omega+k(\epsilon,J)$. Eq.(3.36) could be solved iteratively by choosing a starting population, $g_o(\epsilon,J)$, which is qualitatively correct, and then evaluating successively improved approximations to $g(\epsilon,J)$ through Eqs.(3.34) and (3.36). This would be an iterative solution of the two-dimensional

steady-state master equation. A direct method such as this would be a useful test of the accuracy of more approximate methods. However, such a solution would require a large amount of computational time and storage space and therefore be of limited utility.

Two approximations are now introduced which obviate the necessity of the full iterative solution to the two-dimensional master equation : (1) The assumption is made that a single iteration through Eqs.(3.34) and (3.36) is sufficient to determine the J-dependence of the $g(\epsilon,J)$ population and hence the J-averaged $\bar{k}(\epsilon)$ to the accuracy required. This assumption is based on the fact that $H(\epsilon,J)$ and $\bar{k}(\epsilon)$ are average quantities and will not therefore be sensitive to minor deviations of $g_o(\epsilon,J)$ from the actual population distribution. (2) The population distribution $g(\epsilon',J)$ used in Eq.(3.34) is taken to be locally separable about the energy ϵ:

$$g(\epsilon',J) \approx \bar{g}(\epsilon') \; [g(\epsilon,J) \; / \; \bar{g}(\epsilon)] \tag{3.37}$$

The rationale for this "local separability" approximation is as follows. The bulk of the integrand in $\int P(\epsilon,\epsilon')H(\epsilon',J)\bar{g}(\epsilon')d\epsilon'$ in Eq. (3.36) comes from populations with energies, say, in the region $\epsilon' = \epsilon \pm 3\langle\Delta\epsilon_{down}\rangle$. However, for systems exhibiting weak collisional behaviour for both ϵ and J, $\langle\Delta\epsilon_{down}\rangle$ is small (e.g., *ca.* $125cm^{-1}$ for CH_3NCH^+ in He, the reaction studied in this section) and so this energy range is highly localised. A local separability approximation is expected to be acceptable over the energy range of interest because the shape of the rotational distribution varies only slowly with energy, so that in this small range about ϵ the distribution $[g(\epsilon',J)/\bar{g}(\epsilon')]$ will be very similar to that evaluated for $g(\epsilon,J)$. Substituting Eq.(3.37) into Eq.(3.34) shows that under this assumption $H(\epsilon',J)=H(\epsilon,J)$ and Eq.(3.36) reduces to:

$$g(\epsilon,J) = H(\epsilon,J) \; \Xi(\epsilon) \; / \; [\omega + k(\epsilon,J)] \tag{3.38}$$

Eq.(3.38) in conjunction with Eq.(3.19) gives:

$$\bar{k}(\epsilon) = \int k(\epsilon,J)\, H(\epsilon,J)\, [\omega+k(\epsilon,J)]^{-1}\, dJ \;/\; \int H(\epsilon,J)\, [\omega+k(\epsilon,J)]^{-1}\, dJ \qquad (3.39)$$

As a starting population $g_0(\epsilon,J)$ we choose that defined by the method of the previous section which modelled the rotational relaxation with the strong collision assumption. This distribution, defined by Eq.(3.20), will be qualitatively correct but will slightly overestimate the population at higher J values. Substituting Eq.(3.20) into Eq.(3.34) and taking account of the limits on the integrals yields the following formula for $H(\epsilon,J)$ and thence $\bar{k}(\epsilon)$:

$$H(\epsilon,J) = \frac{\int_0^{J_0(\epsilon)} dJ' f(J') P(J,J') \omega^{-1} + \int_{J_0(\epsilon)}^{\infty} dJ' [\omega+k(\epsilon,J')]^{-1} f(J') P(J,J')}{\int_0^{J_0(\epsilon)} dJ' f(J') \omega^{-1} + \int_{J_0(\epsilon)}^{\infty} dJ' f(J') [\omega+k(\epsilon,J')]^{-1}} \qquad (3.40)$$

$$\bar{k}(\epsilon) = \frac{\int_{J_0(\epsilon)}^{\infty} dJ\, [\omega+k(\epsilon,J)]^{-1}\, H(\epsilon,J)\, k(\epsilon,J)}{\int_0^{J_0(\epsilon)} dJ\, H(\epsilon,J) \omega^{-1} + \int_{J_0(\epsilon)}^{\infty} dJ\, H(\epsilon,J) [\omega+k(\epsilon,J)]^{-1}} \qquad (3.41)$$

Note that, since $k_{uni} \ll \omega+k(\epsilon,J)$, k_{uni} has been neglected in the denominator of $g_0(\epsilon,J)$. Also, if $P(J,J') = f(J)$, $H(\epsilon,J)$ reduces to $f(J)$ and Eq.(3.41) reduces to the result of the previous section, Eq.(3.23).

Application to CH_3^+/HCN *Association*

An example of a reaction which requires a weak collisional treatment for both ϵ and J is the association of CH_3^+ with HCN in helium. In this reaction the initial association product is CH_3NCH^+, which may then isomerise to CH_3CNH^+. This reaction has been well

studied experimentally, with measurements being made at low pressures using ion cyclotron resonance (ICR) (Bass *et al.* 1981; Kemper *et al.* 1985) and at higher pressures using the selected ion flow tube (SIFT) technique (Knight *et al.* 1986; Schiff and Bohme 1979; Adams and Smith 1984). Previous theoretical work includes an investigation of the potential surface by DeFrees *et al.* (1985), an analysis of experimental data using the strong collision assumption (Bass *et al.* 1981), and a one-dimensional master equation analysis using the equation for $k(\epsilon)$ that accounts for J-conservation only in the high pressure limit, Eq.(3.24) (Gilbert and McEwan 1985).

Figure 3.5 shows representative experimental data for the fall-off of the association rate coefficient (plotted as the ratio k_{ass}/k_{ass}^{∞}) at 300K with a helium bath gas, and also the results of calculations using methods outlined or developed in this chapter. The appropriate parameters for the calculations are included in Appendix C. The microscopic rate coefficients were calculated using canonical variational transition state theory (CVTST, see Chapter 1), giving, in the high pressure limit, a calculated capture rate coefficient of 7.4×10^{-9} cm^3s^{-1}. This is somewhat larger than the capture rate predicted by trajectory calculations (Su and Chesnavich 1982) of 4.4×10^{-9} cm^3s^{-1}. The reason for this overestimate will be discussed in Chapter 4. It has been assumed that the isomerisation, which proceeds through a tight transition state, is a much slower process and so may be neglected in determining the rate of association for all but very low pressures. Curve A is the fall-off obtained with the strong collision assumption for both ϵ and J (Section II.1a) As is typically the case, this overestimates substantially the rate coefficient in the fall-off regime. Curve B is that obtained with the method of Section II.2a which allows the collisional relaxation of ϵ to be weak but describes the J relaxation with the strong collision assumption. Curve B was calculated with a value for $\langle\Delta\epsilon_{down}\rangle$ of $150cm^{-1}$. It is apparent that the "weak ϵ, strong J" treatment also overestimates the rate coefficients substantially, indicating that slow relaxation by collisions of the angular momentum is an important factor in determining the fall-off behaviour of this reaction. Curve C is that obtained by using the method of this section which allows for weak collisional behaviour in both the ϵ and J relaxation. Values for $\langle\Delta\epsilon_{down}\rangle$ and $\langle\Delta R_{down}\rangle$ of $150cm^{-1}$ allow an

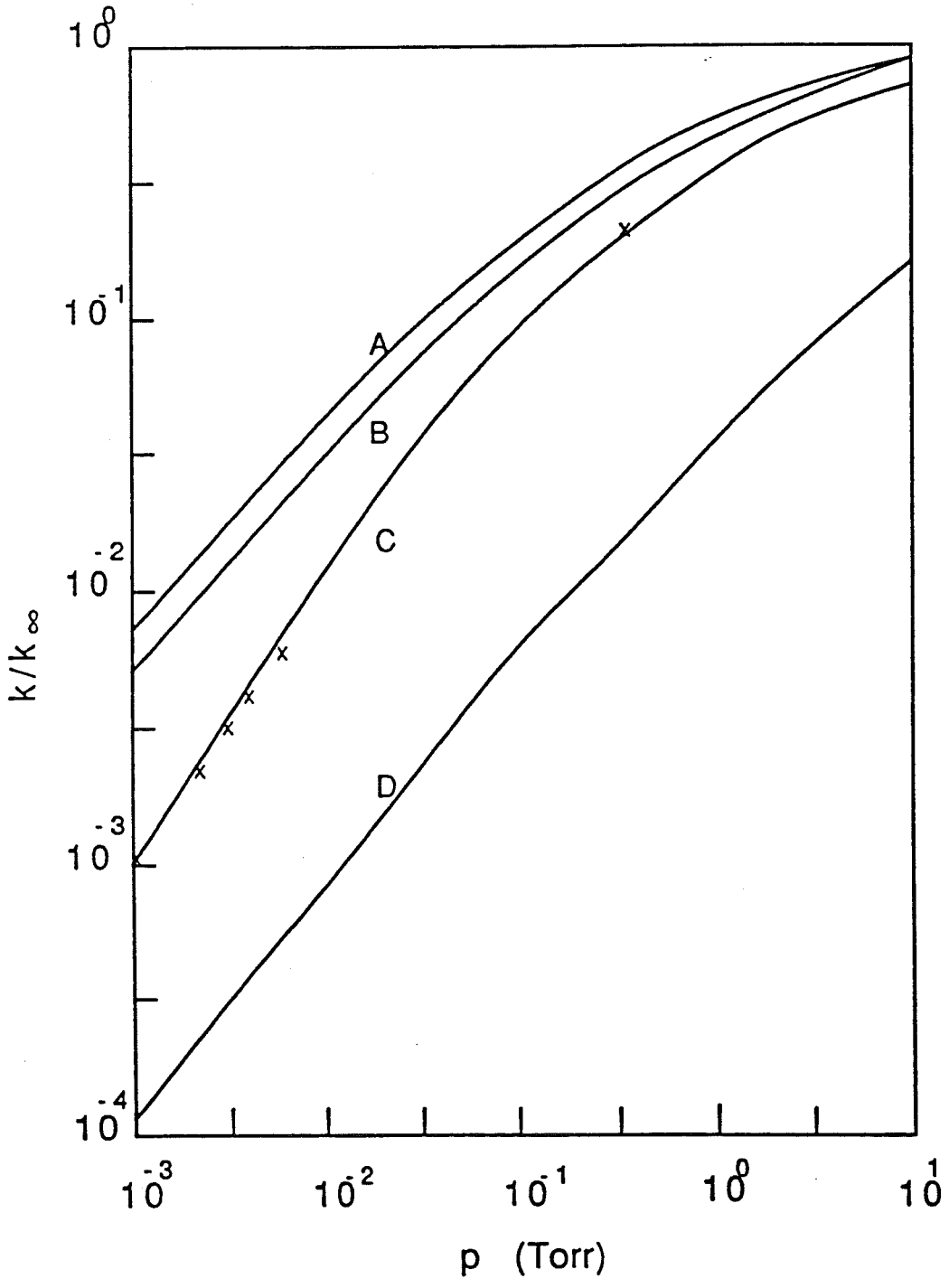

Figure 3.5. Plot of representative experimental data and calculations for the pressure dependence of association rate coefficients for the reaction of CH_3^+ with HCN. Low-pressure points measured by the ICR technique (Kemper *et al.* 1985); high-pressure point measured by the SIFT technique (Knight *et al.* 1986). Curve A: result for strong collisions in both ϵ and R. Curve B: solution of the two-dimensional master equation with the assumption of a strong-collisional form for P(R,R') ($<\Delta\epsilon_{down}>=150cm^{-1}$). Curve C: solution of the master equation for weak relaxation of both ϵ and R ($<\Delta\epsilon_{down}>=<\Delta R_{down}>=150cm^{-1}$). D: solution of the one-dimensional master equation which does not incorporate J-conservation in the fall-off regime ($<\Delta\epsilon_{down}>=150cm^{-1}$).

excellent fit to the data. These two quantities need not have the same value. However, trajectory studies indicate (Date *et al.* 1984, Whyte and Gilbert 1989) that they will be of approximately the same size. For want of further information, $\langle\Delta\epsilon_{down}\rangle$ and $\langle\Delta R_{down}\rangle$ were taken as having the same value for this study. Finally, curve D is that obtained with use of the $k(\epsilon)$ which allows for J–conservation properly only in the high pressure limit, Eq.(3.24). The earlier master equation calculation of Gilbert and McEwan (1985) used this technique to fit experimental data (Bass *et al.* 1981) and determined $\langle\Delta\epsilon_{down}\rangle$ to be *ca.* 700cm^{-1}, a value which was surprisingly large considering that relatively weak collisions are indicated by an experimental β value of 0.1 at low pressures (Bass *et al.* 1981). The reason for this discrepancy is the inadequate account for J–conservation provided by Eq.(3.24) in the fall–off regime: in order to try to fit curve D to the experimental results, one is forced to increase $\langle\Delta\epsilon_{down}\rangle$. Indeed, with the more accurate molecular parameters for the initial association product, CH_3NCH^+, calculated by DeFrees *et al.* (1985), it is not possible to reproduce the experimental data using Eq.(3.24) for $k(\epsilon)$.

The comparison of methods in Figure 3.5 shows that the fall–off data for the CH_3^+/HCN association in helium cannot be reproduced without proper account for both weak collision effects *and* angular momentum conservation. It is admittedly possible to obtain an approximate fit to the fall–off data by inclusion of a collision efficiency into the strong collision treatment. However, as in the CH_3^+/NH_3 reaction (chapter 2), fitting the strong collision curve to the experimental data at high pressures causes the predicted rate coefficients at low pressures to be in error by a factor of *ca.* 2. Furthermore, no quantitative information is obtained concerning the energy transfer in collisions between CH_3NCH^+ and helium, whereas the master equation solution enables such information to be determined from the experimental data.

Before proceeding to the solution of the low–pressure two–dimensional master equation for the case of slow relaxation of ϵ and J, it is necessary to examine the accuracy of the two assumptions introduced in the solution of the general problem, *viz.* the sufficiency of a single iteration to determine the J–distribution and the local

separability approximation. The validity of the assertion that the J-averaged $\bar{k}(\epsilon)$ will be relatively insensitive to a minor deviation of $g_o(\epsilon,J)$ from the true population distribution, and therefore that a single iteration on our starting population is sufficiently accurate, may be easily tested by observing the sensitivity of k_{uni} calculated in the fall-off regime to modifications of the starting population $g_o(\epsilon,J)$. As a test of this sensitivity, a collision efficiency was inserted into Eq.(3.20) to enable the shape of the starting distribution $g_o(\epsilon,J)$ to be varied:

$$g_o(\epsilon,J) = \omega f(J)\, \Xi(\epsilon) \,/\, [\beta\omega + k(\epsilon,J)] \tag{3.42}$$

It was found that on reducing β from 1.0 to 0.2 the greatest change was *ca.* 60% in the calculated k_{uni} at pressures near 0.1 Torr. This moderatedly small change in k_{uni} as a result of a large change in the starting population verifies the relative insensitivity of the final result to the fine details of $g_o(\epsilon,J)$. It should be stressed that this does <u>not</u> imply that the rate coefficient is insensitive to the details of the rotational distribution, since it is not $g_o(\epsilon,J)$ but rather the first-order correction produced by Eq.(3.38) that is used to calculate $\bar{k}(\epsilon)$.

So much for the first approximation. How can the accuracy of the local separability approximation be tested? In order to demonstrate the validity of the local separability approximation, it is useful to note the conditions under which Eq. (3.37) is exact, and those under which it will be most in error. The local separability approximation is exact (i) in the high-pressure limit, where $g(\epsilon,J) = f(\epsilon,J) = f(\epsilon)f(J)$ [the high-pressure population] and also (ii) when $P(J,J')$ depends only on the final state J (as in Section II.2). It will be least accurate at low pressures where the non-equilibrium nature of the populations $g(\epsilon,J)$ is most manifest, and hence the shape of the rotational distribution is more sensitive to energy. The critical accuracy test is then at the low pressure limit. As will be demonstrated in the next section, the low-pressure-limiting two-dimensional master equation can be solved without recourse to the local separability assumption. This allows us to test the accuracy of this approximation where it is likely to cause most error.

II.3b *Slow Relaxation of ϵ and J: the Low-Pressure Limit.*

The solution of the low-pressure-limiting two-dimensional master equation, for the case where a weak collisional description of both the ϵ and J relaxation is required, proceeds by assuming separability of $P(\epsilon,J,\epsilon',J')$ (see, e.g., Penner and Forst 1975) and introducing into Eq.(3.25) the J-averaged quantity:

$$H_0(\epsilon',J) = \frac{\int_0^{J_0(\epsilon')} dJ'\ P(J,J')g(\epsilon',J')}{\int_0^{J_0(\epsilon')} dJ'\ g(\epsilon',J')} \tag{3.43}$$

to produce the equation:

$$-k_0 g(\epsilon,J) = \int_0^{E_0} d\epsilon'\ P(\epsilon,\epsilon')H_0(\epsilon',J)\bar{g}(\epsilon') - g(\epsilon,J) \tag{3.44}$$

where $\bar{g}(\epsilon)$ is as defined in eq(3.18). Note that the upper limits on the integrals in Eq.(3.43) are $J_0(\epsilon')$: this is because perturbation theory shows (Gilbert and Ross 1971) that as $\omega\to 0$ the population of states with excitation above the reaction threshold $\epsilon_0(J)$ [or $J_0(\epsilon)$] approaches zero. The quantity $P(\epsilon,\epsilon')H_0(\epsilon',J)$ represents the average probability that a molecule with energy ϵ' is left in an (ϵ,J) state after a collision.

Integrating Eq. (3.44) over J gives:

$$-k_0\bar{g}(\epsilon) = \int_0^{E_0} d\epsilon'\ P(\epsilon,\epsilon')Q(\epsilon,\epsilon')\bar{g}(\epsilon') - \bar{g}(\epsilon) \tag{3.45}$$

where

$$Q(\epsilon,\epsilon') = \int_0^{J_0(\epsilon)} dJ\ H_0(\epsilon',J) \qquad (3.46)$$

The quantity $Q(\epsilon,\epsilon')$ is the average proportion of collisional transitions from ϵ' to ϵ which go into *stable* J states with $J<J_0(\epsilon)$. Eq.(3.46) has the same form as the J-independent low-pressure master equation of Chapter 1 [Eq.(1.19)] except for $Q(\epsilon,\epsilon')$. The effect of $Q(\epsilon,\epsilon')$ is to discount collisional influx into the energy level ϵ that goes into unstable states [with $J>J_0(\epsilon)$].

It can be seen that, provided the quantity $Q(\epsilon,\epsilon')$ can be accurately approximated, Eq. (3.45) is readily soluble by minor modification of standard techniques (e.g., Gilbert 1983). Integrating Eq. (3.45) over $\epsilon<E_0$ and rearranging, one finds that k_0, the eigenvalue solution of Eq.(3.45), may be written in terms of $\bar{g}(\epsilon)$ as:

$$k_0 = \int_0^{E_0} \bar{g}(\epsilon) \left[\int_0^{\infty} [1-Q(\epsilon',\epsilon)]P(\epsilon',\epsilon)\ d\epsilon' \right] d\epsilon \ / \int_0^{E_0} \bar{g}(\epsilon) d\epsilon \qquad (3.47)$$

Evaluation of $Q(\epsilon,\epsilon')$ via Eqs. (3.43) and (3.46) requires an appropriate functional form for P(J,J') and a knowledge of the J-dependence of $g(\epsilon,J)$. However, as in the solution above for the fall-off regime, an iterative method is appropriate: one uses an approximate starting population $g_0(\epsilon,J)$ for the evaluation of $Q(\epsilon,\epsilon')$. Since $Q(\epsilon,\epsilon')$ is (by nature of being an average quantity) relatively insensitive to the fine details of the distribution $g(\epsilon,J)$, such a technique should yield an accurate solution to the problem.

Various forms for $g_0(\epsilon,J)$ might be chosen. For reliability, it is desirable to choose one which a) results in simple evaluation of $Q(\epsilon,\epsilon')$ and b) provides a rigorous upper bound to the exact solution. For these purposes, we choose for $g_0(\epsilon,J)$ the population distribution defined by the limit of strong collisions in J (Section II.2 above), i.e., setting $P(\epsilon,\epsilon')P(J,J') = P(\epsilon,\epsilon')f(J)$, where $f(J) = (2J+1)\exp(-R/k_BT)$. Substituting Eq.(3.15) into Eq.(3.25), rearranging for $g(\epsilon,J)$ and noting that $k_0 \ll 1$, one obtains for $g_0(\epsilon,J)$:

$$g_o(\epsilon,J) = \Xi(\epsilon)f(J), \quad J < J_o(\epsilon) \qquad (3.48)$$
$$g_o(\epsilon,J) = 0, \quad J > J_o(\epsilon)$$

where $\Xi(\epsilon) = \int P(\epsilon,\epsilon')\bar{g}(\epsilon')d\epsilon'$. It should be emphasised that Eq. (3.48) is used only perturbatively, and that otherwise full account is taken of the functional form of P(J,J'). In evaluating $Q(\epsilon,\epsilon')$ it is convenient first to transform from the angular momentum to the rotational energy as an independent variable, where P(R,R') = P(J,J')/[B(2J+1)]. The form chosen for P(R,R') is the "exponential down" model (see, e.g., Troe 1977a,1987a), in which the probability of energy transfer decreases exponentially as the difference (R–R') increases:

$$P(R,R') = (\gamma+\delta)^{-1} \exp[(R-R')/\gamma], \quad R<R';$$
$$= (\gamma+\delta)^{-1} \exp[(R'-R)/\delta], \quad R>R' \qquad (3.49)$$

where $\gamma = \langle\Delta R_{down}\rangle$, and δ is related to γ by microscopic reversibility: $\delta = \gamma k_B T/(\gamma+k_B T)$. This form of P(R,R') is normalised in the interval $-\infty<R<\infty$, rather than the exact normalisation which should be over $0\leq R<\infty$. This will be quite accurate provided that $\langle\Delta R_{down}\rangle$ is moderately small, as is the case for ion–molecule collisions with inert bath gases. The details of evaluation of $Q(\epsilon,\epsilon')$ using Eqs.(3.48), (3.49), (3.43) and (3.46) are presented in Appendix D.

The solution of Eq.(3.45) using $Q(\epsilon,\epsilon')$ as evaluated in Appendix D provides an upper bound to the exact solution. This can be seen by noting that the only approximation involved in the solution is the choice of the starting population $g_o(\epsilon,J)$ as defined in Eq.(3.48) for the evaluation of $Q(\epsilon,\epsilon')$. This starting population is that defined for strong collisions in J and therefore will overestimate somewhat the J–distribution at high J values. The resulting k_o must therefore overestimate the exact k_o which would be obtained if the true $g(\epsilon,J)$ were used to evaluate $Q(\epsilon,\epsilon')$. Furthermore, note that the local separability approximation is *not required* for the solution, as was the case for the solution in the fall–off regime. In the previous section it was pointed out that the local

separability approximation is most likely to lead to error in the low pressure limit. Solution of Eq.(3.45) therefore allows a rigorous test of the accuracy of the local separability approximation.

Results are presented in Figure 3.6 of calculations carried out for the CH_3^+/HCN association in helium to compare the solution of Eq.(3.45) (curve A) with results obtained using the local separability approximation (curve B). Curve B is obtained by setting $H_o(\epsilon',J) = H_o(\epsilon,J)$ in Eq.(3.44) which leads to $Q(\epsilon',\epsilon) = Q(\epsilon,\epsilon)$ in Eq.(3.45). The results, calculated at 300K, are plotted as the ratio $\beta = k_o/k_o^{sc}$, where k_o^{sc} is the reference strong collision low pressure rate coefficient. β is plotted as a function of $\langle\Delta R_{down}\rangle$ for three different fixed values of $\langle\Delta\epsilon_{down}\rangle$. Recall that the accuracy of the local separability approximation depends on just how "local" the energy range $\epsilon \pm 3\langle\Delta\epsilon_{down}\rangle$ is. For small $\langle\Delta\epsilon_{down}\rangle$, the approximation is expected to be accurate. This is borne out by the results of Figure 3.6. Curve B agrees well with the more rigorous curve A for $\langle\Delta\epsilon_{down}\rangle \leqslant 300cm^{-1}$ ($1.5k_BT$), but diverges from the more accurate result when $P(\epsilon,\epsilon')$ becomes broad. This comparison indicates that the local separability approximation used in Section II.3a for solving the two-dimensional master equation in the fall-off regime is accurate for systems which require a weak collisional treatment for both ϵ and J, since these reactions will generally have $\langle\Delta\epsilon_{down}\rangle$ and $\langle\Delta R_{down}\rangle$ of the order of k_BT or less ($k_BT \approx 200cm^{-1}$ at 300K).

Fitting the low pressure ICR data of Kemper *et al.* (1985) for the CH_3^+/HCN association [which corrects data of an earlier study (Bass *et al.* 1981)], using the exact upper bound solution to the low-pressure two-dimensional master equation developed in this section, enables the experimental termolecular association rate coefficient of 2.2×10^{-25} $cm^6\ s^{-1}$ to be reproduced with values for $\langle\Delta\epsilon_{down}\rangle$ and $\langle\Delta R_{down}\rangle$ of $100cm^{-1}$. For this fitting, both $P(\epsilon,\epsilon')$ and $P(R,R')$ were represented by the exponential down form, i.e., $P(R,R')$ as defined in Eq.(3.49) and $P(\epsilon,\epsilon')$ defined as (see, e.g., Gilbert and King 1980):

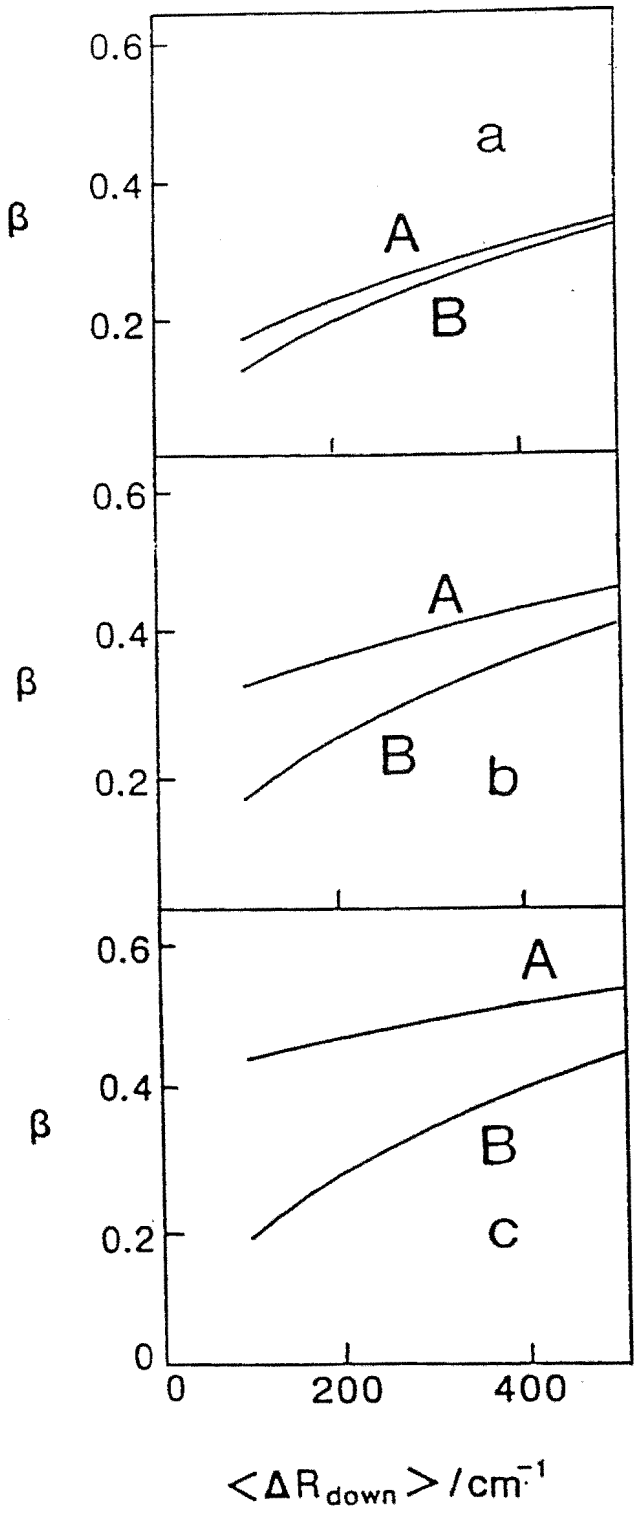

Figure 3.6. Sample calculations of low-pressure rate coefficents for CH_3^+/HCN association to compare results obtained with and without use of the local separability approximation. Curves labelled A calculated without the local separability approximation; curves labelled B calculated with the local separability approximation. k_o (plotted as the ratio $\beta=k_o/k_o^{sc}$) calculated as a function of $<\Delta R_{down}>$, for $<\Delta\epsilon_{down}>$ values of (a) $100cm^{-1}$, (b)$300cm^{-1}$, and (c)$600cm^{-1}$.

$$P(\epsilon,\epsilon') = [1/N(\epsilon')]\exp(\epsilon-\epsilon')/\alpha \ , \qquad \epsilon < \epsilon'$$
$$P(\epsilon,\epsilon') = [f(\epsilon)/f(\epsilon')]P(\epsilon',\epsilon) \ , \qquad \epsilon > \epsilon' \qquad (3.50)$$

where $\alpha = \langle\Delta\epsilon_{down}\rangle$, and the normalising factor $N(\epsilon')$ is evaluated exactly (Gilbert and King 1980). These values for $\langle\Delta\epsilon_{down}\rangle$ and $\langle\Delta R_{down}\rangle$ are consistent with the values of $150cm^{-1}$ determined by fitting the experimental data over the full fall-off range with the more approximate solution of the previous section. The present study therefore indicates that reliable estimates of the average internal and rotational energy transfers in collisions between CH_3NCH^+ and helium at 300K are $125cm^{-1}$ ± 50%. It should be noted that the molecular and transition state properties for the CH_3^+/HCN system are well characterised, and so the fitting allows meaningful values to be assigned to the average energy transfer parameters.

The methods of solution of the two-dimensional master equation developed in this chapter will now be compared and contrasted with the only previous means of approaching this problem: the solutions of Penner and Forst (1975,1976) and Troe (1977,1987a) which apply to the low-pressure-limiting case.

III. Comparison of Solutions to the Two-Dimensional Master Equation

The solution developed in the previous section for the low-pressure master equation with weak collisions in both ϵ and J may be compared with alternative solutions to this limiting case developed by Penner and Forst (1975,1976) and Troe (1977,1987a). Both works start with the two-dimensional master equation, Eq.(3.25), and introduce varying degrees of approximations in obtaining a solution. The Troe solution is the more general of the two, and will be considered in greater detail after comparing the present solution with that of Penner and Forst.

In the following, the "fixed v" solution of Penner and Forst (1976) is derived in a way which illustrates the relationship with the present solution. Eq.(3.45) is reexpressed as:

$$-k_0\bar{g}(\epsilon) = \int_0^{E_0} d\epsilon' \; P(\epsilon,\epsilon')[1-S(\epsilon,\epsilon')]\bar{g}(\epsilon') - \bar{g}(\epsilon) \tag{3.51}$$

where $S(\epsilon,\epsilon') = 1 - Q(\epsilon,\epsilon')$. Specific formulae for the evaluation of $Q(\epsilon,\epsilon')$ and $S(\epsilon,\epsilon')$ are included in Appendix D. In Eq.(3.51), $S(\epsilon,\epsilon')$ is the proportion of collisional transitions from ϵ' to ϵ which go into unstable J states, i.e., $J>J_0(\epsilon)$. Separating out the terms in $S(\epsilon,\epsilon')$, one has:

$$-k_0\bar{g}(\epsilon) = \int_0^{E_0} d\epsilon' \; P(\epsilon,\epsilon')\bar{g}(\epsilon') - \bar{g}(\epsilon) - \langle k_v \rangle \tag{3.52}$$

where

$$\langle k_v \rangle = \int_0^{E_0} d\epsilon' \; P(\epsilon,\epsilon')S(\epsilon,\epsilon')\bar{g}(\epsilon') \tag{3.53}$$

The "fixed v" approximation of Penner and Forst assumes that $P(\epsilon,\epsilon')$ is sufficiently sharply peaked that $\langle k_v \rangle$ may be approximated by setting $P(\epsilon,\epsilon')=\delta(\epsilon-\epsilon')$, yielding (Penner and Forst 1976):

$$\langle k_v \rangle = S(\epsilon,\epsilon)\bar{g}(\epsilon) \tag{3.54}$$

Some explanation of notation may be required: Penner and Forst denote ϵ as E_v, R as E_r, $\bar{g}(\epsilon)$ as $S(E_v)$, $g(\epsilon,J)/\bar{g}(\epsilon)$ as $R(E_r',E_v)$, $P(\epsilon,\epsilon')$ as $q_v(E_v',E_v)$, $P(R,R')$ as $q_r(E_r',E_r)$, $R_0(\epsilon)$ as $E_r^{max}(E_v)$, and ωk_0 as k_0†.

Eqs.(3.52) and (3.53) are identical to Eq.(3.45) above. Hence it can be seen that whereas the solution developed in this chapter is equivalent to solving Eq.(3.52) with complete evaluation of the $\langle k_v \rangle$ term as defined in Eq.(3.53), the model of Penner and Forst solves Eq.(3.52) with the more restricted $\langle k_v \rangle$ term of Eq.(3.54). Since the Penner and Forst model underestimates the $\langle k_v \rangle$ term, their method will also underestimate the resulting k_0. It should be noted that the local separability approximation used above for the solution in the fall-off regime also requires that $P(\epsilon,\epsilon')$ not be too broad. However, the condition for validity of the local separability approximation is not as stringent as that

for the validity of Eq.(3.54). This may be seen by recalling that the local separability approximation in the low pressure limit corresponds to setting $Q(\epsilon,\epsilon') = Q(\epsilon,\epsilon)$, hence $S(\epsilon,\epsilon') = S(\epsilon,\epsilon)$ and one obtains for $\langle k_v \rangle$:

$$\langle k_v \rangle = S(\epsilon,\epsilon) \int_0^{E_0} d\epsilon' \; P(\epsilon,\epsilon')\bar{g}(\epsilon') \tag{3.55}$$

The Penner and Forst solution should therefore produce results which are smaller than both curves in Figures 3.6a–3.6c.

Troe (1977,1987a) has developed an analytic solution to the low–pressure–limiting two–dimensional master equation for the specific case of collisional transition probability $P(\epsilon,\epsilon')$ which varies exponentially both for $\epsilon<\epsilon'$ and for $\epsilon>\epsilon'$. In general, the upward side of $P(\epsilon,\epsilon')$ is dictated by detailed balance as in Eq.(3.50), and may not be of exponential form. However, provided the molecular density of states $\rho(\epsilon)$ varies in an approximately exponential fashion at the energies of interest (Troe 1977a), the upward side of $P(\epsilon,\epsilon')$ may be accurately approximated as exponential. For the exponential–down model, P(R,R') will be exactly exponential on the upward side, Eq.(3.49), since the density of states of the external rotation is a constant. The simple normalisation adopted for P(R,R'), which is independent of the initial state [Eq.(3.49)], is also used for $P(\epsilon,\epsilon')$. With these assumptions, an analytic solution is obtained (Troe 1977a) which expresses the non–equilibrium population distribution $g(\epsilon,J)$ as the product of the equilibrium distribution $f(\epsilon,J)$ and a non–equilibrium term $h(\epsilon,J)$ which is unity for states well beneath the threshold, but becomes depressed from unity for states close to the threshold. Using the simple analytic form for $P(\epsilon,\epsilon')$ and P(R,R'), the rate coefficient is obtained by evaluating the total rate of collisional activation from the non–equilibrium population to states above the threshold. Using the Whitten–Rabinovitch semi–classical approximation to the density of states to evaluate $f(\epsilon,J)$, an analytic expression for the ratio $\beta = k_o/k_o^{sc}$ is determined after some factoring [note that the later reference (Troe 1987a) corrects errors in the earlier (Troe 1977a)].

Calculations were carried out for the association of CH_3^+ with HCN in helium to compare the results of the Troe solution with those of the solution developed in the previous section. The results, calculated at 300K, are presented in Figure 3.7. The value of $<\Delta\epsilon_{down}>$ has been fixed at a typical value of $200cm^{-1}$, and the ratio $\beta = k_o/k_o^{sc}$ plotted as a function of $<\Delta R_{down}>$. Line E represents the result obtained from the solution (Section II.2b) which models the rotational relaxation with strong collisions. This is therefore the correct asymptotic limit for the solution as $<\Delta R_{down}>$ becomes large with $<\Delta\epsilon_{down}>$ fixed at $200cm^{-1}$. Curve A is that obtained from the solution of this chapter (Section II.3b); curve D is that resulting from Troe's analytic solution for β. Also included are two improved versions of Troe's solution (curves B and C), discussed below.

It is immediately apparent from Figure 3.7 that, whilst all methods show the correct qualitative trends for low $<\Delta R_{down}>$, none has the correct behaviour as $<\Delta R_{down}>$ becomes large.

The origin of the inapplicability for large $<\Delta R_{down}>$ is as follows. The exponential form of P(R,R'), Eq. (3.49), is normalised on the range $-\infty < R < \infty$; this gives a simple analytic form for the normalised P(R,R'). Exact normalisation would be evaluated numerically over the range $0 < R < \infty$ (Gilbert and King 1980). The simpler normalisation breaks down as $<\Delta R_{down}>$ becomes large and comparable to the average rotational energy. It has been shown (Gilbert *et al.* 1983) that an incorrect value of β will be obtained in such circumstances. In addition, this functional form also becomes physically inapplicable under such circumstances, and even with exact normalisation will not produce the correct "strong collision in J" limit (line E). This is because as the rotational relaxation becomes fast the functional form of P(R,R') changes from a form depending on R–R' towards the strong collision form. The breakdown of the exponential form for P(R,R') for large $<\Delta R_{down}>$ indicates that it should only be used in cases where the average rotational energy of reacting species is much greater than $<\Delta R_{down}>$. For systems where this criterion does not hold, such as ion–molecule reactions involving *polyatomic* bath gases and most neutral reactions, the preferred method of calculation will

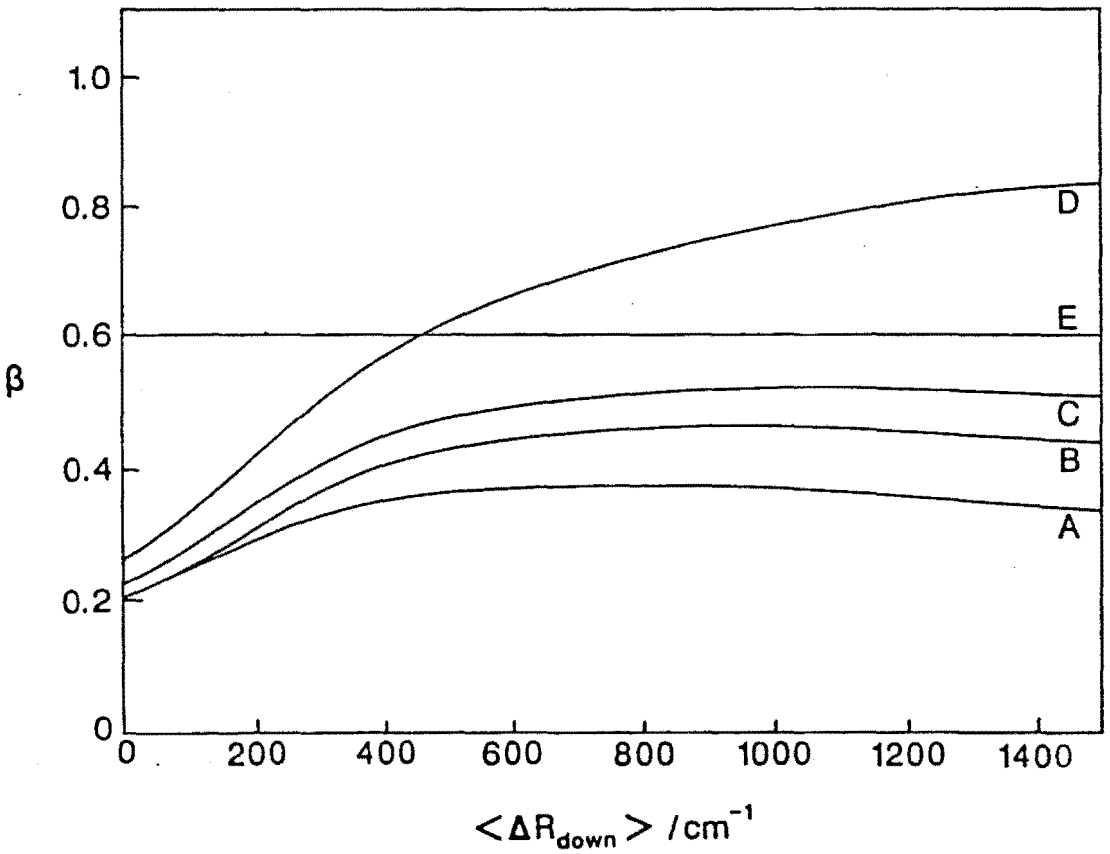

Figure 3.7. Low-pressure-limiting rate coefficients calculated from: (A) The exact upper bound solution of the present work [i.e.,Eq. (3.45)], (B) The exact numerical solution of Troe's model (see Appendix E), (C) Improved analytic solution to the Troe model (see Appendix E), (D) Troe's approximate analytic solution, and (E) The exact asymptotic solution as $<\Delta R_{down}>$ becomes large (i.e., rotational relaxation becomes fast, see section II.2b). k_o plotted as the ratio $\beta=k_o/k_o^{sc}$ as a function of $<\Delta R_{down}>$ for $<\Delta \epsilon_{down}>$ fixed at $200cm^{-1}$.

be that which models the rotational relaxation with strong collisions (Section II.2 above).

The current method (curve A) is now compared in Figure 3.7 with the Troe solution (curve D), given the understanding that these models can only be expected to be applicable for small to moderate $<\Delta R_{down}>$ (less than 500 cm^{-1}). Firstly, recall that Eq. (3.45) yields a rigorous upper bound to the rate coefficient, given $P(\epsilon,\epsilon')$ and $P(R,R')$. Fig. 3.7 shows that the Troe solution gives values significantly larger (by up to a factor of 2) than those of the present method. Since the present method is an upper bound, the Troe solution must therefore overestimate the exact solution.

What is the origin of this discrepancy? Troe's solution consists of several steps. He first develops an analytic expression for the population $g(\epsilon,R)$ [Troe 1987a, Eqs. (27) and (28)]. He then carries out steps which lead to an analytic expression for k_o. Now, if one takes Troe's formula for $g(\epsilon,R)$ and calculates the rate coefficient without any intermediate factoring or semi-classical approximations to $f(\epsilon,R)$, good agreement (curve B) is obtained with the upper bound from present method. The details of this evaluation of the rate coefficient are included in Appendix E. This agreement between two quite different approximate solutions strongly suggests the accuracy of both. The reason for the overestimate of k_o by the Troe solution must therefore be the breakdown of the factorisation approximation used to obtain his analytic formula for β. This is proven (in the midst of considerable algebra) in Appendix E. In addition, an improved analytic approximation to β, which avoids much of the error introduced in Troe's factoring, is derived (curve C in Figure 3.7).

A test of the insensitivity of the solution of Eq.(3.45) to the fine details of $g_o(\epsilon,R)$ can be obtained by substituting Troe's approximate $g(\epsilon,R)$ for $g_o(\epsilon,R)$, instead of Eq. (3.48). The resultant k_o is only marginally smaller (*ca.* 10%). This verifies the insensitivity of the present method to the precise form of the first approximation to the population used in the perturbative treatment, and suggests that it is of quite acceptable accuracy.

IV. Extension to Multichannel Reactions

Many unimolecular dissociation reactions involve two or more competing channels through which dissociation may occur. It is therefore important to extend solutions of the master equation to calculate rate coefficients for such multiple channel systems. In addition to multiple channel dissociations, chemical activation reactions are also multichannel systems. The solution to the master equation for chemical activation reactions presented in Chapter 2 assumes that one is able to solve the multiple channel dissociation problem.

Methods of solving the master equation for multichannel unimolecular dissociation in the J-*independent* case have been developed previously (Gaynor *et al.* 1978b). One notes (see, e.g., King *et al.* 1971) that it is the total $k(\epsilon)$ [$= \sum_i k^i(\epsilon)$] which occurs in the master equation and causes depletion of the populations of excited states. Once the master equation has been solved for the non-equilibrium populations $g(\epsilon)$ and the overall rate coefficient for dissociation k_{uni}, the rate coefficients for dissociation through individual channels are evaluated as:

$$k_{uni}^i = \int k^i(\epsilon)g(\epsilon)d\epsilon / \int g(\epsilon)d\epsilon \qquad (3.56)$$

Note that from Eq.(3.56) $\sum_i k_{uni}^i = k_{uni}$.

No adequate means of incorporating angular momentum conservation into the multichannel unimolecular master equation has hitherto been available. The only method which has been used for calculation of rate coefficients in the fall-off regime is to multiply $k(\epsilon,J=0)$ by the ratio $(I^\dagger/I)$ as in Eq.(3.24) above (e.g., Gaynor *et al.* 1978b). However, the comparison for the methyl recombination reaction, Figure 3.4, shows that this method only works at high pressures and can be grossly in error in the fall-off regime. An approximate method of incorporating J-conservation into the low-pressure master equation has been suggested by Just and Troe (1980). However, as will be discussed below, this has very limited applicability.

The extension of the solutions developed or outlined in this chapter to multichannel reactions is straightforward. Briefly, the appropriate formulae are now presented.

IV.1 *Fast Relaxation of ϵ and J*

The rate coefficient for dissociation through channel i, k_{uni}^{i}, is obtained simply by replacing $k(\epsilon,J)$ in Eq.(3.11) by $k^{i}(\epsilon,J)$. Note that Eq.(3.10) for the population $g(\epsilon,J)$ remains the same, with the understanding that $k(\epsilon,J) = \sum_i k^{i}(\epsilon,J)$. In the low pressure limit, Eq.(3.13) is modified as follows (see, e.g., Just and Troe 1980):

$$k_{uni}^{i} = (\omega/Q)\int\int f(\epsilon,J)[k^{i}(\epsilon,J)/k(\epsilon,J)]d\epsilon dJ \tag{3.57}$$

IV.2 *Slow Relaxation of ϵ, Fast Relaxation of J*

The J-averaged microscopic rate coefficient for the i^{th} channel will be given by:

$$\bar{k}^{i}(\epsilon) = \frac{\int_{J_0}^{\infty} dJ\ [\omega+k(\epsilon,J)]^{-1}\ f(J)\ k^{i}(\epsilon,J)}{\int_{0}^{J_0} dJ\ f(J)\omega^{-1} + \int_{J_0}^{\infty} dJ\ f(J)[\omega+k(\epsilon,J)]^{-1}} \tag{3.58}$$

The one-dimensional J-averaged master equation, Eq.(3.17), is then solved with the understanding that $\bar{k}(\epsilon) = \sum_i \bar{k}^{i}(\epsilon)$, and k_{uni}^{i} is evaluated as:

$$k_{uni}^{i} = \int\bar{k}^{i}(\epsilon)\bar{g}(\epsilon)d\epsilon / \int\bar{g}(\epsilon)d\epsilon \tag{3.59}$$

For the solution of the low-pressure multichannel problem, the *overall* k_o has the same definition as in Eq.(3.29): the total rate of collisional activation from the non-equilibrium population $\bar{g}(\epsilon)$ to states above the reaction threshold $\epsilon_o(J)$ [or $J_o(\epsilon)$].

For the i^{th} channel, the low-pressure rate coefficient is given by:

$$k_0^i = \int_0^{E_0} \bar{g}(\epsilon)\left[\int_0^{\infty}[1-Z(\epsilon')]P(\epsilon',\epsilon)\bar{p}_i(\epsilon')d\epsilon'\right]d\epsilon \;/\; \int_0^{E_0} \bar{g}(\epsilon)\,d\epsilon \qquad (3.60)$$

where $\bar{p}_i(\epsilon)$ is the probability of reaction occuring via the i^{th} channel in the low-pressure limit, and is given by:

$$\bar{p}_i(E) = \lim_{\omega\to 0} \bar{k}^i(E) \;/\; \bar{k}(E) \qquad (3.61)$$

Eqs.(3.60) and (3.61) are a straightforward extension of earlier work (Greenhill *et al.* 1986).

IV.3 *Slow Relaxation of* ϵ *and* J

The multichannel equivalent to Eq.(3.41) for the J-averaged microscopic rate coefficient is:

$$\bar{k}^i(\epsilon) = \frac{\displaystyle\int_{J_0(\epsilon)}^{\infty} dJ\ [\omega+k(\epsilon,J)]^{-1}\ H(\epsilon,J)\ k^i(\epsilon,J)}{\displaystyle\int_0^{J_0(\epsilon)} dJ\ H(\epsilon,J)\omega^{-1} + \int_{J_0(\epsilon)}^{\infty} dJ\ H(\epsilon,J)[\omega+k(\epsilon,J)]^{-1}} \qquad (3.62)$$

where $H(\epsilon,J)$ is evaluated as before [Eq.(3.40)]. The J-averaged master equation, Eq.(3.17), is solved using the total $\bar{k}(\epsilon)$ to obtain $\bar{g}(\epsilon)$ and the overall k_{uni}, whereupon k_{uni}^i is evaluated from Eqs.(3.62) and (3.59).

For the low pressure limit, Eq.(3.45) is solved as before. k_0^i is then evaluated from

the equation:

$$k_0^i = \int_0^{E_0} \bar{g}(\epsilon) \left[\int_0^{\infty} [1-Q(\epsilon',\epsilon)]P(\epsilon',\epsilon)p_i(\epsilon')d\epsilon' \right] d\epsilon \Big/ \int_0^{E_0} \bar{g}(\epsilon)\, d\epsilon \qquad (3.63)$$

where $p_i(\epsilon)$ is evaluated from Eq.(3.61) with the $\bar{k}^i(\epsilon)$ therein given by Eq.(3.62).

It can be seen that calculation of k_0^i via a J-averaged one-dimensional master equation requires a knowledge of the J-averaged microscopic rate coefficients $\bar{k}_i(\epsilon)$. The only alternative to this approach is to solve the full two-dimensional low-pressure-limiting master equation. This equation and its formal solution have been discussed by Just and Troe (1980). They point out that none of the analytical solutions to the master equation are able to cope adequately with angular momentum effects in multichannel reactions. An exact numerical solution would require considerable computational resources and, whilst worthwhile as a test of faster and easier solutions, would be of limited utility. In the light of these considerations, Just and Troe suggest a simplified analytical solution to the multichannel problem [Just and Troe 1980, Eq. (37) therein]. Straightforward algebra shows that their solution is equivalent to that of the full two-dimensional low-pressure master equation in the case where P(J,J') may be represented by a delta function, $\delta(J-J')$: i.e., the transfer of angular momentum in collisions with the bath gas is negligible. Such an approximation, however, is unlikely to be a good physical description of the dynamics of collisions, since cross sections for rotational energy transfer are generally found to be *larger* than those for vibrational energy transfer: it is therefore highly unlikely for collisions to exchange vibrational energy but not angular momentum.

IV.4 *Application to 1-iodopropane Multichannel Dissociation*

A number of the reactions studied in the present work are multichannel systems. For example, the chemical activation reactions studied in Chapters 2 and 4, *viz.* that of CH_3^+ with NH_3 and that of CH_3^+ with CH_3CN, are multichannel systems which, because of the

sensitivity of ion–molecule reactions to angular momentum effects, could not have been modelled without the solutions to the two-dimensional master equation for multichannel reactions developed in this chapter. Both of these reactions require use of the solution for weak collisions in ϵ and J (Section IV.3).

As an example of a multichannel dissociation where the average angular momentum will not be as large, and hence the rotational relaxation is better modelled with strong collisions, sample calculations for the thermal dissociation of 1–iodopropane are presented. This reaction provides a useful model for an illustrative calculation on the effects of angular momentum conservation for multichannel reactions in the fall–off regime, since it has been well studied experimentally (Gaynor *et al.* 1978; King *et al.* 1971) and its two channels are such that one should show only minor J–conservation effects but the other should show large ones. The results show that the effect of angular momentum conservation on the branching ratios can be even more dramatic than its effect on the size of the overall rate.

The two channels are the elimination of hydrogen iodide (channel 1) and bond fission to produce iodine (channel 2):

$$\begin{aligned} &CH_3CH_2CH_2I \rightarrow C_3H_6 + HI; && E_o(1)= 203 \text{ kJ mol}^{-1} \\ &CH_3CH_2CH_2I \rightarrow C_3H_7 + I \rightarrow CH_3 + C_2H_4 + I; && E_o(2) = 221 \text{ kJ mol}^{-1} \end{aligned} \qquad (3.64)$$

The RRKM parameters used in the calculation are detailed in Appendix F. The elimination involves a four–centre transition state and, since $I^{\dagger}/I \approx 1$, is relatively insensitive to angular momentum effects. The frequencies for both transition states were as used by Gaynor *et al.* (1978), with a minor modification of the lowest frequency for the elimination channel to fit the high–pressure A–factor. The bond fission channel occurs via a simple–fission transition state. The optimal method of treating such a reaction is to use microcanonical variational theory (see Chapter 1, and references therein), which has multiple (ϵ– and J–dependent) transition states. However, for the purpose of the present

illustrative calculation a single transition state, taken at a separation of 3.18 Å (King *et al.* 1971), is used. This allows the high-pressure Arrhenius parameters for this channel (Gaynor *et al.*, 1978; King *et al.* 1971) to be reproduced.

In solving the master equation it is necessary to specify the probability function for collisional energy transfer, $P(\epsilon,\epsilon')$. In addition, certain multichannel systems have pressure-dependent behaviour which is sensitive to the nature of $P(\epsilon,\epsilon')$ (Chow and Wilson 1962). For the present illustrative purposes, we have chosen to use (i) the simple "exponential down" form with the average downward energy transfer $\langle\Delta\epsilon_{down}\rangle$ = 500 cm^{-1}, and (ii) the form specified by the "biased random walk" model (Gilbert 1984; Lim and Gilbert 1986) with the same $\langle\Delta\epsilon_{down}\rangle$. Comparison of the calculated pressure dependence for the two different forms of $P(\epsilon,\epsilon')$ will indicate whether the 1-iodopropane reaction has pressure-dependent behaviour which is sensitive to the assumed form of $P(\epsilon,\epsilon')$.

For comparative purposes, the pressure dependence of the thermal rate coefficients for the two channels was calculated by the "strong J" method of Section IV.2 and by the use of Eq.(3.24) (hitherto the only method available for incorporation of J effects into the multichannel master equation). Calculations were carried out for a temperature of 1000K. Figure 3.8 presents the fall-off curves for the two channels. Both methods produce the same high-pressure limiting behaviour, since Eq.(3.24) takes correct account of angular momentum behaviour at high pressures. At intermediate and low pressures, however, Eq.(3.24) results in a large error.

The effect of angular momentum conservation is qualitatively different for the two channels. For channel 1 (elimination), incorporating angular momentum conservation slightly *reduces* the predicted rate coefficient in the fall-off region. This is because $I^{\dagger}<I$ for the four-centre transition state. Conservation of angular momentum throughout the reaction therefore requires that the external rotational mode acquire extra energy from the internal modes as the transition state is approached, thus reducing the amount of energy

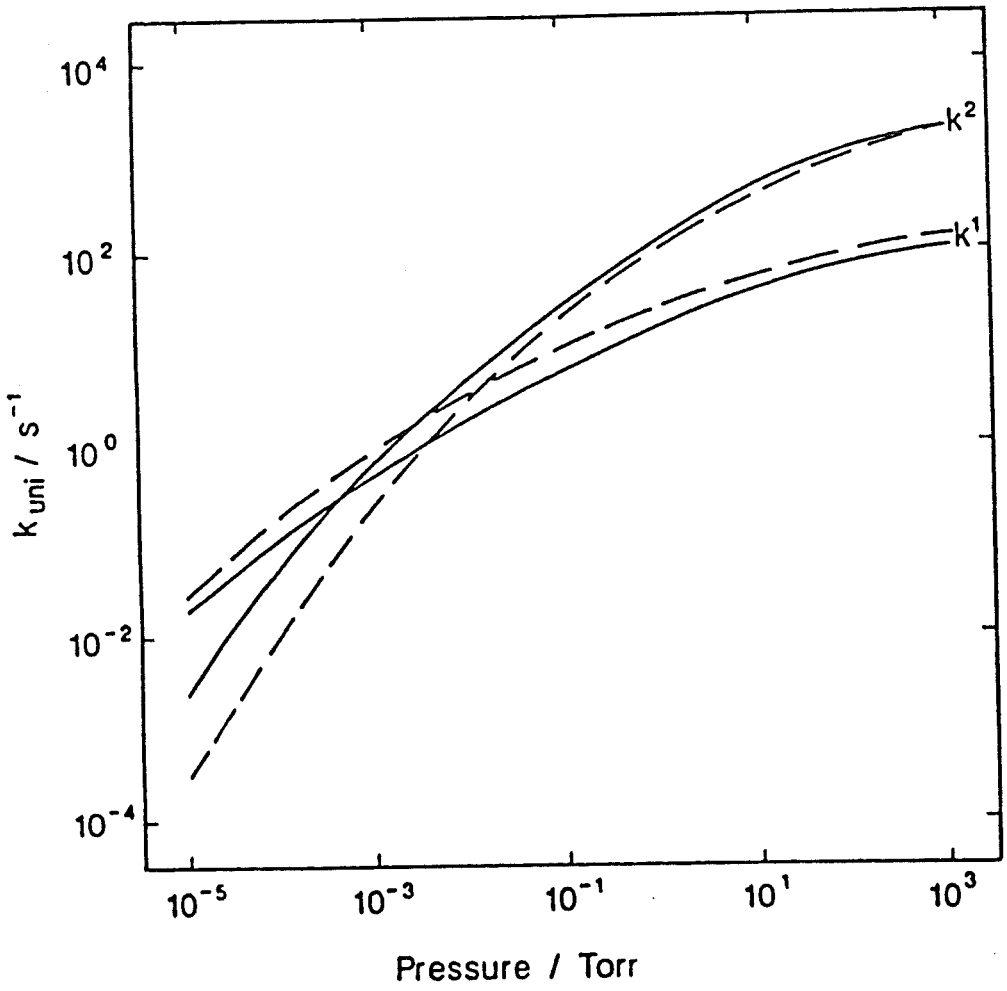

Figure 3.8. Pressure dependence of k_{uni}^1 and k_{uni}^2 for the two-channel dissociation of 1-iodopropane at 1000K. The solid lines are from solution of the two-dimensional master equation where rotational relaxation has been treated as fast. The dashed lines were calculated by solution of the one-dimensional master equation which does not conserve angular momentum in the fall-off regime.

available for barrier crossing (Section I and references therein).

In the case of channel 2 (bond fission), incorporation of angular momentum conservation dramatically *enhances* the predicted rate of reaction in the fall-off regime, since $I^{\dagger} > I$ for the simple-fission type transition state. Conservation of angular momentum then requires that energy be released from the external inactive rotational mode into the internal modes, thus increasing the amount of energy available for barrier crossing (Section I and references therein). Thus, in the fall-off regime, the *different* way in which J-conservation affects the calculated rates for the elimination and simple-fission channels causes a major change in the predicted branching ratio (k_{uni}^{1} / k_{uni}^{2}).

In order to determine whether the 1-iodopropane reaction will exhibit pressure dependence which is sensitive to the assumed form of $P(\epsilon,\epsilon')$, the branching ratio for this reaction was calculated as a function of pressure for the two differing forms of $P(\epsilon,\epsilon')$ specified above. The branching ratios are indistinguishable within the bounds of experimental error throughout the pressure range of Figure 3.8, indicating that the fall-off behaviour of the reaction is insensitive to the precise form chosen for $P(\epsilon,\epsilon')$. Modelling of basic fall-off data is therefore unlikely to provide information beyond the first moment of the distribution, $<\Delta\epsilon_{down}>$. It has been shown (King *et al.* 1981), however, that certain multichannel reactions do exhibit fall-off behaviour which is sensitive to the functional form for $P(\epsilon,\epsilon')$ when studied under conditions where both weak (gas/gas) and strong (gas/wall) collisional activation contributes to reaction (the technique of pressure-dependent very low-pressure pyrolysis, VLPP).

The low-pressure limiting rate coefficients, calculated using the method for fast relaxation of J and slow relaxation of ϵ above [Eqs.(3.26)-(3.29), (3.58), (3.60), and (3.61)], are compared in Table 3.1 with those calculated from the appropriate generalisation to multichannel reactions of the J-independent low-pressure master equation [Greenhill *et al.* 1986: Eqs.(18) and (19) therein]. The method of this work including J conservation is labelled A and the J-independent method is labelled B. The branching

ratios (k_o^1 / k_o^2) are also given. It can be seen that the latter method produces gross errors at lower pressures. This can be understood qualitatively by considering the effect of angular momentum on the threshold energy for reaction $\epsilon_o(J)$.

The reaction threshold (the minimum internal energy, ϵ, at which reaction can occur for a given J) can be represented on a plot with axes ϵ and J (Penner and Forst 1975,1976). Figure 3.9a is a schematic plot of the threshold lines, plotted as functions of the rotational energy R, for the multichannel reaction studied in this work. For reasons explained above, the threshold for channel 1 (elimination) increases with J, whereas the threshold for channel 2 (simple-fission dissociation) decreases with J. A molecule which has a state in the region below the threshold line for channel i will have insufficient energy to react through channel i. At low pressures, the population outside the shaded region (i.e. where $k(\epsilon,J) > 0$) is negligible, and the total rate of reaction is the rate at which molecules are collisionally activated to levels outside the shaded region. Channel 1 has the lower threshold for small J. However, this situation is reversed at somewhat larger J, and so the second channel makes a small but still significant contribution to reaction in the low-pressure limit.

	k_0^1 /10^{11} $cm^3mol^{-1}s^{-1}$	k_0^2 /10^{11} $cm^3mol^{-1}s^{-1}$	B.R.
B	2.56	0.003	992
A	1.88	0.14	13.7

Table 3.1. Low-pressure rate coefficients at 1000 K for multichannel 1-iodopropane dissociation: channel 1 (k_o^1), channel 2 (k_o^2) and branching ratio (B.R. = k_o^1 / k_o^2). Rate coefficients calculated using J-averaged method of sections II.2b and IV.2 (slow relaxation of ϵ, fast relaxation of J, labelled A) and using the J-independent master equation solution (which does not include angular momentum effects outside the high-pressure limit, labelled B).

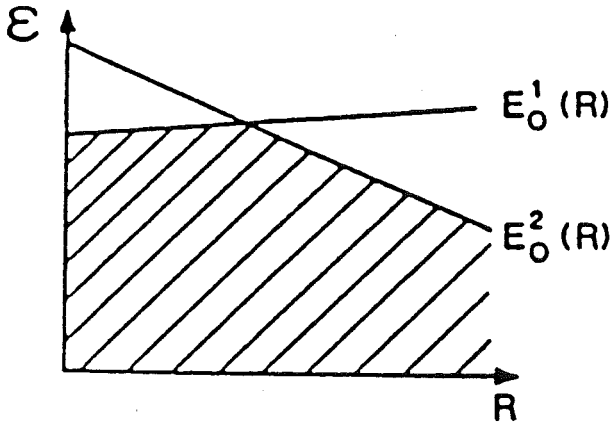

Figure 3.9a. Schematic plot of the reaction thresholds ϵ_o^1 and ϵ_o^2 for the two-channel dissociation of 1-iodopropane. Channel 1 is the elimination of HI, channel 2 is the loose transition state for the iodine-carbon bond fission. The shaded region represents the states that are stable with respect to dissociation.

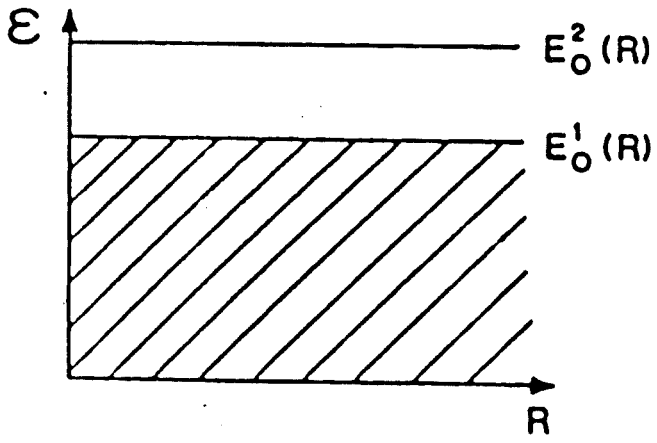

Figure 3.9b. Schematic plot of the reaction thresholds that are assumed for the two-channel dissociation of 1-iodopropane in the J-independent solution of the (one-dimensional) master equation. Threshold lines and shaded region are as defined in Figure 3.9a.

Figure 3.9b shows schematically the corresponding thresholds for the J-independent calculation. The thresholds are here assumed to be independent of angular momentum, and so channel 1 always has the lowest threshold. The rate of reaction is again the rate at which collisions activate molecules to levels outside the shaded region. The difference between the two barriers is *ca.* 1500 cm^{-1}, and since the average energy transfer is considerably less than this, the calculation erroneously produces a very large branching ratio ($k_o^1 \gg k_o^2$).

The illustrative calculations presented above indicate that proper account of angular momentum conservation is essential in the interpretation of multichannel data in the falloff regime. Just and Troe (1980) have presented representative calculations of branching ratios in the fall-off regime using an approximate strong collision treatment. Whilst similar qualitative conclusions to those of the present paper may be drawn from their work, the very approximate nature of their calculations excludes a meaningful comparison with fall-off curves calculated using the current method.

V. Summary

In the current chapter, the problem of including angular momentum effects into the calculation of unimolecular rate coefficients has been addressed. The solution for reactions exhibiting strong collisions is well known (see, e.g., Marcus 1965; Waage and Rabinovitch 1970). Methods available hitherto for solving the master equation with J-conservation apply only to the low pressure limit: Troe (1977,1987a) has developed a solution for weak collision, exponential transition probabilities $P(\epsilon,\epsilon')$ and P(R,R'), and Penner and Forst (1975,1976) have developed a more limited solution which applies to cases where $P(\epsilon,\epsilon')$ is essentially a delta function.

It is shown that the two-dimensional master equation may be exactly reduced to a one-dimensional "J-averaged" master equation involving a microscopic rate coefficient

$\bar{k}(\epsilon)$ which is an average of the $k(\epsilon,J)$ over the angular momentum distribution pertaining in the reaction. This distribution may be determined exactly when $P(J,J')$ is dependent only on the final state J [as is the case for $P(J,J')=f(J)$, the strong collisional form], and perturbatively when $P(J,J')$ is dependent rather on the difference between the initial and final states, $(J-J')$ (i.e., a weak collisional form).

An important category of solution to the two-dimensional master equation has been developed (Section II.2) which models the internal energy relaxation with weak collisions and the rotational relaxation with strong collisions (or, more generally, a form for $P(J,J')$ which is independent of the initial angular momentum J'). In many reactions (*viz.*, most neutral dissociation and recombination reactions, and essentially all reactions with polyatomic bath gases), the nature of angular momentum transfer in collisions is best approximated with a form for $P(J,J')$ which is independent of the intital state.

The other major category for which a solution has been developed is when the collisional relaxation of both ϵ and J is weak. This solution, which models both $P(\epsilon,\epsilon')$ and $P(R,R')$ with weak collisions (Section II.3), may be compared in the low-pressure limit with the best alternative solution to this problem (Troe 1977a, 1987a). Comparison shows that that the Troe solution accurately determines the non-equilibrium population for this problem. However, Troe's analytic formula for β overestimates, by up to a factor of 2, the rate coefficient. Improvements to the Troe formula for β have been derived (Section III and Appendix E) which give good agreement with the present solution.

Importantly, the solutions which have been developed above apply throughout the fall-off regime. This allows one to calculate rate coefficients at any pressure without recourse to approximate interpolation techniques (e.g., Troe 1983, Gilbert *et al.* 1983).

The extension to multichannel reactions of the solutions developed is straightforward. This allows multichannel dissociation and, with the relationships developed in chapter 2, chemical activation reactions to be rigorously treated with full account of angular

momentum conservation.

Angular momentum conservation is especially important for ion–molecule reactions. In these reactions, the long range potential causes $I^{\dagger}$ to be much larger than I, making the microscopic rate coefficients $k(\epsilon,J)$ particularly sensitive to J.

CHAPTER 4

MICROSCOPIC RATE COEFFICIENTS FOR ION-MOLECULE REACTIONS

Chapters 1-3 have considered the calculation of thermal rate coefficients for unimolecular dissociation, recombination (association), and chemical activation reactions via solution of the master equation. The input to the master equation consists of the microscopic rate coefficients $k(\epsilon,J)$ and parameters describing the collisional energy transfer. Some consideration of the calculation of microscopic rate coefficients for ion-molecule reactions is necessary, since the usual RRKM method requires modification for these reactions.

The importance of calculating microscopic rate coefficients *variationally* via microcanonical variational transition state theory (μVTST) has been discussed previously by a number of authors (see, e.g., Truhlar and Garrett 1984; Garrett and Truhlar 1979; Bunker and Patengill 1968; Hase 1976; Quack and Troe 1977; Chesnavich *et al.* 1981; Chesnavich 1984). This involves choosing a transition state variationally for each separate (ϵ,J) value: one does this by calculating $k(\epsilon,J)$ (in practice, the sum of states $W^{\dagger}$) at a range of separations of the moieties and choosing as the transition state that which gives the minimum value for $k(\epsilon,J)$.

A quantity often used for comparison of theories is the capture rate (i.e.,the high pressure limiting association rate), since this depends only on $k(\epsilon,J)$. Use of μVTST in calculating the microscopic rate coefficients has a significant effect on calculated capture rates, particularly at high temperatures.

In section I, ion/induced-dipole reactions are considered. It is shown that, provided the transition state is chosen microcanonically to be at the position of the centrifugal barrier, the RRKM treatment reduces exactly to the same high pressure association rate (i.e., capture rate) as predicted by the simple Langevin capture model (Langevin 1905).

The calculation of microscopic rate coefficients for ion–dipole reactions is considered in section II. The hindrance to the rotation of the dipole has a very important effect on $k(\epsilon,J)$. An exact method of incorporating this effect into an RRKM calculation is developed (section II.1).

A physical constraint on the dynamics of reactive trajectories which is accounted for in capture models but not in RRKM theory is the absence of coupling between of many degrees of freedom and the reaction coordinate on the long range, electrostatic part of the potential surface. Simply, this means that at large separation the energy in these modes is unavailable for motion along the reaction coordinate (i.e., barrier crossing), due to the absence of coupling. Capture theories (of which the Langevin model is the simplest) account for this implicitly by not including degrees of freedom that are not involved in the dynamics of long range electrostatic capture. In section II.2 a modification to the standard RRKM derivation of the microscopic rate coefficient is presented which produces an expression for $k(\epsilon,J)$ that incorporates such uncoupling. The complete uncoupling of certain degrees of freedom from the reaction coordinate at long–range is a restricted example of an adiabatic constraint. The new derivation utilises principles inherent in the Statistical Adiabatic Channel Model (SACM) (Quack and Troe 1974,1977; Troe 1983b) and also the work of Marcus and co–workers (see, e.g., Wardlaw and Marcus 1987). It is then illustrated (section II.3) that the capture expression which results on thermal averaging of our new formula for $k(\epsilon,J)$ is formally equivalent to that derived in the capture model of Chesnavich *et al.* (1980), with the difference that their model does include angular momentum conservation.

The modelling of the CH_3^+/NH_3 chemical activation reaction (see Chapter 2) is briefly reconsidered in the light of the adiabatic and variational effects considered in the present chapter.

Application to the chemical activation reaction between CH_3^+ and CH_3CN is presented in section II.4. Rate data spanning the fall–off regime have been obtained using the SIFT

technique (Knight *et al.* 1986) and ICR (McEwan *et al.* 1989). In this reaction correct treatment of the dipole is essential as methyl cyanide has a very large permanent dipole (3.98 Debye). The importance of correct incorporation of the effect of the dipole moment is apparent from comparison of results obtained with the present technique (which incorporates the dipole hindrance) and those obtained by use of Phase Space Theory (Herbst 1988), which treats the reacting fragments as freely rotating (Chesnavich and Bowers 1976,1977).

A quantity which is of interest in chemical activation and association reactions is the average lifetime of the collision complex in the low density limit. This gives an indication of the probability of occurrence of other non-collisional processes such as radiative stabilisation. Section III details the results of lifetime calculations for some of the ion-molecule reactions which have been studied in this work. These results indicate that the lifetimes of some ionic collision complexes may be very much longer than previously estimated. Long lifetimes with regard to unimolecular dissociation permit radiative stabilisation to become a major cause of stabilisation of the complex, a conclusion which has some significance at the low temperatures and pressures of interstellar clouds.

I. Ion/Induced-Dipole Reactions

The class of ion/induced-dipole reactions is the simplest to treat since the transition states occur (except at high energies) at separations of the reactant moieties large enough that anisotropies in the potential due to chemical forces or steric interaction are negligible. The potential of interaction is therefore central and the separate moieties are free rotors: the transition state parameters are simply those of the separate reactants. The central nature of the potential and the large separation of the moieties implies that the eigenvalues of active modes of the transition state (i.e., the density of states) will be independent of the position of the transition state, so long as it occurs at a sufficiently large separation where the long-range electrostatic forces will dominate. The significance of this is that variational selection will always result in choosing the transition state at the

centrifugal barrier, since, in the absence of changes in the state density pattern with separation, the maximum in the effective potential will always be the position of the minimum sum of states. This is illustrated schematically in Figure 4.1.

Given that, for this ion/induced-dipole case, the variationally chosen transition state is at the position of the centrifugal barrier for any given angular momentum, it is intuitively to be expected that the RRKM treatment will lead to the same high pressure association rate as the simple Langevin capture model. This is because implicit in RRKM theory is the transition state assumption: all trajectories passing through the transition state surface are assumed to go on to react. The positioning of the transition state then implies that, for a given angular momentum, all trajectories with enough energy to surmount the centrifugal barrier are assumed to go on to react. This is identical to the capture assumption involved in the Langevin model.

The equivalence of the statistical approach to the Langevin approach for

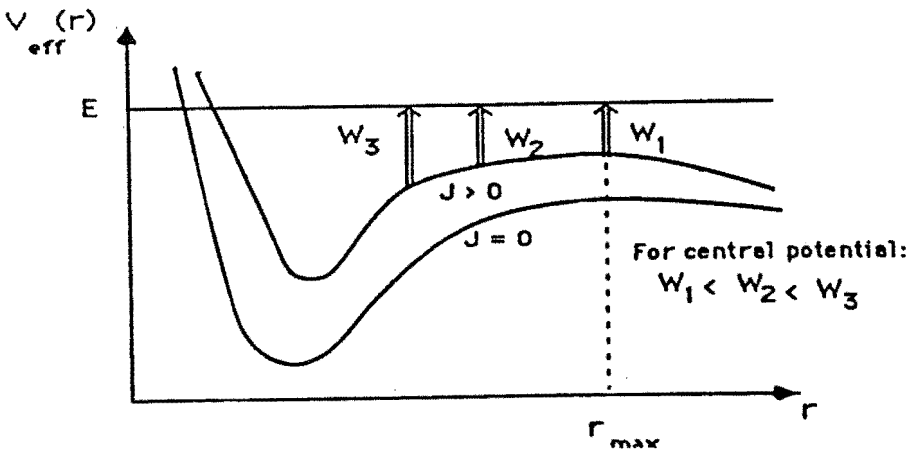

Figure 4.1. Schematic representation of the scheme for microcanonical variational selection of the minimum sum of states in the case of a central potential. For a central potential, the density of states will be the same at each of W_1, W_2 and W_3. Hence the minimum sum of states will always fall at the maximum in the effective potential, where the sum is over the smallest amount of energy.

ion/induced-dipole reactions has been demonstrated before by Chesnavich and Bowers (1982) with Transition State Theory and by Troe (1985) in terms of the Statistical Adiabatic Channel Model. The new proof presented below in terms of RRKM theory is included as it provides useful insight into the connection between the RRKM approach and the capture approach in the limit of a central potential.

Recall from Chapters 1 and 3 that the RRKM result for the microscopic rate coefficient, expressed in terms of the internal energy ϵ and the rotational energy R [= BJ(J+1)], is:

$$k(\epsilon,R) = W^{\dagger}(\epsilon,R)/h\rho(\epsilon) \quad , E > V_{eff}(r_m) \tag{4.1}$$

where $E = \epsilon + R$, and $W^{\dagger}(\epsilon,R)$ is a sum of states for the transition state (see, e.g., Forst 1973) located at a distance s:

$$W^{\dagger}(\epsilon,R) = \int_0^{\epsilon+R-V_{eff}(s)} \rho^{\dagger}(E_+)\, dE_+ \tag{4.2}$$

In general, the position s in Eq. (4.2) will be determined variationally as that which gives the minimum value for $k(\epsilon,J)$. For an ion/induced-dipole system, this will be the position of the centrifugal maximum, r_m, since (for all except high energies and high angular momenta) the minimum sum of states $W^{\dagger}$ will be at this barrier, as explained above. The high-pressure dissociation rate is the thermal average of $k(\epsilon,R)$:

$$k_{uni} = \int\int d\epsilon dR\; k(\epsilon,R)f(\epsilon,R) \tag{4.3}$$

where

$$f(\epsilon,R) = \rho(\epsilon)\exp[-(\epsilon+R)/k_BT] \;/\; k_BTQ_i \tag{4.4}$$

and Q_i is the partition function for the active modes of the molecule. Substituting

Eqs.(4.1), (4.2) and (4.4) into Eq. (4.3), one obtains:

$$k_{uni}^{\infty} = \int_0^{\infty} dR \, \frac{e^{-R/k_BT}}{k_BT} \left[\int_{V_{eff}(r_m)-R}^{\infty} d\epsilon \frac{\rho(\epsilon) e^{-\epsilon/k_BT}}{Q_i} \left[\frac{1}{h\rho(\epsilon)} \int_0^{\epsilon+R-V_{eff}(r_m)} dE_+ \rho^{\dagger}(E_+) \right] \right] \tag{4.5}$$

where it is assumed that $k(\epsilon,R)$ has been evaluated at the centrifugal barrier. Straightforward simplification of this expression leads to:

$$k_{uni}^{\infty} = \frac{1}{hQ_i k_BT} \int_0^{\infty} dR \, e^{-R/k_BT} \left[\int_{V_{eff}(r_m)-R}^{\infty} d\epsilon e^{-\epsilon/k_BT} \left[\int_0^{\epsilon+R-V_{eff}(r_m)} dE_+ \rho^{\dagger}(E_+) \right] \right] \tag{4.6}$$

One then alters the order of integration to obtain:

$$k_{uni}^{\infty} = \frac{1}{hQ_i k_BT} \int_0^{\infty} dR e^{-R/k_BT} \left[\int_0^{\infty} dE_+ \rho^{\dagger}(E_+) \left[\int_{E_+ + V_{eff}(r_m)-R}^{\infty} d\epsilon e^{-\epsilon/k_BT} \right] \right] \tag{4.7}$$

Note that this inversion depends on the fact that the transition state lies at the centrifugal barrier, since if variational effects draw it away from the barrier then $\rho^{\dagger}$ would not be independent of ϵ. The inner integral is straightforward, giving:

$$k_{uni}^{\infty} = \frac{1}{hQ_i} \int_0^{\infty} dR \, e^{-V_{eff}(r_m)/k_BT} \int_0^{\infty} dE_+ \, \rho^{\dagger}(E_+) e^{-E_+/k_BT} \tag{4.8}$$

(note that r_m is a function of R). The second integral in Eq. (4.8) is the partition function of the moieties in the transition state. Since these moieties are completely separate in the transition state, this second integral is simply the partition function for separate reactants $Q_A Q_B$. Re-locating the zero-point energy of the transition state relative to the critical (i.e., dissociation) energy of the two moieties, E_0, one obtains:

$$k_{uni}^{\infty} = \frac{Q_A Q_B}{hQ_i} e^{-E_0/k_BT} \int_0^{\infty} dR\ e^{-[V_{eff}(r_m)-E_0]/k_BT} \tag{4.9}$$

The integral is evaluated using the Langevin interaction potential:

$$V_{eff}(r) - E_0 = -(q^2\alpha/8\pi\epsilon_0 r^4) + (I/mr^2)R \tag{4.10}$$

where q is the electronic charge, α the polarizability of B and ϵ_0 the permittivity of free space. The usual Langevin treatment gives for the effective potential at the centrifugal maximum:

$$V_{eff}(r_m)-E_0 = 2\pi\epsilon_0 I^2R^2/(q^2m^2\alpha) \tag{4.11}$$

Substituting Eq. (4.11) into Eq. (4.9) and multiplying the resultant k_{uni}^{∞} by the equilibrium constant:

$$K_{eq} = \frac{(k_BT/B)Q_i}{Q_{rt}\ Q_A\ Q_B} e^{-E_0/k_BT} \tag{4.12}$$

[where Q_{rt} is the relative translational partition function for the reactants (containing the reduced mass)], one obtains for the capture rate:

$$k_{rec}^{\infty} = 2\pi q(\alpha/4\pi\epsilon_0 m)^{\frac{1}{2}} \tag{4.13}$$

This is identical to the Langevin rate coefficient calculated directly from the rate of capture across the centrifugal barrier.

From this result, we may conclude that RRKM theory will be sufficiently accurate for application to ion/induced-dipole reactions, since the Langevin result is generally accepted as a good approximation to the dynamics of such reactions at low energies. It should be noted, however, that for the case of polyatomic moieties interacting with a central potential, it is possible to take more exact account of angular momentum conservation by

including, in addition to the orbital angular momentum L, the contribution to the total angular momentum J of the individual angular momenta of the separate moieties, J_1 and J_2. This approach, generally termed Phase Space Theory (PST), has been developed for polyatomic species by Chesnavich and Bowers (1976,1977).

II.1 Ion-Dipole Reactions

The application of RRKM theory to ion–dipole reactions is somewhat more complicated. The main difficulty is the non–central nature of the electrostatic potential, which implies that the rotation of the dipole is not free, but rather hindered by a sinusoidal potential. This effect has been discussed by several authors (Chesnavich *et al.* 1980; Troe 1985,1987b; Clary 1985). All of these approaches have, however, been capture models. A capture model calculates the rate of electrostatic capture of the neutral by the charged species, and therefore explicitly excludes all degrees of freedom within the molecules that are not involved in the dynamics of electrostatic capture. In order to calculate a microscopic rate coefficient for unimolecular decomposition (e.g., as required for calculation of fall–off curves and lifetimes), however, one necessarily deals with *all* active degrees of freedom of the molecule. The capture models therefore predict only the high pressure limiting association rate, and a means of including the dipole hindrance into Eq. (4.2) (or the equivalent sum of states in PST) is required before the pressure dependence of such reactions can be accurately modelled. We now proceed to develop a method for this.

The electrostatic potential is written:

$$V(r,\theta) = E_o - (q\mu\cos\theta/r^2 + q^2\alpha/2r^4) \;/\; 4\pi\epsilon_o \qquad (4.14)$$

where q is the charge on the ion, μ is the dipole moment and α the polarizability of the neutral, ϵ_o the permittivity of free space, and θ the angle of orientation of the dipole

with respect to the axis between the two moieties, illustrated in Figure 4.2.

In Eq. (4.14) r, the reaction coordinate, is fixed for the purposes of evaluating the density of states at the transition state. It will then be apparent that the non-central interaction between an ion and a dipolar molecule can be treated as a two-dimensional hindered rotor, whose interaction potential is sinusoidal in the angle of orientation. The evaluation of $k(\epsilon,J)$ therefore requires the density or sum of states for a system which includes such a sinusoidal hindered rotor. An exact semi-classical result is now deduced for the density of states of this system.

Firstly, the partition function for a two-dimensional sinusoidally-hindered rotor is evaluated. The Hamiltonian is:

$$H_{rot} = \frac{1}{2I}\left[P_\theta^2 + \frac{P_\varphi^2}{\sin^2\theta}\right] + \frac{V_0}{2}(1-\cos\theta) \qquad (4.15)$$

where θ, φ, P_θ and P_φ are the angular coordinates and their corresponding momenta. For an ion-dipole interaction, $V_0 = 2q\mu/4\pi\epsilon_0 r^2$. Evaluating the integral of $\exp(-H_{rot}/k_BT)$ over phase space, one obtains the semi-classical partition function for the hindered rotor:

$$Q_{hr} = \frac{(k_BT)^2}{B_{hr}V_0}\left[1-\exp(-V_0/k_BT)\right] \qquad (4.16)$$

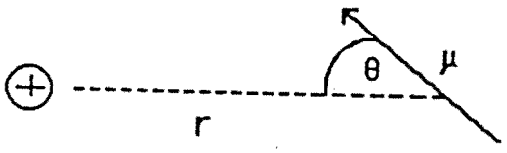

Figure 4.2. Illustration of the definition of θ and r for an ion/dipole system.

B_{hr} being the rotational constant of the hindered rotor. Taking the inverse Laplace transform of Q_{hr} yields the semi-classical result for the density of states:

$$\rho_{hr}(\epsilon) = \epsilon/B_{hr}V_o \quad , \epsilon \leq V_o \qquad (4.17)$$
$$= 1/B_{hr} \quad , \epsilon > V_o$$

It is also possible to derive this result from a direct integral over the phase space of the two-dimensional rotation, constrained by a delta function in the energy. This alternative derivation is presented in Appendix G. For later reference, it may be noted at this stage that the sum of states for a sinusoidally hindered two-dimensional rotor, obtained by integrating Eq. (4.17) over energies, has the form:

$$W_{hr}(\epsilon) = \epsilon^2/2BV_0, \quad \epsilon < V_0;$$
$$= (\epsilon - V_0/2)/B, \quad \epsilon > V_0 \qquad (4.18)$$

The total rotational density of states of the system is obtained by convoluting the density of states of the hindered rotor with the density of states of free rotors (Astholz *et al.* 1979). For a system with p two-dimensional free rotors, s one-dimensional free rotors and one sinusoidally-hindered rotor, one obtains:

$$\Omega(\epsilon) = \frac{\Gamma(1/2)^s}{\Gamma[p+(s/2)+2]}\left[\prod_{i=1}^{s}\left(\frac{1}{B_i}\right)^{\frac{1}{2}}\right]\left[\prod_{n=1}^{p}\left(\frac{1}{B_n}\right)\right]\left[\frac{1}{B_{hr}V_o}\right]\epsilon^{p+(s/2)+1}$$

$$\rho_r(\epsilon) = \Omega(\epsilon) \quad , \epsilon < V_o \qquad (4.19)$$
$$\rho_r(\epsilon) = \Omega(\epsilon) - \Omega(\epsilon - V_o) \quad , \epsilon > V_o$$

where B_{hr} is the rotational constant of the hindered rotor. This result enables the effect of the hindrance to the dipole rotor in the transition state to be easily incorporated into a standard RRKM program, as an extension of the method of Astholz *et al.* (1979). This procedure involves convolution of the rotational density of states with vibrational modes through the Beyer-Swinehart direct count algorithm (1973).

II.2 The Effect of Uncoupled Modes

It is desirable to establish formally the relationship between the RRKM approach to ion–dipole reactions and the capture approach. This can be done by comparison of the resulting capture rate expressions, as has been done above for ion/induced–dipole reactions. Such a comparison brings a much clearer understanding of the assumptions in each approach and, once the exact relationship has been established, a good test of numerical accuracy and physical applicability.

The words "capture approach" oversimplify the situation: there are a number of ion–dipole capture theories (e.g., Su *et al.* 1978; Chesnavich *et al.* 1980; Sakimoto 1982; Clary 1985; Troe 1985,1987b). The capture model most readily comparable with the RRKM approach is that of Chesnavich *et al.* (1980). This is formulated within the context of μVTST and deals with a reduced number of degrees of freedom (those "pertinent" to long–range ion–dipole capture), determining a "reduced" microscopic rate coefficient, $k_{red}(E)$. Their model does not attempt specifically to include angular momentum conservation.

Before a comparison can be made, it is necessary to consider the precise nature of the assumption, implicit to capture theories, that many degrees of freedom are not involved in the dynamics of electrostatic capture and so may be ignored.

The assertion that certain degrees of freedom are irrelevant to the rate of electrostatic capture will be valid provided those degrees of freedom are unable to exchange energy with the reaction coordinate, and hence unable to affect motion along this coordinate, on the electrostatic part of the potential surface. It is in this restricted sense that the term *adiabatic* is used in the present chapter to describe these modes.

The normal RRKM formulation for $k(\epsilon,J)$ does not explicitly account for the absence of coupling between certain modes and the reaction coordinate from the transition state

out to products. The derivation presented in Chapter 1 of the RRKM microscopic rate coefficient is now presented in more detail, together with a modification which allows for the absence of coupling to the reaction coordinate of some degrees of freedom.

Given the ergodic hypothesis (i.e., that there is sufficiently strong coupling between the active degrees of freedom of the molecule to enable rapid randomisation of energy in the metastable complex), the classical expression for the microscopic rate coefficient, expressed as the ratio of the reactive flux per unit time to the statistical ensemble population, is (see, e.g., Garrett and Truhlar 1979):

$$k(\epsilon,R) = \frac{\int\ldots\int d\Gamma \frac{p_r}{m} \delta(r-s) S[p_r] \chi(\Gamma) \delta(E-H-R^\dagger)}{\int\ldots\int d\Gamma \delta(E-H-R)} \qquad (4.20)$$

H is the total Hamiltonian for the active degrees of freedom in the system, which are represented by Γ. $R^\dagger$ is the external rotational energy which (due to angular momentum conservation) will vary with the separation r of the moieties: $R^\dagger = [I/mr^2]R$, where I is the moment of inertia of the molecule and m the reduced mass at a separation r of the two moieties (Chapter 3). Briefly, the $\delta(E-H-R^\dagger)$ function constrains the integral in the numerator to a constant energy surface ($H + R^\dagger = E$ at all positions r along the reaction coordinate). The $\delta(r-s)$ function defines the numerator as an integral over a surface at r=s which divides the reactant and product regions. $S[p_r]$ is a step function which specifies that only positive momenta p_r be counted (i.e., trajectories passing *from* reactants *to* products). Finally, $\chi(\Gamma)$ is a characteristic function which has the value one for trajectories that go directly on to products without recrossing and zero for trajectories which recross the dividing surface. With the above definitions, the numerator counts trajectories passing from the reactant region to products, consistent with the defined energy and angular momentum. The denominator counts the statistical ensemble population.

χ may be determined in a classically exact fashion by following trajectories computationally (or alternatively making use of the traditional fast student with special

abilities). The advantage of a statistical theory, however, is in avoiding the necessity of large-scale trajectory calculations (and sweating students). It is therefore necessary to seek the optimum prescription for χ within the statistical framework. The transition state assumption which is invoked in RRKM theory assumes that *all* trajectories crossing the dividing surface with positive p_r and sufficient total energy to surmount the centrifugal barrier will go on to react without recrossing. This corresponds to the following definition for $\chi(\Gamma)$:

$$\chi(\Gamma) = S[E-V_{eff}(r_m)] \tag{4.21}$$

Suppose that at large separation of the moieties the Hamiltonian for the active modes is separable into a term H_u for modes which are completely uncoupled from the reaction coordinate (i.e., remain *exactly* unchanged from the transition state all the way out to products) and a term H_c for modes which are coupled to the reaction coordinate. The term H_u is then a conserved quantity from the transition state out to products. Neglecting curvature in the reaction coordinate at the transition state (Marcus 1966: this means that any cross term between p_r and the other coordinates is assumed negligible), one then has:

$$H = p_r^2/2m + H_c + H_u + V(r,\theta=0) \tag{4.22}$$

The partitioning of energy into coupled versus uncoupled modes (i.e., the value of the energy term H_c as opposed to H_u) in dissociating molecules is determined by statistical probability. However, once a trajectory representing a dissociating system has reached the long-range part of the potential surface, the term H_u constitutes a conserved quantity due to the absence of coupling with the reaction coordinate or any of the coupled modes. Hence the term H_u may be included in the effective, or "adiabatic" potential representing energy unavailable for motion along the reaction coordinate. An effective potential $V_{eff}'(r)$ is therefore defined which includes the term H_u:

$$V_{eff}'(r) = V(r,\theta=0) + [I/mr^2]R + H_u$$
$$= V_{eff}(r) + H_u \qquad (4.23)$$

Note that θ is set to zero since, given R and the energy H_u "frozen" in the uncoupled modes, the effective potential defines the *minimum* energy pathway. Furthermore, $V_{eff}'(r)$ is valid as an effective potential *only on the long-range part of the potential surface* [at smaller separations of the reactant moieties, where all of the active modes are coupled, one would use rather the effective potential $V_{eff}(r) = V(r,\theta=0)+(I/mr^2)R]$. $V_{eff}'(r)$ correctly describes the adiabatic long-range potential which the system must surmount in order to react. An improved prescription for χ is therefore obtained by using $V_{eff}'(r_m)$ instead of $V_{eff}(r_m)$ in Eq. (4.21):

$$\chi(\Gamma) = S[E-V_{eff}'(r_m)] \qquad (4.24)$$

The construction of an effective potential in this fashion is in the spirit of the SACM of Quack and Troe (1974,1977). However, it should be noted that this uncoupling approximation is much more restricted than the adicbatic approximation of the SACM. In their theory, Quack and Troe construct adiabatic potentials, or "channels", which include *all* degrees of freedom, even where these degrees of freedom are coupled by the potential surface to the reaction coordinate. Their definition of the term *adiabatic* requires that a particular reactant state correlate directly along an "adiabatic channel" to a specific product state; hence it does not require that a degree of freedom be completely uncoupled from the reaction coordinate. Thus, in the SACM a distinction between coupled and uncoupled modes is not made: all modes are considered adiabatic in a more general sense.

Equation (4.20) reduces to the normal RRKM expression as follows. One notes that the denominator is h^n times the classical density of states for active modes of the reactant $\rho(\epsilon)$ (n being the dimensionality of the system). The numerator is converted to a sum of states of the transition state by carrying out the integration over r (i.e., evaluating the

integrand at the transition state r=s) and changing one variable of integration from p_r to E_r, where $E_r = p_r^2/2m$. With χ as defined in Eq. (4.21), and neglect of curvature in the reaction coordinate at the transition state, one then obtains the standard RRKM result, Eqs.(4.1) and (4.2). For the case where certain modes are uncoupled at long range, denote the number of coupled modes by c and uncoupled by u; one has n = u+c+1 (the last coordinate being the reaction coordinate). With the use of Eq. (4.24) for $\chi(\Gamma)$, the evaluation of Eq. (4.20) proceeds as follows. Invocation of the $\delta(E-H-R^\dagger)$ allows the integral over coordinates Γ to be written as a convolution of sub-integrals over coordinates $\{r,p_r,\Gamma_c\}$ and the coordinates Γ_u for uncoupled modes. Simple substitution for E and $V_{eff}'(r_m)$ in Eq. (4.24) shows that $\chi[E-V_{eff}'(r_m)]$ is equivalent to the constraint that the energy E' available for barrier crossing, $E' = p_r^2/2m + H_c$, must exceed $\Delta V = V_{eff}(r_m)-V_{eff}(r)$. The $\chi[E-V_{eff}'(r_m)]$ term therefore imposes the requirement that E' range from a minimum of ΔV to a maximum $E-V_{eff}(r)$. The corresponding limits on the energy of the uncoupled modes are then defined by energy conservation. This leads to:

$$k(\epsilon,R) = \frac{\int dr \int_{\Delta V}^{E-V_{eff}(r)} dE' \left[h^c \int_0^{E'} dE_r \rho_c^\dagger(E'-E_r)\right] h^u \rho_u^\dagger[E-V_{eff}(r)-E'] \delta(r-s)}{\int \ldots \int d\Gamma \delta(E-H-R)} \qquad (4.25)$$

where the integral over p_r (in the range 0 to ∞ due to the step function $S[p_r]$) has been converted to one over E_r, and the choice of r in order to minimise $k(\epsilon,R)$ has yet to be made. The subscripts on the densities of states imply that these quantities are evaluated with reference to the uncoupled or coupled Hamiltonian at the position r. The term in large parentheses in Eq. (4.25) is the sum of states of the coupled modes evaluated at the position r and at energy E', $W_c^\dagger(E')$. Changing the variable of integration from E' to the energy in the uncoupled modes, $E_u = E-V_{eff}(r)-E'$, one has:

$$k(\epsilon,R) = \frac{\int dr \int_0^{E-V_{eff}(r_m)} dE_u \, W_c^\dagger[E-V_{eff}(r)-E_u] \, \rho_u^\dagger(E_u) \, \delta(r-s)}{h\rho(\epsilon)} \qquad (4.26)$$

It remains now to determine the correct choice of r in order to minimise $k(\epsilon,R)$ variationally. Firstly, one notes that the limits of the inner integral in Eq. (4.26) are independent of r, as is the density of states $\rho_u^\dagger$ for the uncoupled modes, and so the integral over r may be brought within that over E_u, yielding:

$$k(\epsilon,R) = \frac{\int_0^{E-V_{eff}(r_m)} dE_u\ \rho_u^\dagger(E_u) \int dr\ W_c^\dagger[E-V_{eff}(r)-E_u]\delta(r-s)}{h\rho(\epsilon)} \qquad (4.27)$$

The derivation of Eq. (4.27) invokes the assumption that every trajectory with sufficient energy *in the coupled modes* that crosses the dividing surface does so irreversibly. This energy in the coupled modes is $E-V_{eff}(r)-E_u$. Exact variational implementation of Eq. (4.27) therefore requires $W_c^\dagger[E-V_{eff}(r)-E_u]$ be determined variationally *prior* to convolution with $\rho_u^\dagger(E_u)$. Since $W_c^\dagger[E-V_{eff}(r)-E_u]$ in Eq. (4.27) is a function of E_u as well as r, it is apparent that the choice of r to minimise $k(\epsilon,R)$, r=s, will be dependent on the energy E_u in the uncoupled modes. The reactive flux, represented by the numerator of Eq. (4.27), is *not evaluated at a single surface.* Rather, it is a sum (or integral in continuum notation) of terms representing the flux for different allowed values of E_u, each term being determined variationally on a *different* surface $r=s(E_u)$. Evaluating the integral over r in Eq. (4.27) therefore yields:

$$k(\epsilon,R) = \frac{\int_0^{E-V_{eff}(r_m)} dE_u\ \rho_u^\dagger(E_u)\ W_c^\dagger[E-V_{eff}(s)-E_u]}{h\rho(\epsilon)} \qquad (4.28)$$

where s is an implicit function of E_u as discussed above. This is the required result. The numerator of Eq. (4.28) represents the overall sum of reactive states (classically, the flux of reactive trajectories) in the case where a number of modes are completely uncoupled with respect to the reaction coordinate from the transition region out to products. Note that Eq. (4.28) becomes equivalent to the standard RRKM result, Eqs. (4.1) and (4.2), if the transition state is chosen at the centrifugal barrier (i.e., $s=r_m$). Otherwise, $k(\epsilon,R)$ as

evaluated from Eq. (4.28) must be smaller than the RRKM value of Eq. (4.1), since trajectories with insufficient energy in the coupled modes that are counted as reactive in Eq.(4.1) are rejected in Eq.(4.28). Of course, full account of the dipole hindrance is made through the method outlined above.

It has not yet been specified precisely which degrees of freedom are coupled to the reaction coordinate in an ion–dipole reaction: these are the "pertinent" degrees of freedom included in capture models. The two–dimensional dipole rotation is clearly coupled to the reaction coordinate via the electrostatic potential, Eq. (4.14). The coupling of the other active degrees of freedom to the reaction coordinate at large separation is essentially negligible in comparison, i.e., these other modes are as they would be in the separated products and are not significantly perturbed by the electrostatic potential. It would seem, then, that only the dipole rotation will be included in the coupled Hamiltonian H_c. The uncoupled modes are then the vibrations and the remaining active rotational degrees of freedom, whose densities of states we denote $\rho_{vib}^{\dagger}$ and $\rho_{rot}^{\dagger}$ respectively. Eq. (4.28) may then be written:

$$k(\epsilon,R) = \frac{\displaystyle\int_0^{E-V_{eff}(r_m)} dE_+ W_c^{\dagger}[E-V_{eff}(s)-E_+] \int_0^{E_+} dE' \rho_{vib}^{\dagger}(E') \rho_{rot}^{\dagger}(E_+-E')}{h\rho(\epsilon)} \qquad (4.29)$$

It should be noted in passing that expressing $\rho_u^{\dagger}$ as a convolution of $\rho_{rot}^{\dagger}$ and $\rho_{vib}^{\dagger}$ in this way is only exact if these two sets of modes are uncoupled from each other. However, this assumption is not crucial to the result since very little error in the final density of states is introduced by such an approximation. Changing the order of integration yields:

$$k(\epsilon,R) = \frac{\int_0^{E-V_{eff}(r_m)} dE' \rho_{vib}^{\dagger}(E') \int_{E'}^{E-V_{eff}(r_m)} dE_+ W_c^{\dagger}[E-V_{eff}(s)-E_+] \rho_{rot}^{\dagger}(E_+-E')}{h\rho(\epsilon)} \qquad (4.30)$$

Exact implementation of Eq. (4.28) in the case of an ion/dipole reaction therefore requires $W_c^{\dagger}$ to be determined as the minimum sum of states for the two-dimensional hindered dipole rotor. One then carries out the convolution of $W_c^{\dagger}[E-V_{eff}(s)-E_+]$ with $\rho_{rot}^{\dagger}$ and $\rho_{vib}^{\dagger}$ as indicated in Eq. (4.30) to determine the optimum variationally selected $k(\epsilon,R)$. It will be shown in the following section (see also Table 4.1) that, in the high pressure limit, ensemble averaging of the $k(\epsilon,R)$ so obtained leads to a capture rate that is the same (barring a small difference due to the treatment of angular momentum) as that of Chesnavich, Su and Bowers (1980).

The minimum sum of states for the dipole rotor may be determined analytically as shown in Appendix H. Unfortunately, the expression for the minimum sum of states does not allow analytic convolution with the density of states of other rotational modes, a step that is crucial for rapid evaluation of the sum of states by extension of the method of Astholz *et al.* (1979). This method, starting with an analytic form for the overall rotational sum of states, utilises the Beyer-Swinehart direct-count method for convolution with the vibrational density of states. Exact implementation of Eq. (4.30) is therefore at the expense of a considerable amount of computational time, and it is of use to examine how good an approximation to the true capture rate is provided by more approximate variational methods. Note in this regard that Eq. (4.19), which does *not* include adiabatic effects, does provide an analytic expression for the total rotational density of states in the transition state and hence is suitable for use in implementing Eqs. (4.1) and (4.2) with the method of Astholz *et al.* (1979). Hence the more usual RRKM equations (4.1) and (4.2) are much easier to implement variationally.

In the next section the capture expression resulting from exact variational implementation of Eq. (4.28) is derived and compared with results calculated from the

capture expression of Chesnavich *et al.* (1980), trajectory results (Su and Chesnavich 1982), and two variational methods that are more easily implemented.

II.3 High-Pressure Capture Rate

In the following derivation it is assumed that $W_c^{\dagger}[E-V_{eff}(s)-E_+]$ in Eq. (4.28) has been determined variationally prior to convolution with $\rho_u^{\dagger}(E_+)$. The high-pressure dissociation rate is the thermal average of k(E,J):

$$k_{uni}^{\infty} = \int dR\ f(R) \int d\epsilon\ f(\epsilon)k(\epsilon,R) \tag{4.31}$$

where f(R) and $f(\epsilon)$ are the normalised equilibrium populations: $f(\epsilon) = \rho(\epsilon)\exp(-\epsilon/k_BT)/Q_i$ and $f(R) = (k_BT)^{-1}\exp(-R/k_BT)$; here $Q_i = \int\rho(\epsilon)\exp(-\epsilon/k_BT)d\epsilon$ is the partition function for the internal degrees of freedom. From Eq. (4.31), one then has:

$$k_{uni}^{\infty} = \frac{1}{k_BThQ_i}\int_0^{\infty} dR\ e^{-R/k_BT}\int_{V_{eff}(r_m)-R}^{\infty} d\epsilon\ e^{-\epsilon/k_BT}\int_0^{E-V_{eff}(r_m)} dE'\rho_u^{\dagger}(E')W_c^{\dagger}[E-V_{eff}(s)-E'] \tag{4.32}$$

Inverting the order of integration, and noting the effects on the limits of integration, one has:

$$k_{uni}^{\infty} = \frac{1}{k_BThQ_i}\int_0^{\infty} dR\ e^{-R/k_BT}\int_0^{\infty} dE'\rho_u^{\dagger}(E')\int_{E'+V_{eff}(r_m)-R}^{\infty} d\epsilon e^{-\epsilon/k_BT}W_c^{\dagger}[E-V_{eff}(s)-E'] \tag{4.33}$$

Changing the integration variable to $\hat{\epsilon} = \epsilon+R-E'-\Delta H_o$, where ΔH_o is the bond energy, yields:

$$k_{uni}^{\infty} =$$

$$\frac{1}{k_B T h Q_i}\int_0^{\infty} dR e^{-R/k_B T}\int_0^{\infty} dE' \rho_u^{\dagger}(E')\int_{V_{eff}(r_m)-\Delta H_0}^{\infty} d\hat{\epsilon}\, e^{-(\hat{\epsilon}-R+E'+\Delta H_0)/k_B T} W_c^{\dagger}[\hat{\epsilon}+\Delta H_0-V_{eff}(s)] \qquad (4.34)$$

On performing the second integral, this becomes:

$$k_{uni}^{\infty} =$$

$$\frac{Q_u e^{-\Delta H_0/k_B T}}{hQ}\int_0^{\infty}\frac{1}{B}dR \int_{V_{eff}(r_m)-\Delta H_0}^{\infty} d\hat{\epsilon}\, e^{-\hat{\epsilon}/k_B T} W_c^{\dagger}[\hat{\epsilon}+\Delta H_0-V_{eff}(s)] \qquad (4.35)$$

where $Q = Q_i Q_{rot}$ is the total internal partition function, $Q_{rot}=k_B T/B$ being the rotational component; $Q_u = \int \rho_u^{\dagger}(\epsilon)\exp(-\epsilon/k_B T)d\epsilon$ is the partition function of the uncoupled transition state modes. The equilibrium constant for the reaction involves the product of partition functions for reactants $Q_A Q_B$. These may alternatively be factored as $Q_c^r Q_u^r$, where Q_c^r is the partition function for those reactant modes which become coupled with the reaction coordinate as the two moieties approach. Multiplying Eq. (4.35) by the equilibrium constant, the partition function for uncoupled modes in the transition state, Q_u, cancels against that for the same reactant modes, Q_u^r, since these modes are unchanged between the transition state and the completely separate reactants. One thus has the final result:

$$k_{rec}^{\infty} = \frac{1}{hQ_c}\int_0^{\infty}\frac{1}{B}\, dR \int_{V_{eff}(r_m)-\Delta H_0}^{\infty} d\hat{\epsilon}\, e^{-\hat{\epsilon}/k_B T} W_c^{\dagger}[\hat{\epsilon}+\Delta H_0-V_{eff}(s)] \qquad (4.36)$$

This is identical to the capture rate expression of Chesnavich *et al.* (1980) except that the Chesnavich model does not attempt to incorporate angular momentum conservation explicitly, including the external rotation rather as an active mode (a two-dimensional free rotor with moment of inertia mr^2) in the sum of states $W_c^{\dagger}$.

Table 4.1 shows a comparison of capture rates obtained from trajectory calculations (Su and Chesnavich 1982) with a number of different levels of variational transition-state theory. The parametrized results of trajectory calculations of the electrostatic ion/dipole capture rate by Su and Chesnavich (1982) are labelled A. Those labelled B are the optimum statistical capture rates obtained from Eq. (4.36). As shown above, this is the capture rate obtained from exact implementation of Eq. (4.28), through Eq. (4.30) with the $W_c^{\dagger}$ therein determined variationally ("uncoupled" μVTST). The results of variational implementation of Eqs. (4.1) and (4.2) [via Eq. (4.19)] are labelled C: this method is the more usual form of μVTST, wherein the reactive flux is evaluated at a single surface r=s chosen to minimise k(ϵ,R), (Garrett and Truhlar 1979; Wardlaw and Marcus 1987; see also Chapter 1). Method C is that which is utilised for cases where there are no uncoupled modes (this method will be referred to as "fully coupled" μVTST). The results labelled D are obtained by *canonical* variational implementation of Eqs. (4.1) and (4.2) ("fully coupled" CVTST), wherein the same value r=s is used for *all* k(ϵ,R) and this value is chosen to minimise the overall capture rate (Garrett and Truhlar 1979; see also Chapter 1). Finally, we have included for comparison the results of the capture model of Chesnavich, Su and Bowers (1980) (E). As shown above, their expression is equivalent to Eq. (4.36) in all respects except that whereas Eq. (4.36) includes angular momentum conservation (under the approximation that J≈L), their method instead treats the orbital

	Capture Rate Coefficient / 10^{-9} cm^3 s^{-1}				
	A	B	C	D	E
CH_3^+/NH_3	2.7	2.85	3.65	4.65	3.1
CH_3^+/HCN	4.4	4.7	5.35	7.4	5.15
CH_3^+/CH_3CN	5.5	5.8	8.6	12.0	6.35

Table 4.1. Comparison of capture rate constants calculated by different methods for selected ion/dipole reactions: CH_3^+ with NH_3, HCN and CH_3CN respectively. A: parametrized trajectory calculations of Su and Chesnavich (1982). B: results of Eq. (4.36), corresponding to optimum variational implementation of Eq. (4.28) ("uncoupled" μVTST). C: results of variational implementation of Eqs. (4.1) and (4.2) ("fully coupled" μVTST). D: results of canonical variational implementation of Eqs. (4.1) and (4.2) ("fully coupled" CVTST). E: Capture model of Chesnavich, Su and Bowers (1980).

rotation as fully coupled. Calculations were carried out for three typical ion/dipole reactions with varying strengths of dipole: CH_3^+ reacting with NH_3 (1.47 Debye), with HCN (2.98 Debye) and with CH_3CN (3.92 Debye). The RRKM parameters used are those of Chapter 2 for CH_3^+/NH_3 (see also Appendix A); Chapter 3 for CH_3^+/HCN (see also Appendix C); and the present chapter (see below and also Appendix I) for CH_3^+/CH_3CN.

The results indicate that the optimum "uncoupled" microcanonical variational method (B) is an excellent approximation to the trajectory results of Su and Chesnavich (1982) (overestimating in the range 5–7% for the examples studied). This is corroborated by the results for the closely related capture expression of Chesnavich, Su and Bowers (1980) (E) which overestimate in the range 15–17%. The "fully coupled" μVTST approach (C) gives capture rates somewhat larger (overestimating in the range 22–56%) but still significantly more accurate than the CVTST results (D: overestimating in the range 68–118%).

The advantage of applying the "fully coupled" μVTST (C) is that it requires substantially less computational time than the more accurate "uncoupled" μVTST (B), an important consideration when modelling fall–off data which requires solution of the master equation over a wide range of pressures and temperatures. The error thus introduced is moderate and is easily estimated by comparison with the more accurate capture model results. Furthermore, it should be noted that this error becomes negligible at low pressures, where appropriate perturbation theory [Gilbert and Ross 1971] shows that (for single channel systems) the solution of the master equation is independent of microscopic rates and depends rather on the rates of collisional activation and deactivation. Hence information concerning collisional energy transfer rates obtained by modelling of low pressure Ion Cyclotron Resonance data for the CH_3^+/HCN reaction (Chatper 3) is not affected by the conclusions of this chapter.

Refitting the CH_3^+/NH_3 Chemical Activation Reaction.

In Chapter 2 the association of CH_3^+ with NH_3 in a helium bath gas at 298K was modelled. This chemical activation reaction has two exothermic product channels, the major product channel involving elimination of H_2 from the collision complex $(CH_3NH_3^+)^*$ to produce $CH_2NH_2^+$ (see Eq. 2.33). The RRKM parameters for the transition state leading to the $CH_2NH_2^+$ product and those for the collision complex $(CH_3NH_3^+)^*$ have been calculated by Nobes and Radom (1983). Herbst (1985) in modelling this reaction with Phase Space Theory correctly highlighted the importance of angular momentum effects in the system, but was forced to use an "effective dipole" for NH_3 of 0.3 Debye, much less than the actual dipole of 1.47 Debye, because of the inability of PST to correctly account for the hindrance to the dipole rotation in the orbiting transition state of the entrance channel. For the calculations presented in Chapter 2, the RRKM parameters used were those calculated by Nobes and Radom (1983) except that it was found necessary to reduce the barrier height for the major exit channel from the calculated value of 367 kJ mol^{-1} to 348 kJ mol^{-1}. This was in order to reproduce the experimental data of Saxer *et al.* (1987) with physically reasonable values of 156cm^{-1} (0.75k_BT) for the average downward transfer of the internal energy, $<\Delta\epsilon_{down}>$, and the external rotational energy, $<\Delta R_{down}>$. The microscopic rate coefficients $k(\epsilon,J)$ were calculated by CVTST, producing, in the high pressure limit, a capture rate of 4.65×10^{-9} cm^3 s^{-1}. The comparison of Table 4.1 shows that this capture rate is a factor of *ca.* 1.7 greater than the capture rates predicted by trajectories (Su and Chesnavich 1982) or Eq. (4.36). Since the data of Saxer *et al.* (1987) are close to the saturation limit, the correction to calculations at these pressures to allow for uncoupling will be essentially the same as that implied by Table 4.1 for capture rates. The data can therefore be refitted with the correction for adiabatic and variational effects implied by Table 4.1. Refitting the data by applying this correction and maintaining all other quantities as before, the experimental data shown in Figure 2.1 are reproduced with *no adjustment of the transition-state parameters calculated by Nobes and Radom.* The fit, using values of 156cm^{-1} for $<\Delta\epsilon_{down}>$ and $<\Delta R_{down}>$ and 367 kJ mol^{-1} for E_o^2 (this replaces the barrier height of 348kJ mol^{-1} indicated in Figure 2.2), is essentially the same

as that shown in Figure 2.1. This result verifies in a very satisfactory manner the combined accuracy of the methods developed in this work for solution of the master equation with conservation of angular momentum and accurately calculated microscopic rate coefficients. The removal of any inconsistency between the barrier height for the $CH_2NH_2^+$ product channel inferred by kinetic modelling and the quantum-chemical results of Nobes and Radom (1983) incidentally also allows greater confidence to be placed on the collisional energy transfer parameters estimated from fitting of the experimental data of Saxer *et al.* (1986). The accuracy of the estimate (i.e., *ca.* 150 cm^{-1} for both $<\Delta\epsilon_{down}>$ and $<\Delta R_{down}>$) is, however, still limited by fact that the data are not far from the pressure-saturated region and so are not strongly sensitive to the values assumed for $<\Delta\epsilon_{down}>$ and $<\Delta R_{down}>$.

II.4 Application: The CH_3^+/CH_3CN Chemical Activation Reaction

The reaction between CH_3^+ and CH_3CN is of chemical activation type, with two exit channels producing product ions $C_2H_5^+$ and H_2CN^+ being observed. The reaction scheme is shown in Eq. (4.37).

$$CH_3^+ + CH_3CN \rightleftharpoons [CH_3CNCH_3^+]^* \qquad (4.37a)$$

$$[CH_3CNCH_3^+]^* \longrightarrow C_2H_5^+ + HCN \qquad (4.37b)$$

$$[CH_3CNCH_3^+]^* \longrightarrow H_2CN^+ + C_2H_4 \qquad (4.37c)$$

$$[CH_3CNCH_3^+]^* \xrightarrow{M} \cdots \longrightarrow CH_3CNCH_3^+ \qquad (4.37d)$$

The reaction has been studied over a wide range of pressures in a helium bath gas, yielding data which cover the full fall-off regime. Measurements at high pressures (≈0.4 Torr) using the SIFT apparatus (Knight *et al.* 1986) showed that at these pressures association is the dominant process with a rate coefficient of 4.0×10^{-9} cm^3 s^{-1}, which is close to the calculated saturation value of 5.5×10^{-9} cm^3 s^{-1} (Su and Chesnavich 1982). The

reaction has been studied in the range 8×10^{-8} – 1×10^{-3} Torr using the ICR technique (McEwan *et al.* 1989). The association is observed to be termolecular at pressures in the range 3×10^{-5} – 1×10^{-3} Torr with a rate coefficient of 1.0×10^{-23} cm^6 s^{-1}. At lower pressures the bimolecular products are dominant, with an overall bimolecular rate coefficient of 1.8×10^{-9} cm^3 s^{-1}. A point of interest, which will be discussed further in Section III, is that at pressures below 10^{-5} Torr the rate of association does *not* continue to decrease in proportion with the bath gas pressure, as would be expected in the absence of any alternative means of stabilisation, but rather levels out to a small but constant value with the bimolecular rate coefficient 9×10^{-11} cm^3 s^{-1}.

Representative data (plotted as the ratio k_{ass}/k_{ass}^{∞}) for the pressure dependence of the association rate coefficient at 300K are shown in Figure 4.3, along with the results of calculations using the methods developed in this work. The parameters for the calculation are presented in Appendix I with appropriate references. Microscopic rate coefficients were determined in these calculations by CVTST, leading to a calculated capture rate of 12.0×10^{-9} cm^3s^{-1}.

Not all of the information required for the calculation of fall-off in this system is available. The relative energies of the reactants, association product and bimolecular products are known, and structural parameters for the association product have been calculated (Deakyne and Meot-Ner 1988). For the association transition state, Eq. (4.37a), structural parameters are simply those of the separate reactants, with the effect of the dipole accounted for as detailed above, and the threshold energy E_o^1 is the difference in energies (E_o^1 = 410 kJ mol^{-1}). Moments of inertia for the reactants were calculated assuming standard bond lengths and angles.

The structual parameters for the exit channels [Eqs. (4.37b) and (4.37c)] have not been calculated. Experimental determination of the translational energy release distribution (McEwan *et al.* 1988) indicates that there is a barrier of the order of 10–20 kJ mol^{-1} to reverse reaction for the exit channels. Intuitively, one expects some rearrangement of the

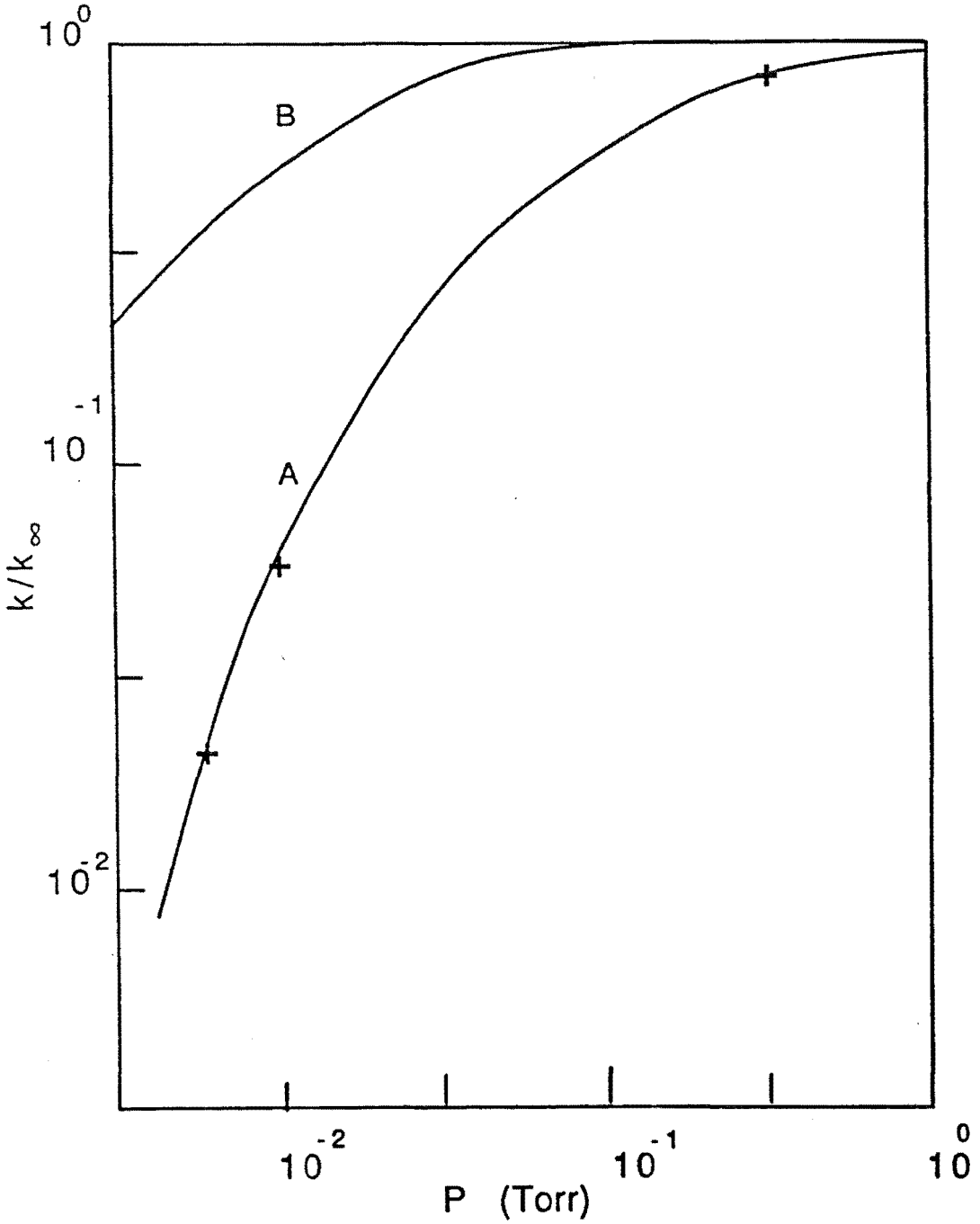

Figure 4.3. Representative experimental data and calculated rate coefficients for the association of CH_3^+ with CH_3CN in helium at 300K. The two points at low pressures represent data measured by the ICR technique (McEwan *et al.* 1989); the point at high pressure was measured using a SIFT (Knight *et al.* 1986). Curve A: solution of the two-dimensional master equation with weak relaxation for both ϵ and R ($<\Delta\epsilon_{down}>=<\Delta R_{down}>=150cm^{-1}$). Curve B: calculated strong collision association rate coefficients.

collision complex before eventual fragmentation to produce products in Eqs. (4.37b) and (4.37c). The transition states for the exit channels are therefore expected to be low–entropy ("tight") in nature, with barrier heights somewhat in excess of the energy differences with respect to the $CH_3CNCH_3^+$ molecule.

In the absence of further knowledge regarding the structural parameters for the exit transition states, it was assumed that both channels proceed initially via a common transition state. This transition state was assigned frequencies equal to those of the molecule, except that the lowest frequencies were adjusted to reproduce the correct bimolecular rate coefficient for product formation at low pressures (Chapter 2, Section II). Assuming the molecule $CH_3CNCH_3^+$ must bend over on itself in order to rearrange and go on to bimolecular products, the moment of inertia for the external adiabatic rotation of the tight transition state was estimated, for a triangular intermediate, to be approximately half that of the molecule. The threshold energy, E_o^2, for the exit transition state was taken to be slightly higher than the energy difference between the molecule and the less stable products (E_o^2 = 288.7 kJ mol^{-1}). This was chosen as an average of the approximate barrier heights determined for the two channels from the experimental translational–energy release distributions (McEwan *et al.* 1988). The scheme for the potential along the reaction coordinate is represented schematically in Figure 4.4.

The uncertainty in the exit channel transition state parameters precludes the determination of energy transfer parameters from fitting of the data. For the calculations shown, physically reasonable values of 150 cm^{-1} were chosen for both $<\Delta\epsilon_{down}>$ and $<\Delta R_{down}>$ (curve A). These values are of a size consistent with those determined for the CH_3NCH^+ molecule in helium (Chapter 3).

It can be seen from Figure 4.3 that an excellent fit to the experimental results is obtained using physically reasonable parameters for the exit channel transition state. There is certainly a measure of adjustability in the model as described, due to the lack of precise information concerning the transition state(s) for the exit channels. However, the

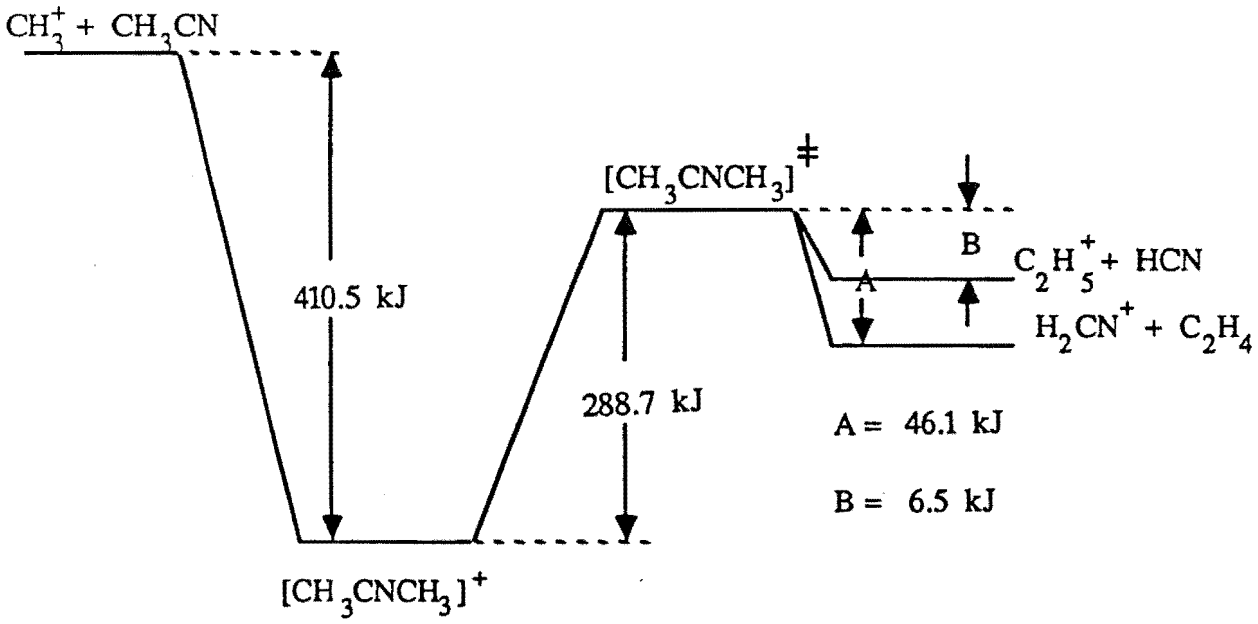

Figure 4.4. Schematic representation of potential along reaction coordinate for CH_3^+/CH_3CN chemical activation reaction, relative to $CH_3CNCH_3^+$ having energy 0.0 kJ mol^{-1}.

study serves as an example of the importance of correct accounting for the dipole moment of the neutral, since it has been found that the experimental results *cannot* be reproduced without making extreme assumptions using Phase Space Theory, which treats the moieties in the association transition state, Eq. (4.37a), as freely rotating under the influence of a central potential (Herbst 1988). In order to try and fit the experimental data of Figure 4.3 with PST, it is necessary to raise the barrier height for the exit channel transition state to *ca.* 390 kJ mol^{-1} and to assume excitation in the CH_3^+ ion equivalent to a rotational temperature of 2000K (Herbst 1988). The translational energy release data (McEwan *et al.* 1988) indicates, however, that the barrier height is much less that 390 kJ mol^{-1}. Whilst there is some discussion as to the extent of suprathermal excitation of ions in the ICR experiment, excitation of the amount required for the PST fit is highly unlikely, since data for a wide range of other reactions are consistent with thermal or close to thermal conditions.

Also illustrated in Figure 4.3 is the association rate coefficient calculated using the strong collision approximation (curve B). It is apparent that for this reaction the strong collision approximation is spectacularly poor. The reason for this is apparent from consideration of the thresholds, $\epsilon_0^1(J)$ and $\epsilon_0^2(J)$, for the two channels. Figure 4.5 shows the behaviour of these thresholds. The upper threshold, $\epsilon_0^1(J)$, is that for the association channel. Collision complexes are formed initially in the shaded region above $\epsilon_0^1(J)$. Before a collision complex can be stabilised, however, its internal energy must be reduced below the *lowest* dissociation threshold of the molecule. As is apparent from Figure 4.5, there is a substantial energy gap between the two thresholds for all except high J values. In reality, many weak collisions will be required to remove the excess excitation of the collision complex and produce a stabilised molecule. This is why the strong collision approximation, which assumes that collisions have unit stabilisation efficiency, overestimates the association rate so much.

In many ion–molecule associations, and indeed in neutral reactions, it is found that the rates measured when using the neutral partner itself as a "parent" bath gas are well

modelled with the strong collision assumption. This is to be expected, since the parent bath gas is a polyatomic molecule and is likely to have vibrational resonances with the collision complex; it therefore will transfer significantly more energy on collisions with the collision complex. The significance of such vibrational resonances in enhancing the rate of energy transfer between polyatomics has been inferred experimentally (Brown *et al.* 1987). In most cases this leads to a high collisional efficiency for stabilisation since enough energy is removed in collisions with the parent bath gas to leave the collision complex well below the dissociation threshold. The reaction between CH_3^+ and CH_3CN is different in this regard because of the large energy gap between the energies of the initially formed collision complexes and the lowest dissociation threshold (Figure 4.5). Figure 4.6 shows the calculated fall-off of the rate of association in the parent bath gas (CH_3CN) (curve A: weak collisions; curve B: strong collisions), along with representative ICR data (McEwan *et al.* 1988). The only parameters changing from the calculations for helium are those describing the collisions of the molecule and bath gas. Following the arguments presented in the previous chapter, it is assumed that the rotational relaxation with a polyatomic bath

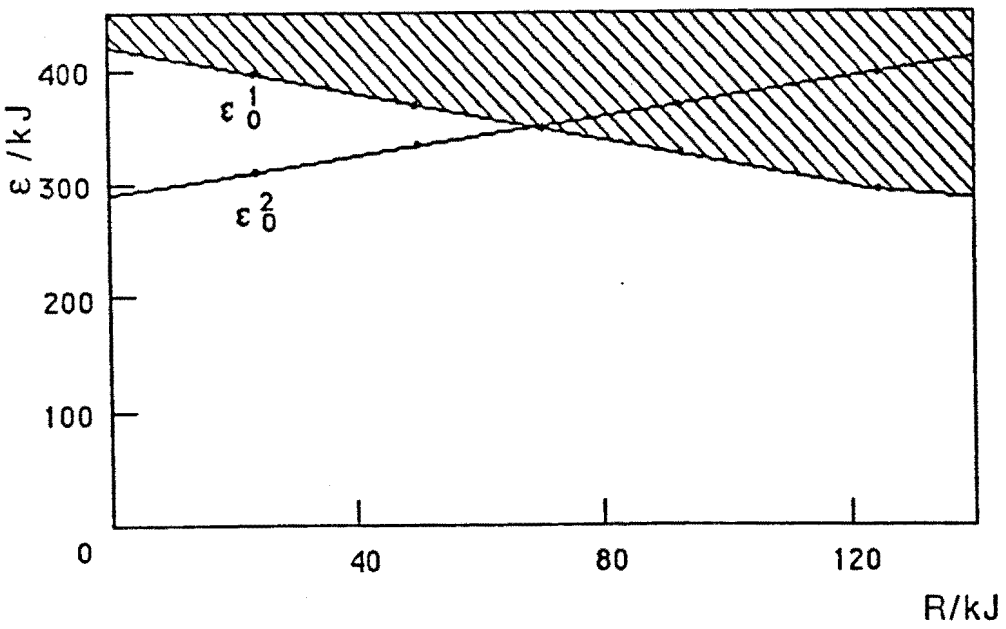

Figure 4.5. Plot of reaction thresholds ϵ_o^1 and ϵ_o^2 for CH_3^+/CH_3CN chemical activation reaction. The shaded area indicates the region of formation of collision complexes by collision between the reactants.

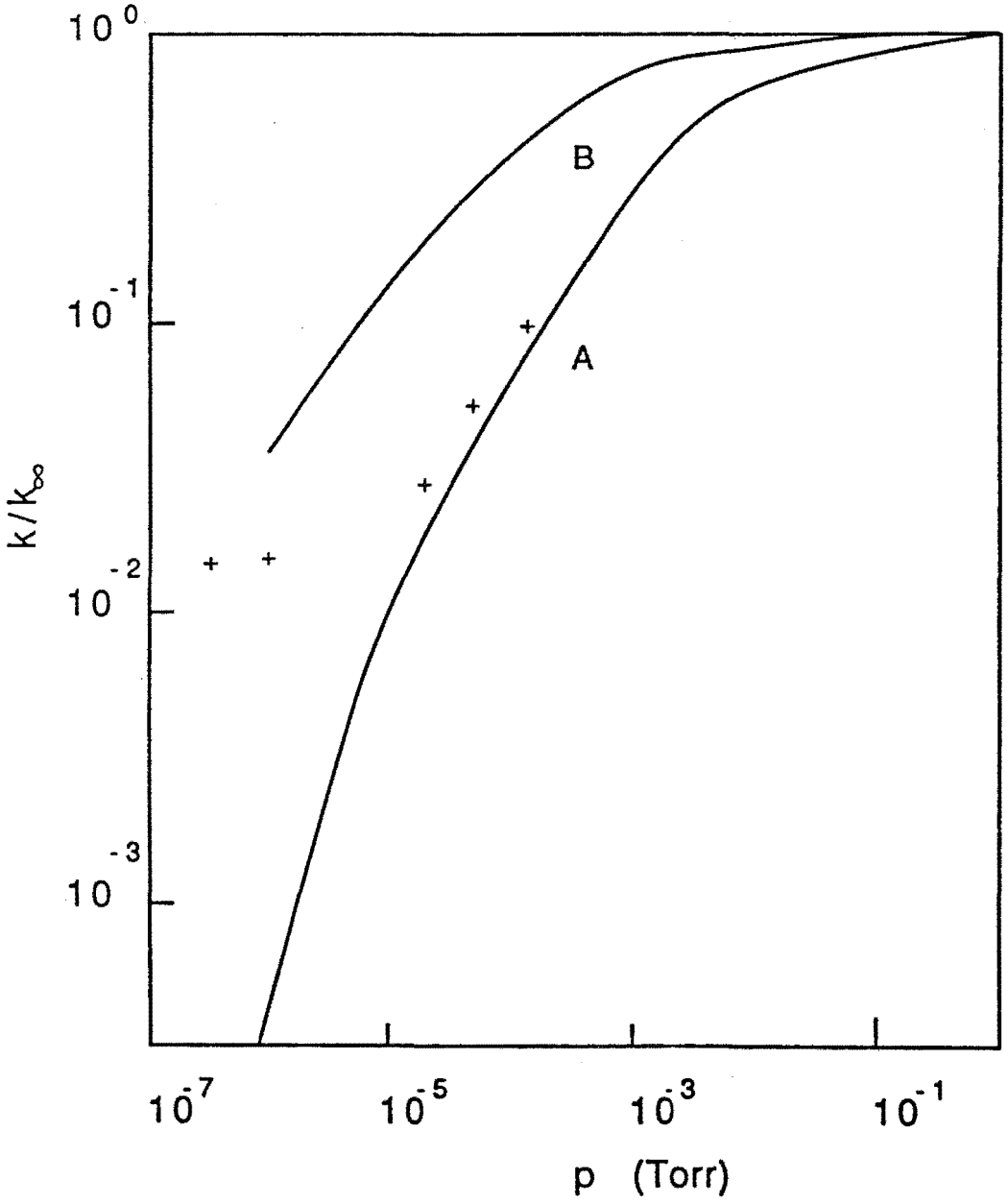

Figure 4.6. Plot of experimental data and calculated rate coefficients for association of CH_3^+ and CH_3CN, with CH_3CN itself as the bath gas. Points are representative ICR data (McEwan *et al.* 1989). Curve A is calculated by solution of the two-dimensional master equation with $<\Delta\epsilon_{down}>$ taken as 165cm^{-1} and rotational relaxation assumed to be fast for the parent bath gas. Curve B: calculated strong collision rate coefficients.

gas is best modelled with strong collisions; for the internal energy relaxation, a value for $\langle\Delta\epsilon_{down}\rangle$ of 165 cm^{-1} was found to reproduce the data quite satisfactorily. The fit obtained is not exact; however, due to the uncertainties in the potential surface, little is to be gained by an exact fitting in this instance and so further adjustment was felt unnecessary. It should be noted that the strong collision curve (curve B) is a poor approximation *even for the parent bath gas* in this reaction. Thus the experimental results indicate that whilst a polyatomic bath gas may appear at times to behave as a strong collider, this may not always be the case and a weak collisional form for $P(\epsilon,\epsilon')$ is the preferred method of modelling such systems.

It is apparent, as noted above, that the experimental rate coefficients for association in Figure 4.6 do not continue to decrease monotonically as the pressure of the parent bath gas decreases below 10^{-6} Torr, but rather level out to a constant bimolecular association rate coefficient of 9×10^{-11} cm^3 s^{-1}. This has been attributed to radiative stabilisation (McEwan *et al.* 1988) and a long lifetime for the collision complex inferred. The calculation of such lifetimes at low pressures will now be discussed.

III. Lifetime of the Collision Complex at Low Densities

At low gas densities, association and chemical activation reactions attain a population distribution for the excited collision complex which is independent of pressure. This distribution is determined by the ratio of reactive influx to dissociative efflux, since collisional events are infrequent and so present a negligible perturbation to the reactive processes. The equations describing the steady state population distribution for collision complex, the dissociation rate constants and the lifetime of the collision complex at low densities have been summarised in Chapter 2. The formula resulting for the average lifetime, τ, of the collision complex in terms of the energy alone, was:

$$\tau = \int\{[1/k(E)]\,[k^1(E)b(E)/k(E)]\}dE \;/\; \int dE\; k^1(E)b(E)/k(E) \qquad (4.38)$$

In Eq. (4.38), [1/k(E)] is the lifetime of the excited molecule with energy E: this is averaged over the low-density-limiting population distribution, which is proportional (see, e.g., Forst 1973) to $k^1(E)b(E)/k(E)$. Taking explicit account of the limits of the integrals in Eq. (4.38) and of angular momentum, the formula for the average lifetime of the collision complex becomes:

$$\tau = \int_0^\infty dJ\ e^{-R/k_BT} \int_{\epsilon_0^1(J)}^\infty d\epsilon\ [k(\epsilon,J)]^{-1}[k^1(\epsilon,J)b(\epsilon)/k(\epsilon,J)]$$

$$\times \left[\int_0^\infty dJ\ e^{-R/k_BT} \int_{\epsilon_0^1(J)}^\infty d\epsilon\ [k^1(\epsilon,J)b(\epsilon)/k(\epsilon,J)]\right]^{-1} \qquad (4.39)$$

where $R = BJ(J+1)$, ϵ_0^1 specifies the association channel threshold, $k^1(\epsilon,J)$ is the microscopic rate coefficient for dissociation via the association channel and $k(\epsilon,J)=\sum_i k^i(\epsilon,J)$.

The lifetime of ionic collision complexes is of importance in interstellar chemistry in relation to proposed synthetic routes to complex species which have been observed in interstellar gas clouds (Herbst 1987; Winnewisser and Herbst 1987). The difficulty in explaining the presence of such species lies in the fact that very low gas densities essentially rule out the possibility of significant association if the only means of stabilisation of the excited complex is by collisions. The means of stabilisation is postulated to be radiative. Estimated lifetimes with respect to emission of infra-red photons are typically in the range 1×10^{-2} to 3×10^{-4} s (Herbst 1987) and so long lifetimes are required at interstellar cloud temperatures if radiative stabilisation is to become competitive with dissociation.

As an investigative exercise, the average collision complex lifetime at low densities was calculated via Eq. (4.39) for the $CH_3CNCH_3^+$ species at room temperature. Analysis of experimental results (McEwan *et al.* 1988) led to an estimated lower bound for this quantity of 1.4×10^{-5} s. Using the method presented in this chapter for calculating $k(\epsilon,J)$

with proper account for dipole and angular momentum effects, and parameters as specified above and in Appendix I, the calculated lifetime at 300K is 4.8×10^{-3} s. The reason for the much smaller experimental estimate appears to be the assumption that the measured rate of association for the parent bath gas corresponds to the strong collision rate. The lifetime inferred from the experimental results increases if the rate measured for the parent bath gas is less than the true strong collision rate. The calculated strong collision rate coefficients for the reaction taking place in the parent bath gas are shown in Figure 4.6 (curve B), along with the measured data (crosses) and the weak collision calculations (curve A). The calculations of Figure 4.6 indicate that the measured rate for the parent bath gas is in fact much lower that the strong collision rate. In order to check that the calculated lifetime is not inconsistent with experiments, it will therefore be necessary to re-analyse the experimental results in the light of the strong collision rate calculated herein (Figure 4.5): this work is in progress (McEwan 1988).

In order to see whether the lifetime calculated for the $CH_3CNCH_3^+$ collision complex is unusual in comparison with other reactions, lifetimes were also calculated for the ion-dipole reactions studied in Chapters 2 and 3: CH_3^+/NH_3 and CH_3^+/HCN respectively. The lifetime resulting for the CH_3NCH^+ collision complex at 300K is 1.1×10^{-6} s. That for the $CH_3NH_3^+$ complex is 2.1×10^{-6} s. The comparison indicates that the $CH_3CNCH_3^+$ lifetime is indeed unusually long. This may be ascribed to the large density of states of the complex, due to low frequency bends and a free internal rotation [it has been shown that the molecule is linear (Deakyne and Meot-Ner 1988)].

McEwan *et al.* (1988) have proposed that the constant rate of association observed at very low pressures in the CH_3^+/CH_3CN reaction (*vide supra*) is due to radiative stabilisation. The very long lifetime calculated for the collision complex in this reaction is consistent with this proposal. Furthermore, corresponding calculations for the CH_3^+/HCN and CH_3^+/NH_3 reactions are consistent with the absence of similar observations in these cases.

IV. Summary

Chapter 4 has dealt with the use of RRKM theory to calculate microscopic rate coefficients $k(\epsilon,J)$ for modelling fall-off behaviour in ion-molecule reactions.

It has been shown that RRKM theory provides results for ion/induced-dipole systems that are equivalent in the high-pressure limit to the well-known Langevin capture rate *provided the transition state is chosen by microcanonical variation as being at the centrifugal maximum.* Since the Langevin capture rate is generally found to accurately predict electrostatic capture rates for such systems, we may conclude that microcanonical variational RRKM theory is sufficiently accurate for such systems.

For ion/dipole reactions, it has been shown that correct incorporation of the hindrance to the dipole rotation in the transition state [see Eqs. (4.17)-(4.19)] is essential for accurate modelling. This is particularly apparent from the modelling of experimental results for the CH_3^+/CH_3CN reaction, where the present theory enables the data to be reproduced with physically very reasonable parameters, whereas Phase Space Theory (which treats the dipole as freely rotating) proves quite inadequate.

Another consideration which is important in modelling ion/dipole reactions is the adiabatic behaviour of a number of degrees of freedom that are completely uncoupled from the reaction coordinate on the long-range electrostatic region of the potential surface. An expression for $k(\epsilon,J)$ has been derived [Eq. (4.28)] which exactly incorporates such non-coupling within the RRKM framework and when determined by microcanonical variation produces, in the high pressure limit, a capture rate which compares very well with the results of capture models and trajectory calculations. In particular, the capture expression obtained [Eq. (4.36)] after ensemble averaging of the new $k(\epsilon,J)$ is formally equivalent to the capture expression derived by Chesnavich *et al.* (1980) in all respects except that the present work includes conservation of angular momentum under the approximation $J \approx L$, whereas the model of Chesnavich *et al.* does not include angular

momentum conservation but rather treats as coupled the external two-dimensional orbital rotation.

The new expression for $k(\epsilon,J)$ which includes uncoupling (from the transition state out to products) of certain degrees of freedom with respect to the reaction coordinate would require considerable computational time if implemented [this would require replacing the analytic result for the total rotational sum of states, Eq. (4.19), by a time-consuming numerical convolution technique]. Comparison of capture rates shows that the more easily implemented "fully coupled" μVTST [i.e., microcanonical variational implementation of Eqs. (4.1) and (4.2) via Eq. (4.19)] produces results in the high pressure limit that overestimate the true rate by *ca.* 20–60%. This error decreases in the fall-off regime and becomes negligible in the low-pressure limit where collisional transitions, as opposed to microscopic rates, are rate determining. It would seem from a pragmatic view point that the "fully coupled" μVTST is the most suitable for modelling of fall-off data, since it is much more computationally economic and its error at higher pressures is easily determined by comparison with more accurate capture expressions such as Eq. (4.36). It may also be noted that μVTST as applied to RRKM theory is much more flexible than electrostatic capture expressions in that it may be applied to systems where transition states in the chemical interaction region (at smaller separation of the moieties) become important in determining the capture rate and hence the electrostatic capture expressions become invalid. This will be the case for most ion/molecule reactions at high temperatures.

CHAPTER 5

UNIMOLECULAR DECOMPOSITION OF A POLYATOMIC ION: AN EXPERIMENTAL STUDY

The rate at which ion–molecule processes occur at elevated temperatures is of interest in a number of applications such as laser physics, plasma etching, combustion and hot interstellar chemistry. As yet no experimental apparatuses have been developed that access high temperature *thermal* conditions for ion–molecule reactions, as distinct from high energy *non–thermal* conditions. It is desirable, therefore, to develop a means of interpreting the results of non–thermal studies to obtain quantitative information about thermal rates of ion–molecule reactions at high temperatures. The development in recent years of the Variable Temperature Selected Ion Flow Drift Tube (VT–SIFDT) (Smith and Adams 1979) has provided a very flexible means of obtaining kinetic data by thermal and non–thermal means. The variable temperature extension enables the thermal temperature range of the SIFT to be extended over the range 80–600K, whilst the drift tube allows higher ion energies to be accessed. The question arises, then, as to whether kinetic data obtained using the drift field to access high ion energies can be interpreted to determine corresponding high–temperature thermal rate coefficients.

The use of the SIFDT to obtain information on the kinetics of ion–molecule reactions at high temperatures has been a topic of active interest, since as yet no truly thermal means of accessing temperatures above about 700K other than in flames have been developed. A significant amount of data has now accumulated from drift tube studies concerning the centre–of–mass energy dependence of ion–molecule reactions. Although there are some applications where reactions involving disparate translational and internal energies occur (e.g. reactions occurring in interstellar shock waves), most applications of interest are essentially thermal in nature.

Smith *et al.* (1985) found an approximate correspondence between the kinetics of the

O_2^+/CH_4 reaction when measured under truly thermal conditions (using the variable temperature extension) and when measured in the drift mode. Adams and Smith (1987) have determined the dependence on field strength of ternary association reactions of the CH_3^+ ion with N_2, H_2 and CO in a helium bath gas. They were able to reproduce this field–strength dependence with a simple model developed as an extension of earlier work on ternary ion–molecule association by Bates (1979) and Herbst (1979). The quantitative interpretation of drift–tube kinetic data for such polyatomic systems is, however, as yet a difficult and unexplored area.

Ferguson (1986) has summarised earlier investigations of collisional quenching of vibrationally excited diatomic and triatomic ions by monatomic and polyatomic neutrals using SIFDT apparatuses. The technique commonly employed is to introduce a neutral species which will charge–transfer only with ions having a sufficient amount of vibrational excitation, providing a "monitor ion" whose signal is a measure of the concentration of the vibrationally excited species. Various quenching gases can then be introduced and the monitor ion signal used to determine the rate of quenching of the vibrationally excited ions by the neutral quencher. Quenching rate coefficients can be determined as a function of the ion centre–of–mass energy. Some qualitative models have been developed (see, e.g., Ferguson 1986) to explain trends in the data, but quantitative modelling of these complex processes is still some way off.

Considerable progress has been made in establishing the relationship between kinetics measured in drift tubes and truly thermal data for reactions involving *monatomic* ions (see, e.g., Albritton *et al.* 1977; Viehland and Mason 1977; Lin and Bardsley 1977). The crucial information required is the steady–state translational energy distribution of the ions relative to the neutral reactant. The translational energy distribution of the ions is determined by their interaction with the bath gas (commonly called the carrier gas in flow– and flow/drift–tube studies), which constitutes the bulk of the system. Once calculated, this distribution can be expressed relative to the neutral reactant. The most commonly used method of obtaining the steady–state translational energy distribution for the ions involves

solving the Boltzmann equation by a method of moments (Viehland and Mason 1977). The results of this theory indicate that, to a first order of approximation, the translational energy distribution of the ions relative to the bath gas may be equated to a thermal (Maxwellian) distribution with the same *mean* kinetic energy. Progressively higher order corrections to the distribution can be obtained (Viehland and Mason 1977).

A theory for determining the energy distributions of polyatomic ions in drift tubes has been formally presented (Viehland *et al.* 1981). In principle, this makes possible the calculation of the steady–state translational energy distribution of a molecular ion in this more complex case. The computational effort required is considerable, and detailed calculations on polyatomic systems have yet to appear. However, the formal structure of the solutions obtained is similar to the monatomic case: it is found that, to a first approximation, the relative translational energy distribution between the ion and the buffer gas may be taken as a thermal distribution with the same mean kinetic energy.

An additional complicating factor is that the polyatomic ion has rotational and vibrational degrees of freedom which participate through inelastic collisions. One therefore has three distinct energy distributions to account for (Viehland *et al.* 1981): (1) The neutral reactant distribution, which will be thermalised at the ambient temperature; (2) The translational energy distribution between neutral reactant and polyatomic ion; and (3) The energy distribution for rotational and vibrational degrees of freedom of the ion which, for a monatomic bath gas, may be assumed to equilibrate with the relative translational energy distribution between the ion and the buffer gas after a sufficient number of collisions (see, e.g., Federer *et al.* 1985). The number of collisions required for the vibrational and rotational degrees of freedom to reach their respective steady–state distributions will depend on the nature of the ion. In general, smaller species such as diatomics and triatomics can require a large number of collisions before the distribution of vibrational energies has reached steady state. Larger polyatomic ions, such as that involved in the present study, may be expected to equilibrate more quickly because the larger number of low–frequency vibrations fascilitates vibrational relaxation.

Quantitative modelling of drift tube kinetics is made substantially easier if negligible error is introduced by the assumption that the steady-state translational energy distribution of the polyatomic ion is a thermal (Maxwellian) distribution with mean kinetic energy given by E_c, the mean centre-of-mass kinetic energy with respect to the bath gas. The formal solution developed by Viehland *et al.* (1981) shows that this is the first level of approximation to the true steady-state distribution. In order to develop more rigorous quantitative kinetic modelling, it is therefore important to examine the accuracy of this approximation.

The study of *unimolecular dissociation* of polyatomic ions in a VT-SIFDT apparatus has a particular advantage in this regard: one has only the interaction between the polyatomic ion and the buffer gas to consider, as distinct from the two separate interactions of the ion with the buffer gas and the neutral reactant that are involved in bimolecular ion-neutral reactions in a drift-field.

In this chapter the results of an experimental study of the dissociation of a polyatomic ion, protonated ethanol ($CH_3CH_2OH_2^+$), in a VT-SIFDT apparatus are presented and discussed. The experiment was designed in order to obtain information about the thermal or non-thermal nature of the energy distributions of polyatomic ions in drift tubes, and also to investigate the rapidity with which the translational, vibrational and rotational degrees of freedom of large ions achieve their respective steady-state distributions.

In Section I the experimental method is summarised. In Section II relevant theory for the modelling of pseudo-thermal dissociation of polyatomic ions in the VT-SIFDT apparatus, via RRKM theory and solution of the two-dimensional master equation, is presented. The assumptions implicit in the analysis of the experiment are discussed. A simple expression for the total non-reactive collision frequency of the ions with the inert carrier gas is derived which extends the Langevin model to take account of the finite size of the species involved. In section III the results of the experiment and theoretical

modelling are presented and discussed. Information is obtained regarding the nature of the internal energy distribution acquired by the protonated ethanol under drift tube conditions, and by inference the nature of the steady-state translational energy distribution. In Section IV the results of the present study are summarised. Conclusions are drawn as to the viability of this experimental approach as a means of obtaining thermal rate data and other information concerning collisional relaxation and energy distributions of polyatomic ions in drift tubes.

I. Experimental Method

The experiment was carried out using the VT-SIFDT apparatus at the Department of Space Research, University of Birmingham in the laboratory of Professor David Smith and Dr Nigel Adams. (Mr Kevin Giles ran the VT-SIFDT and the author looked on!). The reaction was carried out in a helium carrier gas at 300K ambient temperature.

A schematic diagram of the VT-SIFDT apparatus is presented in Figure 5.1 (adapted from Smith and Adams 1987). The principles and operation of the VT-SIFDT have been described in detail elsewhere (Adams and Smith 1984; Smith and Adams 1987). Ions are generated in the ion source region (IS). The ion of choice (in the present case, $CH_3CH_2OH_2^+$) is mass selected by a quadrupole mass spectrometer (QMS1) and then injected into the high pressure flow tube via a venturi nozzle. The injected ions typically have some residual excitation from the ion formation process (usually either electron-impact ionisation or chemi-ionisation), and may also gain some vibrational excitation in the process of injection through the venturi nozzle. This excitation is quenched by collisions with the carrier gas in the field-free region (FFR). This quenching process will be rapid for a polyatomic ion because the large number of degrees of freedom promotes rapid collisional relaxation. The quenching process may not be rapid for diatomic ions, however, as has been illustrated by Federer *et al.* (1985) for the cases of O_2^+ and N_2^+ in helium. A region of the flow tube is lined with insulated rings which may be charged to produce a constant field gradient along the axis of the tube. On

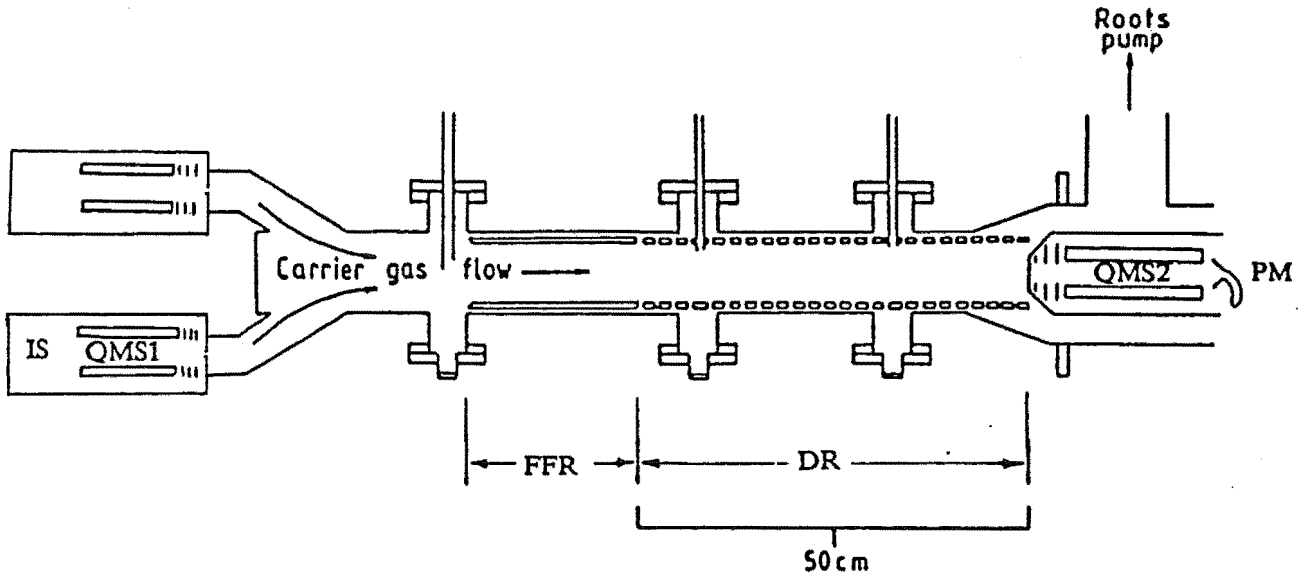

Figure 5.1. Schematic diagram of the Variable-Temperature, Selected-Ion-Flow-Drift Tube (VT-SIFDT), at the University of Birmingham, that was utilised for the present experiment. IS = Ion Source, QMS1 = First Quadrupole Mass Spectrometer, FFR = Field Free Region, DR = Drift Region, QMS2 = Second Quadrupole Mass Spectrometer, PM = Photo-Multiplier.

entering the drift region (DR), the ions are rapidly accelerated to a steady state velocity distribution where the energy gain from the electric field is balanced on average by the energy loss due to collisions. Ions are sampled through an orifice at the end of the drift–region and analysed by mass with a second quadrupole mass spectrometer (QMS2).

The conditions for injection of the ions are optimised to ensure a minimum of fragmentation occurs during this process. Essentially all of the product ions detected are then the result of unimolecular dissociation in the drift–region. The mean centre–of–mass kinetic energy E_c is determined from the drift velocity v_d using the expression (see, e.g., Viehland *et al.* 1981):

$$E_c = (3/2)k_BT + (1/2)M_bv_d^2 \qquad (5.1)$$

where M_b is the carrier gas mass. The drift velocity is the average speed with which the ion drifts through the carrier gas, and is a function of the ratio, E/N, of field strength E to gas number density N. The drift velocity is measured directly by determining the time of transit between two positions. One measures the time for ions to travel from each position to the point of detection by applying a small voltage pulse, and then obtains the difference between the two times. The absolute ion velocity is then the ratio of distance between the positions to the transit time. The drift velocity is the absolute velocity less the flow velocity of the carrier gas.

The unimolecular dissociation rate coefficient is determined in the following manner. For a fixed field strength E and a fixed pressure, the length of the drift region, and hence the reaction time t_r, can be varied by changing the number of drift rings which are charged (the voltage difference and the length must be changed in proportion to maintain a constant E). Let I denote the parent ion signal and P_i the i^{th} product ion signal for a reaction time t_r. Let $I_0 = I + \sum_i P_i$. Provided differential diffusion and mass discrimination effects do not significantly disturb the relative signals for different ions (these can be corrected for if necessary), the ratio I/I_0 is an excellent approximation to the ratio of the

parent ion concentration after reaction time t_r to the initial concentration at time t=0. The slope of a plot of $\log(I/I_0)$ versus the reaction time t_r therefore determines the unimolecular rate coefficient k_{uni}. The VT-SIFDT enables k_{uni} to be determined under a range of conditions by varying the gas number density, the field strength and the thermal temperature.

II.1 Interpretation of Dissociation in a Drift Tube.

Theoretical considerations which must be borne in mind when interpreting this experiment will now be discussed.

On entering the drift region, the swarm of ions is accelerated, gaining energy until a state is reached where the average loss of energy in collisions with the carrier gas is balanced by the energy gained from the field. Not only translational but also the vibrational and rotational degrees of freedom are involved in this process. After an induction period, the vibrational and rotational degrees of freedom of the ion attain a steady state distribution which depends (through solution of the master equation) on the gas number density, the collision frequency, and the probability distribution function for transfer of energy and angular momentum in collisions [$P(\epsilon,J,\epsilon',J')$]. Now, $P(\epsilon,J,\epsilon',J')$ depends implicitly on the translational energy distribution of the ion through detailed balance, which relates the probabilities for upward and downward transfer of energy and angular momentum. The effect of the drift field is to alter the collision frequency ω and create a bias towards higher energies and angular momenta by altering $P(\epsilon,J,\epsilon',J')$ through the detailed balance relationship.

The detailed balance relationship is well understood for thermal systems, where a Maxwellian distribution of translational energies applies. In this case $P(\epsilon,J,\epsilon',J')$ must satisfy the relationship (see, e.g., Tardy and Rabinovitch 1977):

$$P(\epsilon,J,\epsilon',J')f(\epsilon',J') = P(\epsilon',J',\epsilon,J)f(\epsilon,J) \qquad (5.2)$$

where $f(\epsilon,J)$ is the equilibrium (Boltzmann) distribution for the molecule. Determination of the relationship appropriate to a non-Maxwellian translational energy distribution is a non-trivial problem. This would require the averaging of cross sections for collisional transfer of internal energy and angular momentum in the ion over the appropriate non-Maxwellian translational energy distribution. Now, calculations of the exact steady-state translational-energy distribution for polyatomic ions in drift tubes have yet to appear, let alone accurate cross sections for collisional energy and angular momentum transfer. Because of the difficulty of such an undertaking, modelling is made considerably simpler if one can assume that the steady-state translational energy distribution of the ion is essentially thermal with mean translational energy equal to E_c. This allows the usual detailed balance relationship, Eq. (5.2), to be used in solving the master equation. The total collision frequency ω, considered below, is then also calculated assuming a Maxwellian distribution of translational energies.

It should be noted (Whyte *et al.* 1988) that the separation of the total collisional transition rate into a collision frequency ω and a probability distribution function $P(\epsilon,J,\epsilon',J')$ is convenient but not essential: properly the calculation should be done in terms of the collisional transition rate itself. For the present we confine ourselves to the more usual (though less correct) formulation (calculations using the more correct collisional transition rate are being developed).

The steady state distribution of energies in a thermal unimolecular dissociation reaction is given by the eigenvector of the collisional / reactive matrix J that corresponds to the largest eigenvalue $\lambda_1 = -k_{uni}$ (see Chapter 1). The timescale for approach to steady state is usually referred to as the induction period, and is the time required for relaxation of transient terms in the population that involve higher eigenvalues (Montroll and Shuler 1958). These transients must decay rapidly on an experimental timescale in order for single-exponential decay to be observed.

It should be stressed that even if the steady-state translational energy distribution is

Maxwellian (with some mean energy E_c), the steady-state internal and external rotational distributions will *not* be Boltzmann, but rather will be determined by solution of the master equation. Nevertheless, the steady-state *non-equilibrium* population distribution $g(\epsilon,J)$ for the molecular ion will be characteristic of a thermal unimolecular dissociation reaction at the appropriate ion "temperature" and gas number density.

With these considerations in mind, the measured rate of unimolecular dissociation of the polyatomic ion in the drift field will correspond to thermal dissociation at an elevated temperature with mean translational energy E_c if: (1) The steady-state ion translational-energy distribution is, to a sufficient degree of accuracy, Maxwellian with mean energy E_c; and (2) The induction period for unimolecular dissociation of the ion is short compared with the experimental timescale for motion of the ions along the drift tube.

How may these two conditions be tested experimentally? If single exponential decay is observed then it can be assumed that the induction period is sufficiently brief [condition (2)]. As will be shown below, this is indeed the case for the present experiment, i.e., condition (2) applies. In addition, the VT-SIFDT apparatus offers a means of rigorously testing condition (1), since the same value of E_c can be created by different combinations of thermal temperature versus field strength. If condition (1) holds, then the same rate coefficient for unimolecular dissociation should be measured in each of these cases (provided the pressure is adjusted at different thermal temperatures to maintain a constant gas number density). As will be shown below, the results of this test shows that condition (1) does *not* apply for the present reaction.

II.2 Modelling the $CH_3CH_2OH_2^+$ System.

The unimolecular dissociation of $CH_3CH_2OH_2^+$ has been studied previously under truly thermal conditions up to 700K (Meot-Ner 1989) and by Collision Induced Dissociation (CID) with a high energy ion beam (Jarrold *et al.* 1986). Jarrold *et al.* (1986) also

studied dissociation of the metastable $CH_3CH_2OH_2^+$ ion. In the present study, two product channels were observed for the reaction, shown in Eq. (5.3):

$$CH_3CH_2OH_2^+ \longrightarrow H_3O^+ + C_2H_4 \ , \ \Delta H_0 = 136 kJ\ mol^{-1} \qquad (5.3a)$$

$$\longrightarrow C_2H_5^+ + H_2O \ , \ \Delta H_0 = 168 kJ\ mol^{-1} \qquad (5.3b)$$

The second channel, which constituted less than 10% of the overall dissociation rate in the present measurements, was not observed by Jarrold *et al.* (1986). A third possible channel, which produces the most stable products, involves loss of H_2. This third channel was also not observed and appears therefore to have a significant barrier which prevents it from being competitive. The kinetic energy release spectrum obtained by Jarrold *et al.* (1986) for dissociation of the metastable $CH_3CH_2OH_2^+$ ion to produce the H_3O^+ product ion indicates that there is no significant barrier to the reverse association. This is corroborated by the finding of Adams and Smith (1988) that the association of H_3O^+ with C_2H_4 in the temperature range 80–300K has a negative temperature dependence. It appears therefore that any barrier to chemical rearrangement preceding the dissociation is less than the overall threshold energy for dissociation.

The potential profile along the reaction coordinate for the two dissociative channels is unknown. This profile may be quite complex, since each channel may involve some molecular rearrangement via a "tight" transition state before eventual dissociation into ionic and neutral fragments. Accurate evaluation of the microscopic rate coefficients for dissociation would therefore require these to be calculated by microcanonical variational RRKM theory, with inclusion of both a tight transition state and loose, orbiting transition states (see, e.g., Chesnavich *et al.* 1981). Given the appropriate transition state parameters, this microcanonical variational approach is automated in the programme package which has been developed (Smith and Gilbert 1989). However, such an approach is not possible in the present study because of the lack of knowledge of the potential surface. A quantum chemical study of the potential surface would clearly be very useful in this regard.

It is possible, however, to model the *total* rate of dissociation of the $CH_3CH_2OH_2^+$ under the present experimental conditions because the reaction is in the low-pressure regime. The master equation therefore reduces to its low-pressure-limiting form which deals only with collisional activation / deactivation processes:

$$-g(\epsilon,J)\omega k_o = \omega\int_0^{E_o} d\epsilon' \int_0^{J_o(\epsilon')} dJ'\ \hat{P}(\epsilon,J,\epsilon',J')g(\epsilon',J') - g(\epsilon,J) \qquad (5.4)$$

Eq. (5.4) is solved via Eq. (3.26) or Eq. (3.45), depending on the nature of the rotational relaxation. The low-pressure-limiting rate coefficient for overall dissociation, $k_{uni}=\omega k_o$, obtained from solution of Eq. (5.4) is independent of the transition state parameters: it depends rather on the molecular parameters, the average collisional transfer of energy and angular momentum, and the lowest dissociation threshold $J_o(\epsilon)$. Note that the branching ratio for the two channels *does* depend on the transition state parameters, as shown in Chapter 3. The experimental branching ratios for the $C_2H_5^+$ product channel were, however, sufficiently small (<10%) as to make their reliability uncertain, and so the analysis of the current experiment is not greatly handicapped by the inability to predict accurately branching ratios because of the lack of knowledge of the potential surface.

The structural parameters used in the calculations are presented in Appendix J. The frequencies for the $CH_3CH_2OH_2^+$ molecule were taken as those for ethanol with appropriate extra frequencies for the additional hydrogen. The threshold for dissociation was taken as that for the dominant H_3O^+ product channel, Eq. (5.3a) (136kJ mol^{-1}), calculated from standard thermochemical data (Lias *et al.* 1984). Transition state parameters were estimated for the loose, orbiting transition states. As stated above, microscopic rate coefficients so calculated may not give accurate extrapolation of data to higher pressures, but the essential dependence of the dissociation threshold on angular momentum is thereby included.

II.3 Collision Frequency.

It is important to represent correctly the collision frequency ω that pertains to the experimental conditions. This is normally represented as the product of a bimolecular rate coefficient for encounters between ion and carrier gas and the carrier gas number density: $\omega = k_{coll}M$, where M is the carrier gas number density and k_{coll} is the ion/carrier gas collision rate coefficient (often denoted Z).

Firstly, it should be stressed that whilst k_{coll} is calculated appropriate to the ion translational temperature, M is to be calculated rather at the ambient carrier gas temperature.

A simple formula which is commonly used to calculate the encounter rate between an ion and an induced dipole is the Langevin rate coeffient [Chapter 4, Eq. (4.13)]:

$$k_{coll} = k_L = 2\pi q(\alpha/4\pi\epsilon_0 m)^{\frac{1}{2}} \qquad (5.5)$$

As discussed in the previous chapter, this rate coefficient gives the electrostatic capture rate of a point mass with an induced polarizability by a point charge. Such a model will be accurate at low translational energies where the long-range electrostatic potential will determine the dynamics of capture. However, for the present high temperature application the Langevin model requires some refinement to account for the size of the species involved, i.e., the repulsive terms in the potential which describe the steric interaction. An easily evaluated expression for the bimolecular collision rate coefficient is now derived which includes this steric repulsion in terms of the hard sphere collision radii of the species involved. In fact, the definition of a "collision" is somewhat nebulous, and indeed unnecessary, but arises from the convenient separation of the collisional transition rate into an encounter frequency ω and the probability for collisional transition of energy and angular momentum $P(\epsilon,J,\epsilon',J')$ (this point has been discussed in detail by Whyte *et al.* 1988). For the present, the collision event is defined conservatively as an approach of the

two species within the hard-sphere collision diameter. The Langevin condition for this to occur is that the centrifugal barrier must be surmounted. As will be seen below, for species with finite size, this is a sufficient but not always necessary condition for encounter, hence k_L can underestimate the collision rate.

It is useful to present the normal derivation of the Langevin collision rate coefficient, since the result to be derived is a simple extension of this. The long range effective potential for an ion interacting with an induced dipole is written as:

$$V_{eff}(r) = -q^2\alpha/2Gr^4 + mv^2b^2/2r^2 \qquad (5.6)$$

where $G=4\pi\epsilon_0$, v is the magnitude of the relative velocity, b is the impact parameter and r the separation of the two point species. Figure 5.2 indicates these definitions schematically, and Figure 5.3 illustrates schematically the effective potential for several different impact parameters (assuming a fixed translational energy E). The criterion defining a collision is that a trajectory must have sufficient energy to overcome the centrifugal barrier and proceed, in principle, to zero separation. Therefore one determines the maximum impact parameter, b_{max}, for which the energy $E = mv^2/2$ is sufficient to overcome the centrifugal maximum:

$$b_{max} = [4q^2\alpha/Gmv^2]^{\frac{1}{4}} \qquad (5.7)$$

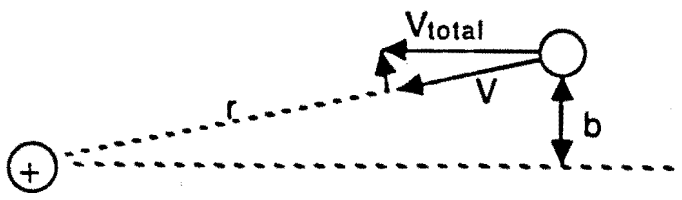

Figure 5.2. Illustration of definition of the impact parameter b, the relative velocity v, and the separation r for ion/induced-dipole system. v_{total} is the velocity of the induced-dipole with respect to the ion.

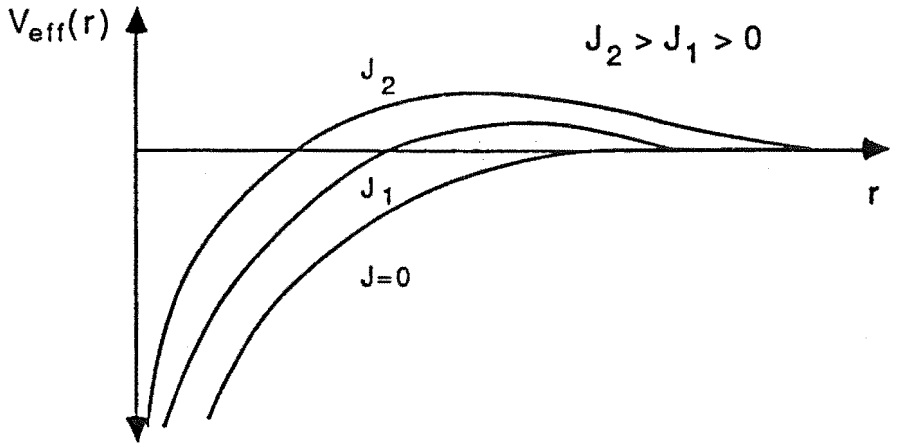

Figure 5.3. Schematic representation of effective potential for ion/induced dipole potential.

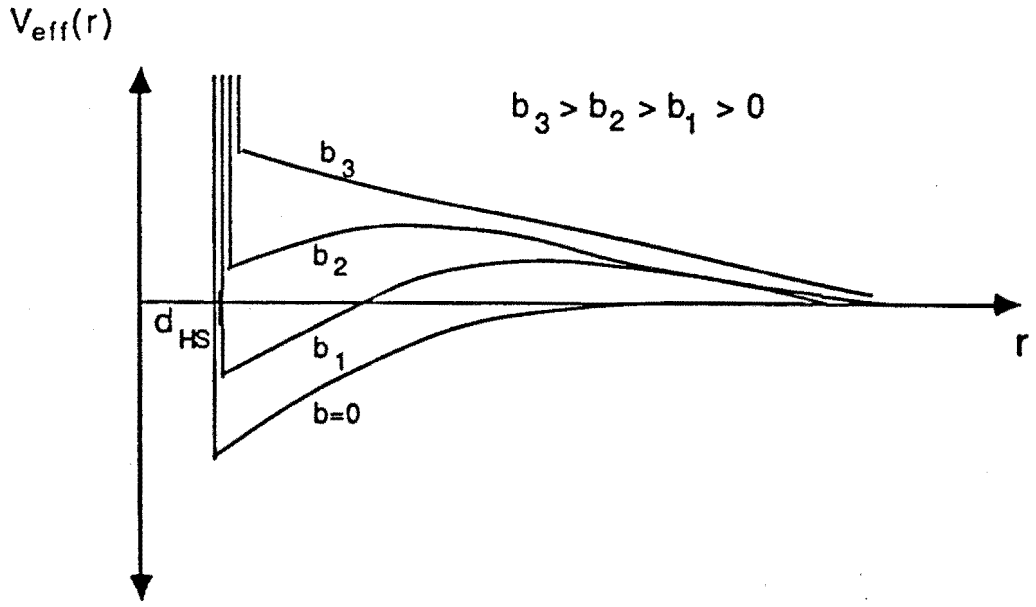

Figure 5.4. Schematic representation of effective potential for an ion/induced–dipole system that includes steric repulsion through the hard–sphere collision diameter (d_{HS}).b represents the impact parameter: for a fixed v_{total}, J increases in proportion to b, where b and v_{total} are defined as in Figure 5.2.

In the Langevin model collisions cannot occur for impact parameters greater than b_{max} because the system, unable to surmount the centrifugal maximum, will reach a distance of closest approach d_{min}, defined by setting V_{eff} equal to the translational energy $mv^2/2$, and then reflect off the effective potential. For later reference, the equation defining d_{min} is:

$$mv^2/2 = -q^2\alpha/2Gd_{min}^4 + mv^2b^2/2d_{min}^2 \tag{5.8}$$

The cross section for non-reactive collisions in the Langevin model is defined as:

$$\sigma(v) = \pi b_{max}^2 = \pi\left[4q^2\alpha/Gmv^2\right]^{\frac{1}{2}} \tag{5.9}$$

The bimolecular rate coefficient for collisions, k_{coll}, is given by:

$$k_{coll} = \int f(v)v\sigma(v)dv \tag{5.10}$$

where f(v) is the Maxwellian velocity distribution:

$$f(v) = 4\pi\left[\frac{m}{2\pi k_BT}\right]^{3/2} v^2 \exp\left[\frac{-mv^2}{2k_BT}\right] \tag{5.11}$$

Substituting Eqs. (5.9) and (5.11) into Eq. (5.10), and transforming the variable of integration from v to E leads to the result of Eq. (5.5).

In order to extend the Langevin formulation to account for the size of the species involved, the effective potential is modified to include the repulsive steric interaction which occurs when the two moieties approach within the hard-sphere collision diameter:

$$V_{eff}(r) = -q^2\alpha/2Gr^4 + mv^2b^2/2r^2 + U(r-d_{HS}) \tag{5.12}$$

where d_{HS} is the hard-sphere collision diameter and $U(r-d_{HS})$ is the Voertkoel wall function: $U(x)=0$, $x>0$, and $U(x)=\infty$, $x<0$. Figure 5.4 illustrates schematically this effective potential for a fixed energy E and varying impact parameters. This effective potential includes only the long range electrostatic and short range (approximate) repulsive parts of the potential. Whilst it would be quite inadequate, for instance, for calculations aimed at determining the *amount* of energy transferred in collisions, it should nevertheless give a reasonable approximation to the average collision frequency. With Eq. (5.12), the criterion defining a collision is that a trajectory must have sufficient energy to reach the separation d_{HS}, whereafter an encounter is ensured. Note that for low energies this criterion will amount to surmounting the centrifugal barrier, since the maximum in the effective potential will lie outside the hard sphere collision diameter d_{HS}. For higher energies, however, the effective potential at large impact parameters will have a maximum at separations smaller than d_{HS}: it is *not* necessary for a trajectory to surmount this barrier to ensure an encounter between the species, only that it reach the separation d_{HS}. Hence for higher energies the repulsive part of the potential causes the collision cross section to be larger than the simple Langevin model would allow. The expressions for the cross sections are derived as follows.

It is easily shown that for $v \leq (q^2\alpha/Gmd_{HS}^4)^{\frac{1}{2}}$, the maximum impact parameter for a collision will be determined by the usual Langevin criterion, leading to a b_{max} as in Eq. (5.7). For velocities higher than this, as one progressively increases the impact parameter b the centrifugal maximum moves within the hard-sphere collision diameter before the Langevin b_{max} is reached. It is then possible for a system with insufficient energy to surmount the centrifugal barrier to undergo a collision nevertheless by virtue of having sufficient energy to approach to d_{HS}. The criterion for collision is now not the capacity to surmount the centrifugal barrier, but rather that the distance of closest approach $d_{min} \leq d_{HS}$. The maximum impact parameter for a collision is then that for which $d_{min}=d_{HS}$, since for impact parameters greater than this the system will reflect off the effective potential before reaching the hard-sphere collision diameter. This b_{max} is determined by setting $d_{min}=d_{HS}$ in Eq. (5.8) and solving for b. These considerations lead to the following

prescription for the maximum impact parameter at a given relative velocity:

$$b_{max} = [4q^2\alpha/Gmv^2]^{\frac{1}{4}} \quad , v \leq (q^2\alpha/Gmd_{HS}^4)^{\frac{1}{2}} \tag{5.13a}$$

$$= d_{HS}[1 + q^2\alpha/mv^2d_{HS}^4G]^{\frac{1}{2}} \quad , v > (q^2\alpha/Gmd_{HS}^4)^{\frac{1}{2}} \tag{5.13b}$$

Thus the non-reactive collision cross-section is:

$$\sigma(v) = \pi[4q^2\alpha/Gmv^2]^{\frac{1}{2}} \quad , v \leq (q^2\alpha/Gmd_{HS}^4)^{\frac{1}{2}} \tag{5.14a}$$

$$= [\pi/d_{HS}^2][d_{HS}^4 + q^2\alpha/Gmv^2] \quad , v > (q^2\alpha/Gmd_{HS}^4)^{\frac{1}{2}} \tag{5.14b}$$

Substituting Eqs. (5.11) and (5.14) into Eq. (5.10) gives an equation involving three integrals, two of which may be evaluated analytically, yielding:

$$k_{coll} = 4\left[\frac{\pi q^2\alpha}{Gm(k_BT)^3}\right]^{\frac{1}{2}} \int_0^{q^2\alpha/2G\sigma_{HS}^4} dE\, E^{\frac{1}{2}}\, e^{-E/k_BT}$$

$$+ \pi d_{HS}^2\left[\frac{8k_BT}{\pi m}\right]^{\frac{1}{2}} e^{-q^2\alpha/2Gd_{HS}^4k_BT}$$

$$+ \frac{2q^2\alpha}{Gd_{HS}^2}\left[\frac{2\pi}{mk_BT}\right]^{\frac{1}{2}} e^{-q^2\alpha/2Gd_{HS}^4k_BT} \tag{5.15}$$

The first integral is easily evaluated numerically. Note that this first integral covers the lower energies where the cross section is simply the Langevin cross section, Eq. (5.14a). If the energy $q^2\alpha/2Gd_{HS}^4$ is large compared with k_BT then k_{coll} reduces to k_L, Eq. (5.5) (the first integral may be determined analytically over the range 0 to ∞). This will be the case if the neutral has a large polarizability and/or the hard-sphere collision diameter is small. If the polarizability is small and the temperature large, however, the second term in Eq. (5.15) dominates and k_{coll} reduces to the hard-sphere bimolecular collision rate coefficient, $k_{HS} = \pi d_{HS}^2[8k_BT/\pi m]^{\frac{1}{2}}$.

For the present case, conditions conspire to make k_L an inadequate representation of the collision rate (a factor of *ca.* 2 too small in the temperature range under study), since helium has a small polarizability and $CH_3CH_2OH_2^+$ a large collision diameter.

III. Results and Discussion

Figure 5.5 illustrates plots of $\ln(I/I_0)$ versus the drift region length (which is proportional to the reaction time) for a number of different values of E_c. The results are obtained at a fixed carrier gas temperature of 300K and pressure of 0.3 Torr by increasing the E/N ratio and hence also the drift velocity and centre-of-mass energy. It is apparent that the ion population undergoes essentially single-exponential decay. The absence of any non-zero intercepts indicates that the internal degrees of freedom of the $CH_3CH_2OH_2^+$ approach the steady state rapidly on the experimental timescale, since if a significant length of the tube were traversed *whilst* the population approached the steady state then one would expect to see an apparently reduced rate of dissociation for shorter drift region lengths. It can therefore be concluded that the induction period is short compared with the timescale for reaction: condition (2) is satisfied.

The measured rate coefficients were found to be directly proportional to the carrier gas pressure, indicating that the dissociation reaction is in the low-pressure regime for the present experimental conditions. This is verified by the fact that k_{uni} calculated from solution of the full master equation (see Chapter 3) is equal to ωk_0 calculated from the low-pressure master equation, Eq. (5.4).

Figure 5.6 shows plots of k_{uni} versus E_c at a number density of 1.0×10^{16} cm^{-3}: curves A and B are experimental results and curve C has been calculated using typical values for the average internal and rotational energy transfer and the parameters set out in Appendix J (the temperature being defined as $2E_c/3k_B$). The lower curve (A) was obtained with a carrier gas temperature of 298K and high drift fields, whilst the upper curve (B) was obtained with a carrier gas temperature of 500K and somewhat lower drift

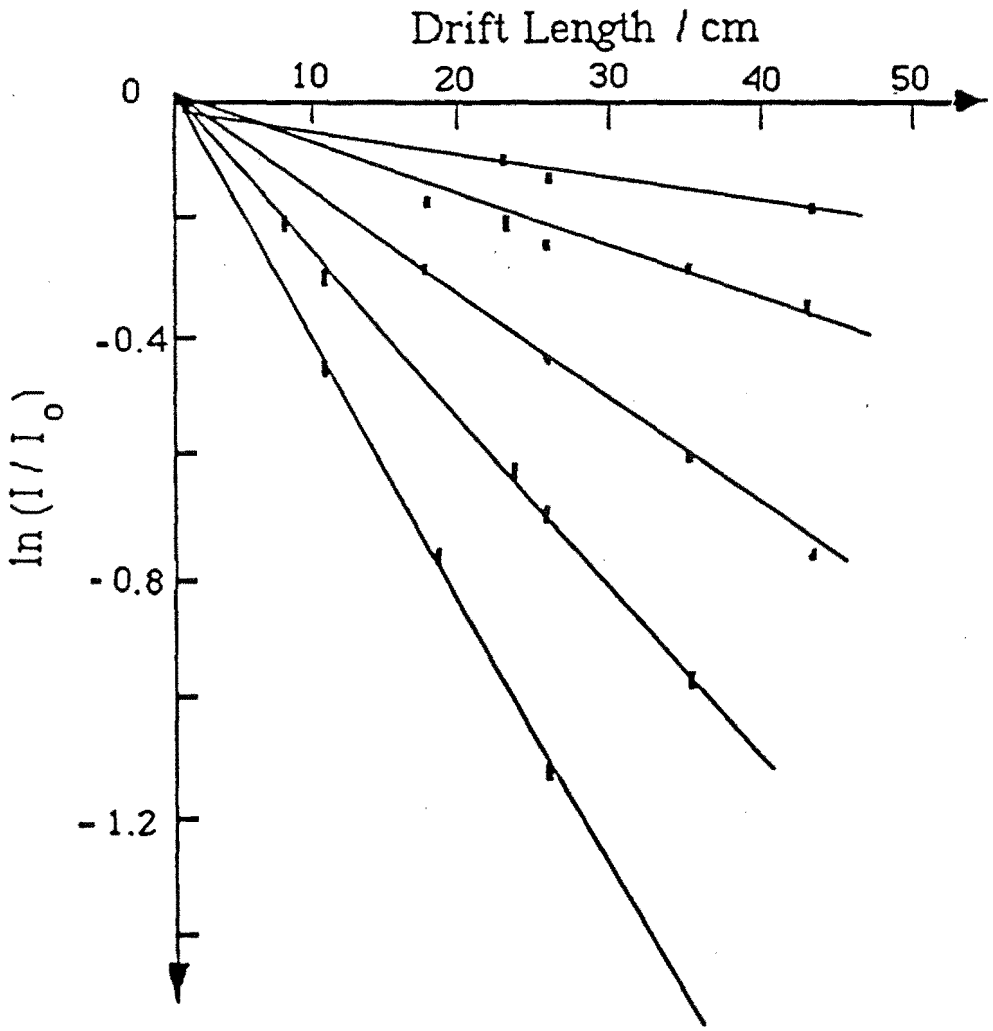

Figure 5.5. Plot of $\ln(I/I_0)$ versus drift region length, where I/I_0 is the ratio of the parent ion signal before to that after the reaction time associated with passage through the drift region.

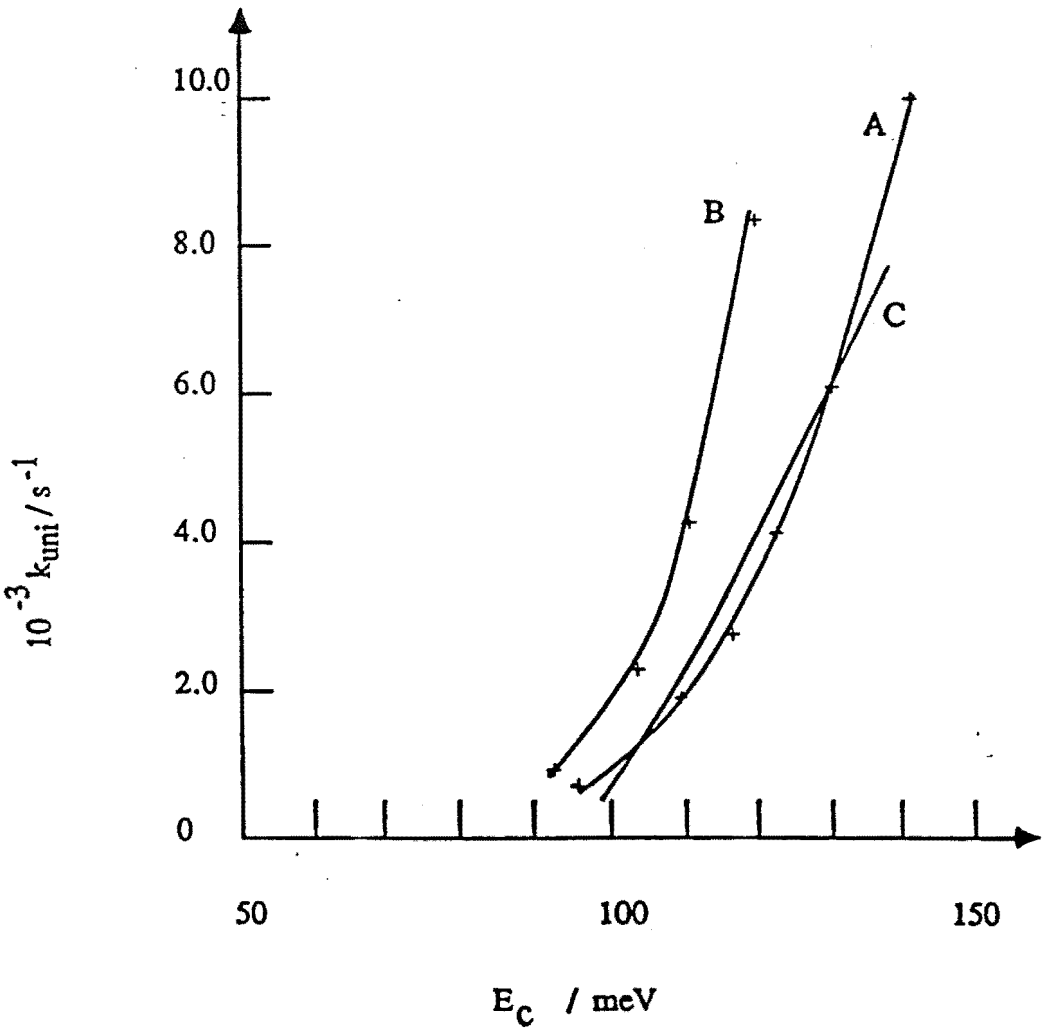

Figure 5.6. Plots of experimental and calculated k_{uni} versus E_c: (A) Ambient temperature = 298K with a range of higher field strengths. (B) Ambient temperature = 500K with a range of moderate field strengths. (C) Thermal rate coefficients calculated for temperatures defined by $T=2E_c/3k_B$. All rate coefficients correspond to a carrier gas number density of 1.0×10^{16} cm^{-3}.

fields. The fact that the measured dissociation rate coefficient changes for different combinations of thermal temperature versus field strength having the same centre-of-mass energy E_c indicates that the translational energy distribution, and hence the internal energy and angular momentum distributions, are changing as the component of E_c caused by the drift field is altered. The rate coefficients measured therefore do not correspond to thermal rate coefficients at elevated temperatures, since the comparison of curves A and B in Figure 5.6 shows that they depend not only on E_c but also on the field strength.

The assumption of a rapid approach to steady state appears to be justified by the absence of significant end-effects in plots such as those of Figure 5.5. Now, the internal degrees of freedom of the ion will attain a distribution which is non-equilibrium due to depletion of reactive levels, but nevertheless characteristic of the translational energy distribution, since this influences the precise nature of the detailed balance relationship for the probability of collisional transition between states. Since the rate coefficients for the low-temperature/high-field measurements (Curve A) are less than those measured under high-temperature/low-field conditions (Curve B), it appears that the steady-state translational energy distribution at high fields is not as broad as that produced by more nearly thermal conditions. This will result in a smaller probability for "upward" collisional transition to the high energy reactive states and hence rates of reaction in curve A which are depressed below the more nearly thermal results of curve B.

The calculated temperature dependence of k_{uni} is not conclusive in indicating what the true thermal rate coefficients ought to be, since the results are sensitive to the size of the threshold for dissociation (the value calculated from thermochemical data has a moderate uncertainty associated with it) and the size of the average downward internal and rotational energy transfers. Curve C of Figure 5.6 has been calculated using values of 150 cm^{-1} for $<\Delta\epsilon_{down}>$ and $<\Delta R_{down}>$, which are typical of the reactions studied thus far (see Chapters 2, 3 and 4). It approximates curve A (coincidentally) quite well, but one could equally well produce a curve that fitted B by altering the threshold and collisional energy transfer parameters within reasonable bounds.

The results clearly indicate that the rates of dissociation measured do not constitute truly thermal data. The question remains: can thermal data be extracted by appropriate analysis? It may be possible to take a series of measurements which have been made at constant number density and E_c, but with a progressively larger thermal contribution to E_c, and extrapolate to zero drift field. The data of Figure 5.6 provide two such points for each value of E_c. A plot of $\ln(k_{uni})$ versus the contribution to E_c of the drift field, $E_d=(1/2)M_b v_d^2$, is shown in Figure 5.7. Some form of extrapolation of this data to zero field may provide essentially thermal numbers for k_{uni}. The form of extrapolation required is not obvious, however. A simple log-linear extrapolation of k_{uni} to $E_d=0$, indicated in Figure 5.7 by dashed lines, gives results for k_{uni} with a temperature dependence which is rather too large to be modelled with physically reasonable parameters. For instance, decreasing the dissociation threshold by 10kJ mol^{-1} (to 126kJ mol^{-1}) allows the approximate magnitude of the extrapolated rate coefficients to be reproduced, but the temperature dependence is too shallow. If the threshold is maintained at 136kJ mol^{-1} an appropriately steep temperature dependence is obtained, but the magnitude of the calculated rate coefficients is then much too small: a value of $<\Delta\epsilon_{down}>$ in excess of 1000cm^{-1} and strong rotational relaxation needs to be assumed in order to fit the absolute magnitude of the extrapolated rate coefficients. These values are much too large to be physically reasonable for a helium bath gas, as is indicated by the values of $<\Delta\epsilon_{down}>$ and $<\Delta R_{down}>$ needed to fit the thermal reactions modelled in Chapters 2, 3, and 4.

The form of extrapolation required may be further investigated by obtaining a more extensive set of data for rate coefficients measured with the same value for E_c and the same number density but varying combinations of thermal temperature versus field strength. Further modelling is also required to suggest the best parameter to be used as a measure of the contribution of the drift field to the dissociation rate: the plot of $\ln(k_{uni})$ against $(1/2)M_b v_d^2$ is an obvious one, but not necessarily the best choice of variable.

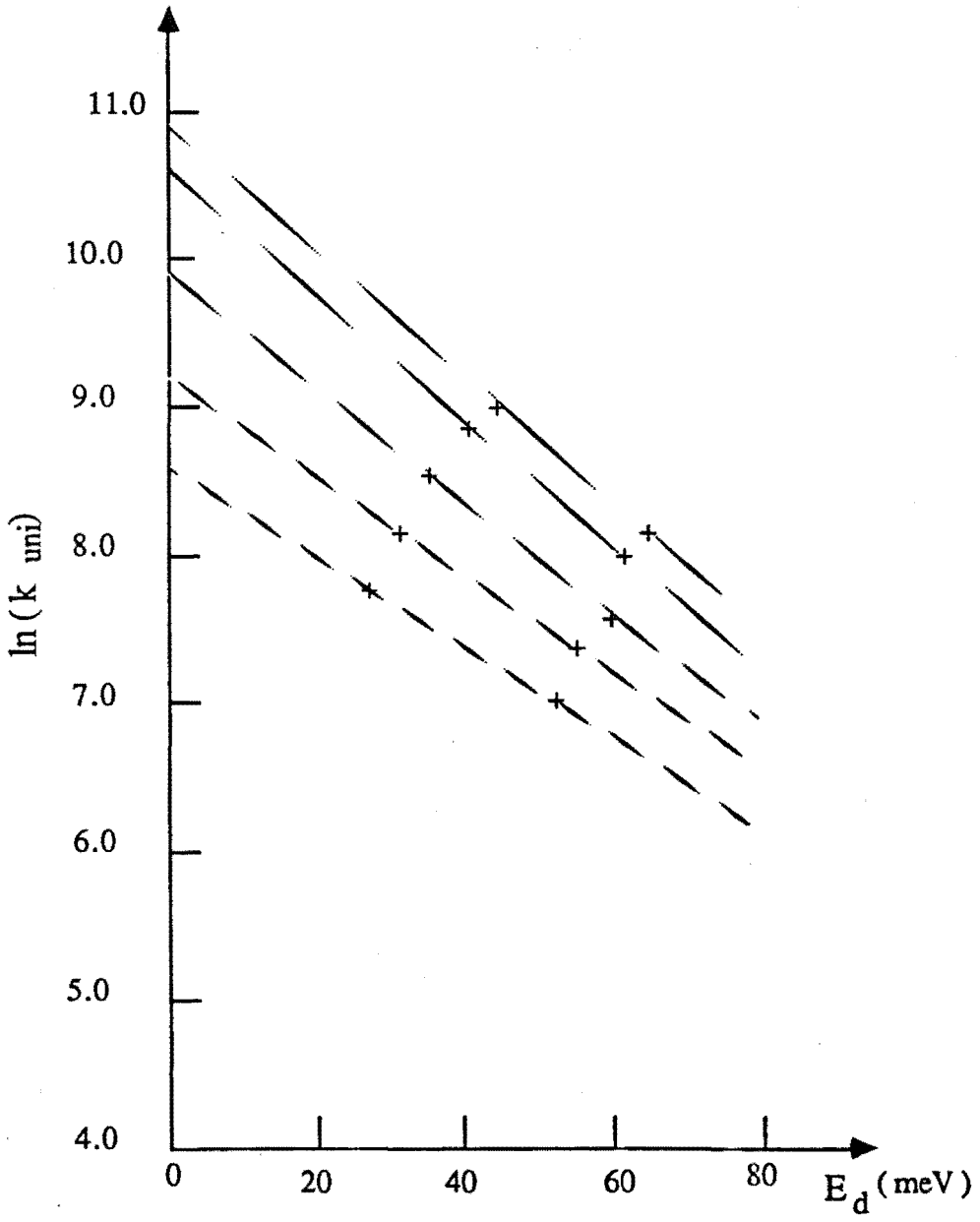

Figure 5.7. Plot of experimental $\ln(k_{uni})$ versus E_d, where $E_d=(1/2)M_b v_d^2$. A log–linear extrapolation of data measured with a fixed value of E_c to zero field is indicated by dashed lines.

IV. Conclusions

The study of unimolecular dissociation in a VT-SIFDT apparatus provides a means of investigating the nature of the steady-state translational and internal energy distributions of polyatomic ions under drift-field conditions. The approach is inherently simpler than study of the reverse association or chemical activation reactions, since only one independent distribution need be considered: the steady-state translational energy distribution.

The experimental results indicate that the vibrational and rotational degrees of freedom of the $CH_3CH_2OH_2^+$ ion approach steady state rapidly on the timescale of motion along the drift tube, since the rate of dissociation is independent of the length of the drift region (and hence the reaction time) to within the accuracy of the observations.

The fact that the measured rate of dissociation depends not only on pressure and "temperature" as defined by E_c, but also on the combination of thermal carrier gas temperature versus drift field strength indicates that, unfortunately, the ion energy distributions vary with field strength for a fixed E_c. Specifically, the internal distributions, and by inference the translational distributions, for a truly thermal system with mean translational energy E_c are broader than the corresponding distributions when a significant amount of the mean translational energy E_c is due to the drift field. This implies that unimolecular dissociation rate coefficients measured with the aid of the drift field will in general not correspond to thermal data. In order to obtain data which may be interpreted by thermal modelling, some form of extrapolation of the results to zero field would be required. Further experimental studies and theoretical modelling will be required in order to determine the best functional form for such an extrapolation and the reliability of the results.

Whilst the present study is sensitive to the non-Maxwellian nature of the steady-state translational energy distribution of the polyatomic ion in the drift field, the magnitude of the deviation from the thermal distribution is not clear. It should be noted that the

experimental rate coefficients do not deviate drastically from those which would be expected on the basis of thermal modelling (generally by up to a factor of five). Relatively small changes in the high energy tail of the translational energy distribution, which in turn determines the detailed balance relationship between the "upwards" and "downwards" collisional transfer of internal energy and angular momentum, can induce changes in the dissociation rate coefficient of this order of magnitude. Again, further model calculations will indicate the sensitivity of the results in this regard.

CONCLUSION

This work has been concerned with the calculation of unimolecular dissociation and recombination rate coefficients. A large portion of gaseous reactions of interest fall into these categories, and development of accurate and reliable methods for predicting rate coefficients and extrapolating experimental data is therefore of fundamental importance.

Rate coefficients for dissociation and recombination reactions show a dependence on the bulk pressure of the system, as determined by the bath gas, often called "fall–off" behaviour. This is manifested as a pressure–independent rate coefficient at high gas densities which decreases as the density decreases and eventually becomes proportional to the bath gas pressure at sufficiently low densities. This pressure dependence results from a complex interplay between collisional activation / deactivation and reaction from excited states: at high pressures the microscopic rate coefficients are rate determining whereas at low pressures the collisional relaxation is rate determining.

Calculation of rate coefficients in the fall–off regime requires the solution of a master equation which describes the rates of collisional transition between, and reaction from, the populations at individual energies. Sophisticated means of solving the one–dimensional master equation (in energy alone) for unimolecular dissociation have been developed (see, e.g., Gaynor *et al.* 1978a; Schranz and Nordholm 1983). Solution of the master equation for recombination reactions and their multichannel equivalent, chemical activation reactions, has generally been restricted to use of the strong collision approximation with a collision efficiency β (see, e.g., Bass *et al.* 1981; Larson *et al.* 1988), although truncated master equation approaches have also been used (see, e.g., Kohlmaier and Rabinovitch 1963). An alternative approach (see, e.g., Troe 1977a, Gilbert and McEwan 1985) has been to assume that the non–equilibrium recombination rate coefficient is, to a good approximation, related to the reverse non–equilibrium unimolecular dissociation rate coefficient by the equilibrium constant. This approach, which is based on approximate

solutions to the master equation for diatomic dissociation and the reverse recombination (Snider 1965; Keck and Carrier 1965), has the advantage that a single computer programme can be used to solve both problems. A rigorous proof of the relationship by solution of the recombination / chemical activation master equation has not, however, been presented. In chapter 2 an exact solution to the recombination / chemical activation master equation has been developed. Analysis of this solution shows that the recombination and dissociation rate coefficients are, in general, related by the equilibrium constant and a non-equilibrium factor which is easily calculated from the solution of the unimolecular dissociation master equation, and has a value between zero and one. In most cases this factor may to an excellent approximation be taken as unity. At high temperatures, however, it can become depressed from unity, a fact which may be significant when modelling high temperature systems.

The solution to the master equation for recombination and chemical activation reactions enables fast and accurate methods which have been developed (Gaynor *et al.* 1978a; Schranz and Nordholm 1983) for solution of the unimolecular dissociation master equation to be used in addition for solution of the reverse problem. It should be noted that this approach, relating back to the pioneering work of Keck and Carrier (1965), is not new. Rather, it is now on a secure theoretical footing and the conditions under which it is not accurate are apparent. Furthermore, where such conditions apply, the required correction is easily calculated.

The calculated rate coefficient for certain types of reactions is sensitive to incorporation of the constraint of angular momentum conservation. Such reactions include dissociations proceeding via a simple-fission transition state: radical-radical recombinations and, in particular, ion-molecule reactions. The feature common to these reactions which makes angular momentum conservation important is that the transition state has moments of inertia $I^{\dagger}$ that differ greatly from those of the reactant (or, for recombination, product) molecule. The importance of accounting for angular momentum conservation in rate calculations has long been recognised, and very sophisticated means of incorporating this

constraint into calculations of capture (equilibrium) rate coefficients and/or microscopic rate coefficients have been developed (see, e.g., Chesnavich and Bowers 1976, 1977; Clary 1985; Troe 1983b,1987b). More generally one requires the *non-equilibrium* (fall-off) rate coefficients, the calculation of which requires solution of a two-dimensional master equation (with independent variables E and J). Means of solving this two-dimensional problem have hitherto been limited to solutions of the low-pressure-limiting master equation (Troe 1977a, 1987a; Penner and Forst 1975,1976). This shortfall in master-equation calculations has, in general, limited analysis of fall-off behaviour in ion-molecule reactions to strong-collision modelling (e.g., Bass *et al.* 1981).

In Chapter 2, general methods of solution of the two-dimensional master equation have been developed. Two categories of solution are identified: (1) where the collisional relaxation of the internal energy is weak and where the collisional relaxation of the angular momentum is best approximated by a transition probability which is independent of the initial state (most simply with the strong-collisional form), and (2) where collisional relaxation of both internal energy and angular momentum is best modelled with a weak collisional form for the transition probability.

The solutions involve extensive (though straightforward) modification of a standard RRKM program (e.g., Gilbert 1983) to facilitate the calculation of the J-averaged microscopic rate coefficients $\bar{k}(\epsilon)$. The solution of the resulting one-dimensional J-averaged master equation then proceeds exactly as for the usual one-dimensional master equation (see, e.g., Gaynor *et al.* 1978a), with $\bar{k}(\epsilon)$ replacing the usual microscopic rate coefficients. Minor modification of a program for solution of the master equation (e.g., Gilbert 1983) is required to incorporate angular momentum conservation into the low-pressure master equation. The solutions are computationally economic, requiring times generally within an order of magnitude of that required for an ordinary RRKM calculation.

Comparison of the present result with the Troe (1977a, 1987a) solution [which applies to category (2)] indicates that the latter can overestimate the collision efficiency β by as

much as a factor of two for a typical ion–molecule reaction (that of CH_3^+ with HCN). The discrepancy between the two solutions has been shown (Appendix E) primarily to be due to factoring approximations made in the Troe solution. Improvements to the Troe solution have been derived that result in good agreement with the solution of this work. In addition it has been shown that the solution of Penner and Forst must in general *underestimate* the rate coefficient.

An important advantage of the solutions derived here is that they apply throughout the fall–off regime. This avoids the necessity of interpolation between low– and high–pressure rate coefficients (Gilbert *et al.* 1983), a procedure which has arisen because hitherto solutions to the two–dimensional master equation have only been applicable to these two limits. Direct solution of the master equation at any pressure is to be preferred for philosophical and pragmatic reasons. The method developed by Troe (1983a) introduces the approximate "broadening factors" F_{LH}, F_{SC} and F_{WC} as a means of interpolating k_{uni} between ωk_0 and k^∞. Modelling of experimental data in this way promotes the description of fall–off behaviour in terms of interpolation parameters rather than more fundamental quantities which determine the rate of reaction through the master equation, i.e., microscopic rate coefficients and average energy transfer parameters. From a more pragmatic point of view, one may ask which approach requires less effort to implement. For modelling a limited set of data, the interpolation technique is probably easier to apply since it is essentially analytical, whereas implementation of the direct numerical solution to the master equation developed in the present work requires a certain amount of acclimatisation with the computer programme. It might also be said, however, that correct utilisation of the interpolation method requires considerable understanding of the principles involved. The direct solutions of the present work offer a substantial advantage over the interpolation method when modelling large amounts of data. Once one has become familiar with the operation of the computer programme, running calculations for a wide range of pressures and temperatures is a trivial matter, whereas such modelling rapidly becomes tedious and time–consuming with the analytic interpolation technique.

The extension of the solutions presented to multichannel systems allows treatment of multichannel dissociation reactions and, with the relations developed in Chapter 2, chemical activation reactions. The combination of the results of Chapters 2 and 3 therefore makes possible the accurate modelling of a wide range of reactions via solution of the two-dimensional master equation. The methods developed in the present work constitute the only currently available means of solving the multichannel dissociation and chemical activation master equations in the fall-off and low-pressure regimes with proper inclusion of angular momentum effects. Angular momentum conservation can dramatically alter the predicted rate coefficients and branching ratios in multichannel systems, as has been illustrated in the application (Chapter 3) to the two-channel dissociation of 1-iodopropane; and the fact that the experimental data for the ion-molecule chemical activation reactions of CH_3^+ with NH_3 (Chapter 2) and CH_3CN (Chapter 4) *cannot* be reproduced, even to within an order of magnitude, without incorporation of J conservation.

There is still much room for improvement in the area of incorporating J-conservation into the master equation. The simple RRKM expression for $k(\epsilon,J)$ (Marcus 1965) used in the present calculations incorporates the gross effects of angular momentum conservation by assuming that the two-dimensional orbital rotation is adiabatic (i.e., the orbital angular momentum, L, is conserved). The choice of the internal energy ϵ and the external ("orbital") rotational energy R as independent variables for solution of the master equation also assumes that the external two-dimensional rotation of a symmetric top molecule is adiabatic. In polyatomic systems, however, the rotational motion of the individual fragments contributes in a complex fashion to the total angular momentum as the dissociation proceeds. Since the total angular momentum is conserved, the orbital angular momentum need not be an exactly conserved quantity, hence the orbital rotational degrees of freedom will not in general be rigorously adiabatic. The solution of the two-dimensional master equation without approximating the external two-dimensional rotation as adiabatic is an open problem. It is likely that the results of such a solution will not be greatly different from those of the techniques developed in this work, as is indicated by the fact that the optimum capture rate for ion/dipole reactions ovestimates the exact trajectory

result (Su and Chesnavich 1982) typically by less than 10% (see Table 4.1). However, comparison with a solution to the more gemeral problem will provide further insight into the nature of the adiabatic approximation as applied to the orbital angular momentum.

A major aim of the present work has been to adapt RRKM theory and master equation solutions to make possible the modelling of the pressure dependence of ion–molecule reactions. The work of Chapters 2 and 3 allows the application of master equation solutions to ion–molecule fall–off data for the first time. In addition, some adaptations to the standard RRKM approach are required for the calculation of microscopic rate coefficients in ion–molecule systems. Chapter 4 deals with this subject.

Ion–molecule reactions involving neutrals with a significant dipole moment have a long range, non–central potential of interaction. This has two important effects: (1) Collision complexes with greater angular momenta can be formed because the strong ion–dipole attraction reduces the size of centrifugal barriers (Herbst 1985), and (2) Hindrance to the dipole rotation (caused by the non–central electrostatic potential) significantly reduces the density of states at the transition state. The solution of the two–dimensional master equation presented in Chapter 3 is essential to take proper account of Effect (1). In Chapter 4 an exact semi–classical solution for the density of states of a sinusoidally–hindered rotor has been presented which enables Effect (2) to be included into the standard RRKM "loose" transition state.

Effect (1) tends to *increase* the rate of capture, whereas effect (2) tends to *reduce* the rate of capture. The net effect on the predicted capture rate is a moderate increase, provided one takes *both* effects into account (see, e.g., Chesnavich *et al.* 1980).

Rate coefficients predicted in the fall–off regime, on the other hand, are very sensitive to incorporation of Effects (1) and (2). The modelling of the CH_3^+/HCN association, presented in Chapter 3, shows that incorporation of angular momentum conservation increases dramatically the predicted rate of association at low pressures. The

importance of Effect (2) is indicated by the inability of Phase Space Theory (which assumes free rotation of the separate moieties in the transition state) to reproduce with physically reasonable parameters the experimental data for the pressure-dependence of the CH_3^+/CH_3CN chemical activation reaction (Herbst 1988).

Consideration has also been taken in Chapter 4 of the effect on predicted rate coefficients of the adiabaticity of all modes that are not coupled with the reaction coordinate by the long-range electrostatic potential. Such adiabaticity is implicit in ion/dipole capture models through their neglect of such uncoupled degrees of freedom. RRKM theory traditionally allows for full coupling of all degrees of freedom in the region of the transition state. A simple modification to the standard RRKM formula for $k(\epsilon,J)$ has been presented in Chapter 4 which accounts exactly for adiabaticity of degrees of freedom that are completely uncoupled from the reaction coordinate in the region from the transition state out to products. The high pressure association rate so obtained is equivalent to the capture model of Chesnavich *et al.* (1980) except that the Chesnavich model does not explicitly include angular momentum conservation.

It has also been noted in Chapter 4 that use of microcanonical variational transition state theory (μVTST) is important when applying RRKM theory to ion/dipole reactions where the electrostatic potential is non-central. In this regard it was pointed out in Chapter 5 that for high temperature applications one should *always* allow for the possibility that the variationally chosen transition state may lie at smaller separation of the moieties where chemical as well as electrostatic forces determine the potential. Hence a variational calculation at high temperatures should include, in addition to long-range "orbiting" transition states, one or more transition states in the chemical interaction region. These considerations for ion-molecule reactions have been stressed previously by Chesnavich *et al.* (1981).

The work presented in Chapter 4 enables RRKM theory to be applied to ion-dipole reactions for the calculation of microscopic rate coefficients $k(\epsilon,J)$ for use in fall-off

calculations. This has not previously been possible: ion–dipole calculations have in the main been limited to the capture rate. This work couples with the development of master equation solutions in Chapters 2 and 3 to allow ion–molecule reaction rates to be reliably modelled and predicted at any pressure or temperature. It therefore constitutes an important improvement, since the only means of calculating pressure–dependence of ion–molecule reactions hitherto available involves use of the strong collision formalism (Bass *et al.* 1981). As has been demonstrated herein and elsewhere (see, e.g., Gilbert *et al.* 1983), use of the strong collision approximation with a collision efficiency β enables data over a limited range of pressures or temperatures to be fitted, but commonly leads to significant error (a factor of *ca.* 2 or 3) when extrapolating over a wide range of conditions.

A direction for future improvement in calculating microscopic rate coefficients, both in ion–molecule and neutral reactions, is in the treatment of adiabatic effects, since adiabatic behaviour (or the lack of it) in certain degrees of freedom affects the evaluation of $k(\epsilon,J)$. As mentioned above in connection with the solution of the two–dimensional master equation, the treatment of the two–dimensional external orbital rotation is one candidate for examination. Quack and Troe (see, e.g., 1974, 1977) have carried out pioneering work in this regard with the development of the Statistical Adiabatic Channel Model (SACM). However, the optimal way of calculating $k(\epsilon,J)$ for unimolecular dissociation and recombination reactions within the statistical framework is not as yet clear.

In Chapter 5 a study of unimolecular dissociation of the protonated ethanol ion in a variable–temperature selected ion flow–drift tube (VT–SIFDT) has been presented. The purpose of this study was to address the question of whether drift–tube apparatuses can be used to gain *quantitative* kinetic information concerning the rates of reactions involving polyatomic ions at elevated temperatures. The reason for studying unimolecular dissociation in a drift field rather than a bimolecular process is because the complexity of analysis is considerably reduced. The study indicates that the induction periods for achieving steady state distributions of translational and internal energies are rapid compared with the

experimental timescale for motion of the $CH_3CH_2OH_2^+$ ions along the drift tube (this contrasts with the timescale for vibrational relaxation illustrated by Federer *et al.* (1985) for the diatomic ions O_2^+ and N_2^+). The study also shows that the dissociation induced by the drift field does *not* correspond directly to thermal dissociation at an elevated temperature with the same centre-of-mass translational energy E_c. Such an assumption would correspond to the first level of approximation that arises out of the detailed theory of molecular ion motion in drift tubes (Viehland *et al.* 1981). It may be concluded that this first level of approximation is not good enough for obtaining quantitative thermal data from drift-tube kinetic studies.

In order to pursue the possibility of obtaining quantitative thermal data for reactions of polyatomic ions at elevated temperatures, it will be important to investigate the dependence of k_{uni} on the strength of drift field for a constant value of E_c, with a view to determining the form of extrapolation to zero-field required.

Finally, a question regarding modelling of ion/molecule reactions in helium [e.g., the modelling studies of the CH_3^+/NH_3 (Chapter 2), CH_3^+/HCN (Chapter 3), and CH_3^+/CH_3CN (Chapter 3) reactions] is raised by the derivation in Chapter 5 of an ion/induced-dipole total non-reactive collision rate coefficient that accounts for the size of the species involved. In Chapter 5 it was shown that for the $CH_3CH_2OH_2^+$/He pair in the range 700-1100K the Langevin collision rate coefficient was too small by a factor of *ca.* 2. Part of the reason for the inadequacy of the simple Langevin model in this case is undoubtably the weak polarizability of He, since an encounter model which includes only the electrostatic potential (neglecting interactions such as steric hindrance) will then be inaccurate. Time has not allowed further investigation of the effect of using the improved collision rates with helium on the modelling of the other ion-molecule reactions mentioned above. The increase in the collision frequency ω may not be as large at 300K (the temperature of the calculations and experiments) as at the higher temperatures of interest in Chapter 5, but it may still be significant. Qualitatively, the effect of an increased collision rate on such modelling is to *reduce* the inferred average collisional energy transfer

parameters. However, this would make for very weak collisions, with average downward energy transfer parameters of, say, somewhat less than $100cm^{-1}$. Such numbers would take some believing in the light of trajectory calculations (Date *et al.* 1984) and typical energy transfer parameters for neutral systems (see, e.g., Tardy and Rabinovitch 1977). The answer may be that molecular ions do indeed display particularly weak energy transfer in collisions as a result of the effect of the charge on the dynamics of collisions with a neutral bath gas. Alternatively, there may be another factor involved such as the effective temperature of the collision complex when formed in the ICR spectrometer. If ions in the ICR spectrometer have an effective temperature that is suprathermal then accounting for this effect would *increase* the inferred energy transfer parameters again, thus counteracting the effect of improving the estimate of the collision frequency. At this stage we cannot say how much these effects influence the results obtained thus far. For future modelling, it will be important to (1) Investigate more closely the accuracy of various estimates of the collision frequency ω (such as the Langevin rate compared with that derived in chapter 5). This is most probably best done by trajectory studies. (2) Investigate more carefully the effective temperature and collision frequency appropriate to the ICR experiment.

APPENDIX A

RRKM PARAMETERS FOR CH_3^+/NH_3 CHEMICAL ACTIVATION REACTION

For the CH_3^+/NH_3 reaction, the two major dissociative channels, i.e., that leading back to reactants [Eq. (2.33a)] and that leading on to the $CH_2NH_2^+$ product ion [Eq. (2.33b)] are included in the calculation.

I. *Reactant Channel.* This channel is modelled with a loose transition state, i.e., vibrational frequencies and moments of inertia were taken as those of the separate reactants (Nobes and Radom 1983; Herzberg 1949). The potential of interaction between the moieties in the simple-fission transition state is that between the positive charge of the methyl cation and the dipole (μ) and isotropic polarisability (α) of ammonia [1.47 Debye (McClellan 1963) and 2.26×10^{-24} cm^3 (Hirschfelder *et al.* 1954) respectively], with the overall threshold energy being being 442 kJ mol^{-1} (Nobes and Radom 1983):

$$V(r) = 442.0 - 6.9492\times10^{26}\alpha/r^4 - 289.21\,\mu/r^2 \text{ kJ mol}^{-1} \qquad (A.1)$$

with α in cm^3, μ in Debye, and r in Å. The separation of the moieties in the transition state, determined by canonical variation (see, e.g., Garrett and Truhlar 1979 or Chapter 1 above) was 10Å. At this separation the only hindrance to rotation of the moieties is that of the dipole NH_3 due to the non-central electrostatic potential. Parameters are included in Table A1. The equilibrium constant, required for converting unimolecular rate coefficients to association rate coefficients, is calculated (see, e.g., McQuarrie 1973) for 300K using the parameters of this appendix to be 2.39×10^{51} cm^3.

II. $CH_2NH_2^+$ *Product Channel.* The structure and vibrational frequencies of the transition state have been calculated by Nobes and Radom (1973). Their frequencies and geometries are used in the present calculation. The threshold energy is taken as 348kJ mol^{-1} (see Chapter 2 for further discussion of this). The parameters are included in Table A1.

III. $CH_3NH_3^+$ *Collision Complex.* Nobes and Radom (1983) have calculated the structure and geometry of this. The parameters are included in Table A2. The collision frequency with the bath gas helium at 300K was assumed to be given by the Langevin model, which gives $\omega = 6.75\times10^{-17}(p/T)$ s^{-1}, where p is the pressure of He (Pa) and T the temperature (K).

TABLE A1. RRKM transition state parameters for the multi-channel dissociation of $CH_3NH_3^+$. Frequencies and rotational constants for the transition states of Eqs. (2.33a) and (2.33b). For the simple fission transition state (2.33a), the rotational constant for the hindered dipole rotation is marked with an asterisk. The frequencies and structure for CH_3^+ are from Nobes and Radom (1983), and those for NH_3 are from Herzberg (1949). For Eq. (2.33b), the frequencies and structure are from Nobes and Radom (1983).

Vibrations : Frequencies[a] (cm^{-1}) (2.33a)	(2.33b)	Type	Rotations : B Values[b] (cm^{-1}) (2.33b)	(2.33a)
950 (1)	452 (1)	External inactive	0.646 (1,2)	0.0205 (1,2)
1628 (2)	822 (1)			
3337 (1)	1001 (1)			
3414 (2)	1061 (1)	External active	2.269 (1,1)	2.543 (3,1)
1350 (1)	1093 (1)			
1370 (2)	1183 (1)			
2903 (1)	1388 (1)	Internal		10.36 (3,1)
3090 (2)	1558 (1)			8.951 (2,2)
	1562 (1)			*9.301 (1,2)
	1731 (1)			
	1805 (1)			
	2106 (1)			
	2517 (1)			
	3299 (1)			
	3403 (1)			
	3701 (1)			
	3821 (1)			

[a]Degeneracies in parenthesis.

[b]Parenthetic quantities are symmetry number and dimension respectively.

TABLE A2. RRKM molecular parameters for $CH_3NH_3^+$ collision complex. Frequencies (appropriately scaled) and structure from Nobes and Radom (1983).

Vibrations : Frequencies[a] (cm^{-1})	Rotations : Type	B Value[b] (cm^{-1})
275 (1)	External inactive	0.648 (1,2)
907 (1)		
1006 (2)	External active	2.725 (3,1)
1348 (2)		
1610 (1)		
1653 (2)		
1703 (1)		
1844 (2)		
3259 (1)		
3367 (2)		
3538 (1)		
3615 (2)		

[a]Degeneracies in parenthesis.

[b]Parenthetic quantities are symmetry number and dimension respectively.

APPENDIX B

RRKM PARAMETERS FOR METHYL/METHYL RECOMBINATION

The illustrative calculations for the methyl/methyl recombination reaction are carried out at 300K. The transition state is chosen using Canonical Variational Transition State Theory (CVTST) at a separation of 4.5 Å. The reaction coordinate potential was approximated as a Morse curve:

$$V(r) = D\{1-\exp[-\beta_m(r-r_e)]\}^2 \qquad (B.1)$$

where $D = E_O = 368\text{kJ mol}^{-1}$, $\beta_m = 2.4575\ \text{Å}^{-1}$, and $r_e = 1.54$ Å. The usual RRKM loose transition state is assumed, wherein the fragments are treated as free rotors except for any steric hindrance (see, e.g., Greenhill *et al.* 1986a). At 4.5 Å separation of the moieties, it was found that the rotations of the methyl fragments are unhindered. The frequencies and rotational constants are taken as those for ethanol and the separate methyl fragments (Greenhill *et al.* 1986b). The relevant parameters are included in Table B1. For conversion from k_{uni} to k_{rec}, the equilibrium constant calculated at 300K with the parameters presented here was 1.02×10^{38} cm^3.

Table B1. RRKM parameters for methyl recombination model used for illustrative calculations. R denotes the reactant (ethane); T denotes the transition state ($CH_3 \cdots CH_3$).
Vibrations: degeneracies in parenthesis.
Rotations: B value = rotational constant (all internal rotors are unhindered). Numbers in parentheses are symmetry number and dimension of rotation, respectively.

Vibrations: Frequencies (cm^{-1})		Rotations:		
		Type	B values (cm^{-1})	
R	T		R	T
303	3125 (4)	ext. inactive	0.658 (2,2)	0.1085 (2,2)
823	1304 (4)	ext. active	2.664 (3,1)	2.42 (3,1)
1016 (2)	1344 (2)	internal		9.67 (3,1)
1246 (2)	2942 (2)			9.67 (2,2)
1438				9.67 (2,2)
1449 (2)				
1526 (2)				
1552				
3043				
1361				
3140 (2)				
3174 (2)				

$E_o(J=0) = 368.2$ kJ mol^{-1}

APPENDIX C

RRKM PARAMETERS FOR CH_3^+/HCN ASSOCIATION

The CH_3^+/HCN association reaction at 300K proceeds via a loose, orbiting transition state, for which the transition state parameters are those of the separate reactants. The frequencies and geometries for separated reactants in the transition state, and for the collision complex CH_3NCH^+ were taken as those calculated by DeFrees *et al.* (1985). The potential of interaction is determined by the interaction of the ion with the dipole moment (μ) and the polarizability (α) of HCN, with the threshold energy calculated from thermochemical data (Knight *et al.* 1986; Rosenstock *et al.* 1977) as 368kJ mol^{-1}:

$$V(r) = 368 - 6.9492\times10^{26}\alpha/r^4 - 289.21\mu/r^2 \text{ kJ mol}^{-1} \qquad (C.1)$$

where μ = 2.98 Debye (McClellan 1963), $\alpha = 2.59\times10^{-24}$ cm^3 (Hirschfelder *et al.* 1954). The collision frequency was assumed to be that given by the Langevin capture model. At 300K, this yields $\omega = 1.336\times10^5P$, where P is the pressure in Pa. The molecular parameters are included in Table C1. For conversion of k_{uni} to k_{ass}, the equilibrium constant was calculated using the parameters herein to be 3.11×10^{38} cm^3 at 300K.

Table C1. RRKM parameters for $(H_3CNCH)^+$ collision complex (C) and transition state (T). Langevin capture rate between collision complex and bath gas at 300 K = $1.336 \times 10^5 p$, where p = pressure in Pa.

Vibrational frequencies (cm^{-1})[a]		Rotational B values[b] (cm^{-1})		
C	T		C	T
323(2)	1350(1)	External inactive:	0.305(1,2)	0.0083(1,2)
757(1)	1370(2)	External active:	5.25(3,1)	4.84(3,1)
837(2)	2903(1)	Internal:		9.68(2,2)
1121(2)	3090(2)			1.48(1,2)
1404(1)	791(2)			
1426(2)	2170(1)			
2286(1)	3274(1)			
2909(1)				
3014(2)				
3200(1)				

[a] The frequencies are from De Frees *et al.* (1985), with a scaling factor of 0.89 (Defrees and McLean 1985). Degeneracies in parenthesis.

[b] Parenthetic quantities are symmetry number and dimension respectively.

APPENDIX D

EVALUATION OF LOW-PRESSURE RATE COEFFICIENTS

In this appendix the details of evaluation of the quantity $Q(\epsilon,\epsilon')$ for the assumed exponential-down form of P(R,R') are presented in order to facilitate solution of the low-pressure two-dimensional master equation via Eqs. (3.45)-(3.47). From microscopic reversibility and normalisation, $H_0(\epsilon,J)$ in Eq. (3.43) may be expressed as:

$$H_0(\epsilon,J) = \frac{f(J)}{Z(\epsilon)}\left[1 - \int_{J_0(\epsilon)}^{\infty} dJ'\ P(J',J)\right] \tag{D.1}$$

where

$$Z(\epsilon) = \int_0^{J_0(\epsilon)} dJ\ f(J) \tag{D.2}$$

From Eq. (3.46), one then finds:

$$Q(\epsilon,\epsilon') = \frac{1}{Z(\epsilon')}\left[Z(\epsilon) - \int_0^{J_0(\epsilon)} dJ f(J) \int_{J_0(\epsilon')}^{\infty} dJ' P(J',J)\right] \tag{D.3}$$

Before introducing Eq. (3.49), it is necessary to transform from J, as an independent variable, to the energy R of the two-dimensional external adiabatic rotation. Correspondingly, one has $P(R,R')=P(J,J')/B(2J+1)$ and $f(R)=(k_BT)^{-1}\exp(-R/k_BT)$.

To evaluate $Q(\epsilon,\epsilon')$, we define the quantity $S(\epsilon,\epsilon') = 1 - Q(\epsilon,\epsilon')$:

$$S(\epsilon,\epsilon') = \frac{1}{Z(\epsilon')}\left[Z(\epsilon') - Z(\epsilon) + \int_0^{R_0(\epsilon)} dR\ f(R) \int_{R_0(\epsilon')}^{\infty} dR' P(R',R)\right] \tag{D.4}$$

The exponential-down form of P(R,R'), [Eq. (3.49)], requires separation of the integrands in Eq. (D.4) into portions where R<R' and R>R'. The form of the result depends on whether $\epsilon'>\epsilon$ or $\epsilon'<\epsilon$.

(1) For $\epsilon'>\epsilon$ one has:

$$S(\epsilon,\epsilon') = \frac{1}{Z(\epsilon')}\left[Z(\epsilon') - Z(\epsilon) + \int_0^{R_0(\epsilon')} dR\, f(R) \int_{R_0(\epsilon')}^{\infty} dR' \frac{e^{(R-R')/\delta}}{\gamma+\delta}\right.$$

$$\left. + \int_{R_0(\epsilon')}^{R_0(\epsilon)} dR\, f(R) \left[\int_{R_0(\epsilon')}^{R} dR' \frac{e^{(R'-R)/\gamma}}{\gamma+\delta} + \int_{R}^{\infty} dR' \frac{e^{(R-R')/\delta}}{\gamma+\delta}\right]\right] \qquad (D.5)$$

After some algebra, Eq. (D.5) reduces to:

$$S(\epsilon,\epsilon') = \frac{\gamma\delta}{k_B T(\gamma+\delta)Z(\epsilon')}\left[e^{R_0(\epsilon')/\gamma}\, e^{-R_0(\epsilon)/\delta} - e^{-R_0(\epsilon')/\delta}\right] \qquad (D.6)$$

where $Z(\epsilon) = 1-\exp[-R_0(\epsilon)/k_B T]$.

(2) For $\epsilon'<\epsilon$ one has:

$$S(\epsilon,\epsilon') = \frac{1}{Z(\epsilon')}\left[Z(\epsilon') - Z(\epsilon) + \int_0^{R_0(\epsilon)} dR\, f(R) \int_{R_0(\epsilon')}^{\infty} dR' \frac{e^{(R-R')/\delta}}{\gamma+\delta}\right] \qquad (D.7)$$

After some more algebra, one obtains:

$$S(\epsilon,\epsilon') = \frac{1}{Z(\epsilon')}\left[Z(\epsilon') - Z(\epsilon) + \frac{\gamma\delta e^{-R_0(\epsilon')/\delta}\left[e^{R_0(\epsilon)/\gamma} - 1\right]}{k_B T(\gamma+\delta)}\right] \qquad (D.8)$$

Eqs. D.6 and D.8 enable $Q(\epsilon,\epsilon')$ to be evaluated, and thus $\bar{g}(\epsilon)$ found from numerical solution of Eq. (3.45), using standard techniques (Gilbert *et al.* 1983). Eq. (3.47) then specifies k_0 in terms of $\bar{g}(\epsilon)$.

APPENDIX E

COMPARISON WITH TROE'S SOLUTION.

In this appendix modifications to Troe's approximate analytic solution to the low-pressure two-dimensional master equation are derived which show that his solution is accurate for the non-equilibrium population $g(\epsilon,J)$, but inaccurate for the collision efficiency β due to factoring approximations made *after* the determination of $g(\epsilon,J)$, in the actual evaluation of k_0.

We commence with Eq. (3.47), re-expressed (Troe 1977a, 1987a) as:

$$k_0 = \int_0^{E_0} d\epsilon\ f(\epsilon) \int_0^{R_0(\epsilon)} dR\ h(\epsilon,R) f(R) T(\epsilon,R) \tag{E.1}$$

where $h(\epsilon,R) = g(\epsilon,R)/f(\epsilon,R)$ and

$$T(\epsilon,R) = \int_{-\infty}^{\infty} dR' \int_{-\infty}^{E_0(R')} d\epsilon'\ P(\epsilon',R',\epsilon,R)$$

$$= \frac{\beta^3 \exp[-(E_0-B^*R-\epsilon)/\beta]}{(\alpha+\beta)(\beta+B^*\gamma)(\beta-B^*\delta)} + \frac{B^{*2}\delta^3 \exp[-(E_0-R-\epsilon)/\delta]}{(\gamma+\delta)(\alpha+B^*\delta)(B^*\delta-\beta)} \tag{E.2}$$

where γ and δ are as defined in Eq. (3.49), α and β are the exponential parameters for $P(\epsilon,\epsilon')$ as used by Troe ($\alpha = \langle\Delta\epsilon_{down}\rangle$, to which β is related by microscopic reversibility), and $B^* = 1-(I/I^\dagger)$; for fully contributing rotations where $I^\dagger \gg I$ (as in the present system), $B^* \approx 1$. Define

$$M(\epsilon) = \int_0^{R_0(\epsilon)} dR\ h(\epsilon,R) f(R) T(\epsilon,R) \tag{E.3}$$

whence

$$k_0 = \int_0^{E_0} d\epsilon f(\epsilon) M(\epsilon) \tag{E.4}$$

We evaluate Eq. (E.3) with the same approximation used by Troe, viz., $E_0(R) = E_0 - B^*R$, implying $R_0(\epsilon)=(E_0-\epsilon)/B^*$. After some algebra, one obtains:

$$
\begin{aligned}
M(\epsilon) = & \frac{\beta^3\left[e^{(\epsilon-E_0)/\beta} - e^{(\epsilon-E_0)/B^*k_BT}\right]}{(1-B^*k_BT/\beta)(\alpha+\beta)(\beta+B^*\gamma)(\beta-B^*\delta)} \\
& + \frac{B^{*2}\delta^3\left[e^{(\epsilon-E_0)/B^*\delta} - e^{(\epsilon-E_0)/B^*k_BT}\right]}{(1-k_BT/\delta)(\gamma+\delta)(\alpha+B^*\delta)(B^*\delta-\beta)} \\
& - \frac{C_1\beta^3\left[e^{(\epsilon-E_0)(1/\beta+Y_1/k_BT)} - e^{(\epsilon-E_0)/B^*k_BT}\right]}{(1-B^*k_BT/\beta-Y_1B^*)(\alpha+\beta)(\beta+B^*\gamma)(\beta-B^*\delta)} \\
& - \frac{C_1B^{*2}\delta^3\left[e^{(\epsilon-E_0)(1/B^*\delta+Y_1/k_BT)} - e^{(\epsilon-E_0)/B^*k_BT}\right]}{(1-k_BT/\delta-Y_1B^*)(\gamma+\delta)(\alpha+B^*\delta)(B^*\delta-\beta)} \\
& - \frac{C_2\beta^3\left[e^{(\epsilon-E_0)(1/\beta+Y_2/k_BT)} - e^{(\epsilon-E_0)/B^*k_BT}\right]}{(1-B^*k_BT/\beta-Y_2B^*)(\alpha+\beta)(\beta+B^*\gamma)(\beta-B^*\delta)} \\
& - \frac{C_2B^{*2}\delta^3\left[e^{(\epsilon-E_0)(1/B^*\delta+Y_2/k_BT)} - e^{(\epsilon-E_0)/B^*k_BT}\right]}{(1-k_BT/\delta-Y_2B^*)(\gamma+\delta)(\alpha+B^*\delta)(B^*\delta-\beta)}
\end{aligned}
\qquad \text{(E.5)}
$$

where Y_1, Y_2, C_1 and C_2 are the quantities in Eqs. (27) and (28) of (Troe 1987a). Evaluation of k_0 through Eqs. (E.4) and (E.5) (which requires numerical evaluation of the integral in Eq. (E.4), since one uses the exact $f(\epsilon)$, rather than any approximation) yields curve B in Figure 3.7. While Troe's original solution (curve D) is much greater than the exact upper bound of Chapter 3 (curve A), that from Eqs. (E.4) and (E.5) exceeds the upper bound by no more than 15%. Equations (E.4) and (E.5) therefore represent an improvement to Troe's original expression. The differences between this and Troe's original expression are that the factorisation approximation is not made, and that all ϵ-dependent quantities are evaluated exactly rather than through various semiclassical approximations. Equations (E.4) and (E.5) require additional effort to evaluate but give a greatly improved agreement with the exact upper bound results obtained by the present method. One sees that the overestimate in the original Troe expression arises because, although his expressions for $g(\epsilon,R)$ appear to be accurate, the exact $f(\epsilon,R)$ =

$(Q_{vib}k_BT)^{-1}\rho(\epsilon)\exp(-[R+\epsilon]/k_BT)$ is replaced with the approximation $f(\epsilon,R) \approx (Q_{vib}k_BT)^{-1}\rho[\epsilon_0(R)]\exp(-[R+\epsilon]/k_BT)$. While this permits analytic evaluation of the final k_0 and thus avoids our last numerical integration, it overestimates $f(\epsilon,R)$ (because $\epsilon_0(R)$ is always greater than ϵ) and thus overestimates the final k_0, by as much as a factor of 2 in the present case.

However, it is not essential when evaluating k_0 to make the approximation that $\rho(\epsilon)\equiv\rho[\epsilon_0(R)]$ in $f(\epsilon,R)$ in order to obtain an analytic solution. Lastly, we derive an improved analytic approximation using the Troe factoring technique, which will give the curve denoted C in Fig. 3.7. Following Troe, we re-write Eq. (E.4) as:

$$k_0 = \int_0^{E_0} d\epsilon\ \rho_{vib}(\epsilon)\exp(-\epsilon/k_BT)\ F_{rot,K}(\epsilon)\ M(\epsilon) \tag{E.6}$$

where Troe's $F_{rot,K}(\epsilon)$ accounts for the effect of the active external rotor on $f(\epsilon)$. Adopting Troe's approximation $F_{rot,K}(\epsilon) \approx F_{rot,K}(E_0)$, and evaluating this by Troe's method, one then has:

$$k_0 = \frac{\rho_{vib}(E_0)}{Q_{vib}}\ F_{rot,K}\ e^{-E_0/k_BT}\int_0^{E_0} d\epsilon \frac{\rho_{vib}(\epsilon)}{\rho_{vib}(E_0)}\ e^{(E_0-\epsilon)/k_BT} M(\epsilon) \tag{E.7}$$

Following Troe's use of the semiclassical Whitten-Rabinovitch approximation, one puts:

$$\rho_{vib}(\epsilon)/\rho_{vib}(E_0) \approx [[\epsilon+a(E_0)E_z]/[E_0+a(E_0)E_z]]^{s-1} \tag{E.8}$$

where a, E_z and s are as defined by Troe. Equation (E.7) may then be evaluated analytically through Eq. (E.5). After some algebra, and ignoring some higher-order terms, one obtains the following approximate analytic expression for the collision efficiency:

$$\beta = \frac{1}{k_BTF_EF_{rot,J}} \sum_{i=1}^{7} \frac{a_i}{(b_i-1/k_BT)} \left[1 - \frac{s-1}{x_i} + \frac{(s-1)(s-2)}{x_i^2}\right] \tag{E.9}$$

where F_E is as defined by Troe, $F_{rot,J}$ is his expression for the contribution to F_{rot} from the inactive external rotations, $x_i = [E_0+a(E_0)E_z](b_i-1/k_BT)$, and the a_i and b_i are given by:

$$
\begin{aligned}
a_1 &= \beta^3/(1-B^*k_BT/\beta)(\alpha+\beta)(\beta+B^*\gamma)(\beta-B^*\delta), & b_1 &= 1/\beta,\\
a_2 &= B^{*2}\delta^3/(1-k_BT/\delta)(\gamma+\delta)(\alpha+B^*\delta)(B^*\delta-\beta), & b_2 &= 1/B^*\delta,\\
a_3 &= -C_1\beta^3/(1-B^*k_BT/\beta-Y_1B^*)(\alpha+\beta)(\beta+B^*\gamma)(\beta-B^*\delta), & b_3 &= 1/\beta + Y_1/k_BT,\\
a_4 &= -C_1B^{*2}\delta^3/(1-k_BT/\delta-Y_1B^*)(\gamma+\delta)(\alpha+B^*\delta)(B^*\delta-\beta), & b_4 &= 1/B^*\delta + Y_1/k_BT,\\
a_5 &= -C_2\beta^3/(1-B^*k_BT/\beta-Y_2B^*)(\alpha+\beta)(\beta+B^*\gamma)(\beta-B^*\delta), & b_5 &= 1/\beta + Y_2/k_BT,\\
a_6 &= -C_2B^{*2}\delta^3/(1-k_BT/\delta-Y_2B^*)(\gamma+\delta)(\alpha+B^*\delta)(B^*\delta-\beta), & b_6 &= 1/B^*\delta + Y_2/k_BT,\\
a_7 &= -(a_1+a_2+a_3+a_4+a_5+a_6), & b_7 &= 1/B^*k_BT. \qquad \text{(E.10)}
\end{aligned}
$$

The seventh term in Eq. (E.9) has a special form when $B^*=1$, in which case $(b_7-1/k_BT)=0$ and the seventh term becomes $a_7[E_0+a(E_0)E_z]/s$.

It can be seen from Fig. 2 that the analytic solution of Eq. (E.9), plotted as curve C, yields a significant improvement over Troe's orginal expression; however, it can be 30% higher than the exact upper bound furnished by the present numerical technique.

APPENDIX F

RRKM PARAMETERS FOR 1-IODOPROPANE TWO-CHANNEL DISSOCIATION

The two-channel dissociation of 1-iodopropane involves one tight transition state (HI elimination, channel 1) and one loose transition state (fission of the carbon-iodine bond, channel 2). Transition state and molecular parameters were taken as those used by Gaynor *et al.* (1978). The molecular RRKM parameters are included in Table F1. RRKM parameters for the two dissociative channels are included in Table F2.

Table F1. RRKM molecular parameters for 1-iodopropane multichannel dissociation.
Vibrations: degeneracies in parenthesis.
Rotations: B value = rotational constant. Numbers in parentheses are symmetry number and dimension of rotation, respectively.

Vibrations (cm^{-1})	Rotations: Type	B value (cm^{-1})
3100 (7)	ext. inactive	0.062 (1,2)
1450 (5)	ext. active	0.333 (1,1)
1150 (6)		
1000 (2)		
700 (1)		
600 (1)		
425 (2)		
300 (1)		
200 (1)		
70 (1)		

Table F2. RRKM transition state parameters for channel 1 (T_1) and channel 2 (T_2). Critical energies for channels 1 and 2 are 203 kJ mol^{-1} and 221 kJ mol^{-1} respectively. For channel 2: interaction between C_3H_7 and I moieties, V(r), taken to be Morse curve, $V(r) = D\ \{1-\exp[-\beta_M(r-r_e)]\}^2$, with $D = E_0$, $\beta_M = 4.925$, $r_e = 2.13$Å. Lennard-Jones reference collision frequency used with collision diameter $\sigma = 6.0$ Å (Gaynor *et al.* 1978) and well depth $\epsilon/k_B = 460$ K.

Vibrations: degeneracies in parenthesis.

Rotations: B value = rotational constant. Numbers in parentheses are symmetry number and dimension of rotation, respectively.

Vibrations: Frequencies (cm^{-1})		Rotations: Type	Rotations: B value (cm^{-1})	
T_1	T_2		T_1	T_2
3100 (6)	3100 (7)	ext. inactive	0.073 (1,2)	0.037 (1,2)
2200 (1)	1450 (5)	ext. active	0.277 (1,1)	0.299 (1,1)
1450 (4)	1150 (4)			
1300 (1)	1000 (2)			
1150 (7)	700 (2)			
1000 (1)	400 (1)			
700 (2)	200 (1)			
300 (1)	130 (3)			
135 (3)	70 (1)			

APPENDIX G

DERIVATION OF THE DENSITY OF STATES FOR A TWO-DIMENSIONAL, SINUSOIDALLY-HINDERED ROTOR FROM THE DIRECT PHASE SPACE INTEGRAL

The semi-classical density of states of a two-dimensional rotor is expressed as an integral over a constant energy surface in the phase space of the system:

$$\rho(E) = h^{-2}\int\int\int\int d\theta d\varphi dP_\theta dP_\varphi \delta(E-H) \tag{G.1}$$

where h is Planck's constant, E the fixed energy and H the Hamiltonian for the sinusoidally hindered rotor, Eq. (4.15). The phase-space integral in Eq. (G.1) evaluated by transforming from the canonical Euler coordinates $\{\theta,\varphi,P_\theta,P_\varphi\}$ to the set of non-canonical coordinates $\{\theta,\varphi,\zeta,L\}$, where θ and φ have the same definitions, L is the total angular momentum, which lies in a plane perpendicular to the axis of the rotor, and ζ describes the angle of orientation of the angular momentum vector $\underline{L}$ in the plane perpendicular to the rotor axis. The vector $\underline{L}$ is expressed as the product of the inertia tensor $\bar{I}$ and the angular velocity with respect to the principal axes, $\underline{\omega}$ (Goldstein 1980):

$$\underline{L} = \bar{I}\cdot\underline{\omega} \tag{G.2}$$

In Eq. (G.2), the angular velocity $\underline{\omega}$ may be expressed in terms of the Euler coordinates (Goldstein 1980):

$$\underline{\omega} = I^{-1}\begin{bmatrix} P_\theta \\ P_\varphi/\sin\theta \\ P_\varphi\cos\theta/\sin^2\theta \end{bmatrix} \tag{G.3}$$

where I is the moment of inertia of the rotor. The inertia tensor $\bar{I}$ for a two-dimensional rotor is given as:

$$\bar{I} = \begin{bmatrix} I & 0 & 0 \\ 0 & I & 0 \\ 0 & 0 & 0 \end{bmatrix} \tag{G.4}$$

Substituting Eqs. (G.3) and (G.4) into Eq. (G.2) gives the required relationship between $\underline{L}$ and the Euler coordinates (Goldstein 1980):

$$\underline{L} = \begin{bmatrix} P_\theta \\ P_\varphi/\sin\theta \\ 0 \end{bmatrix} \tag{G.5}$$

From Eq. (G.5), the projections of $\underline{L}$ onto the two orthogonal principal axes in the plane perpendicular to the body axis are P_θ and $P_\varphi/\sin\theta$. Hence the angle of orientation of $\underline{L}$ in this plane, ζ, is determined in terms of these projections. The equations of transformation from the Euler coordinates $\{\theta,\varphi,P_\theta,P_\varphi\}$ to the new set $\{\theta,\varphi,\zeta,L\}$ are then:

$$\begin{aligned} \theta &= \theta \\ \varphi &= \varphi \\ \tan\zeta &= P_\varphi/P_\theta\sin\theta \\ L^2 &= P_\theta^2 + P_\varphi^2/\sin^2\theta \end{aligned} \tag{G.6}$$

The Hamiltonian for the system in the new set of coordinates is:

$$H = L^2/2I + (V_0/2)(1-\cos\theta) \tag{G.7}$$

In order to carry out the phase-space integral in the new set of coordinates, it is necessary to determine the Jacobian, J, of the transformation. This will differ from unity because the new set of coordinates are not canonical (see, e.g., Goldstein 1980). After some algebra, one finds $J=L\sin\theta$. Hence $\rho(E)$ may now be expressed as:

$$\rho(E) = h^{-2}\int_0^{2\pi} d\varphi \int_0^{2\pi} d\zeta \int_0^{\theta_{max}} d\theta \int_0^{\infty} dL\ L \sin\theta\ \delta(E-H) \qquad (G.8)$$

The range of the integral over θ is determined by the δ function. If $E>V_0$, then θ may take its full range of values ($0<\theta<\pi$). If $E<V_0$ then θ_{max} is determined by setting $(V_0/2)(1-\cos\theta)$ equal to E:

$$\cos\theta_{max} = 1 - 2E/V_0 \qquad (G.9)$$

The integrals over φ and ζ in Eq. (G.8) may be performed immediately, giving:

$$\rho(E) = [2\pi/h]^2 \int_0^{\theta_{max}} d\theta \sin\theta \int_0^{\infty} dL\ L\ \delta(E-H) \qquad (G.9)$$

Let $E'=E-(V_0/2)(1-\cos\theta)$. Given θ, the $\delta(E-H)$ function can also be written as $\delta(R-E')$ where R is the rotational energy: $R= L^2/2I$. Transforming the integral over L to one over R ($LdL=IdR$), Eq. (G.9) becomes:

$$\rho(E) = I[2\pi/h]^2 \int_0^{\theta_{max}} d\theta \sin\theta \int_0^{\infty} dR\ \delta(R-E') \qquad (G.10)$$

The integral over R collapses to unity due to the delta function. Evaluating the integral over θ for the cases where $E>V_0$ and $E<V_0$, one obtains the result:

$$\rho(E) = 8\pi^2 I/h^2 \quad , E > V_0$$
$$\rho(E) = (8\pi^2 I/h^2)(E/V_0) \quad , E < V_0 \qquad (G.11)$$

Substituting into Eq. (G.11) the rotational constant $B=(8\pi^2 I/h^2)^{-1}$ completes the proof.

APPENDIX H

VARIATIONAL SELECTION OF SUM OF STATES FOR COUPLED MODES

We begin by substituting $\xi=E_+-E'$ in Eq. (4.30) to give:

$$k(\epsilon,R) = \frac{\int_0^{E-V_{eff}(r_m)} dE' \rho_{vib}^{\dagger}(E') \int_0^{L_1} d\xi \; W_c^{\dagger}[E-E'-\xi-V_{eff}(s)] \rho_{rot}^{\dagger}(\xi)}{h\rho(\epsilon)} \qquad (H.1)$$

Where $L_1 = E-V_{eff}(r_m)-E'$. As shown in Chapter 4, $W_c^{\dagger}$ in Eq. (H.1), the sum of states for the two-dimensional hindered dipole rotation, must be minimised by variation with respect to the reaction coordinate r. The value of r for which $W_c^{\dagger}$ is minimised is denoted s and will be dependent on the value of ξ. In order to determine s, the differential of $W_c^{\dagger}$ with respect to r is set to zero:

$$\partial W_c^{\dagger}[\zeta + q\mu_d/r^2 + q^2\alpha/2r^4 - IR/mr^2]/\partial r = 0 \qquad (H.3)$$

where ζ has been introduced for convenience and is defined as:

$$\zeta = E-E'-\xi-\Delta H_0 \qquad (H.4)$$

and ΔH_0 represents the bond energy. For purposes of notational clarity, the factor $4\pi\epsilon_0$ is assumed to be implicit in potential energy terms in Eq. (H.3) and below. For later reference, note that ζ can also be written as:

$$\begin{aligned}\zeta &= E - V_{eff}(r_m) - E' - \xi + (IR/m-q\mu_d)^2/2q^2\alpha \\ &= L_1 - \xi + (IR/m-q\mu_d)^2/2q^2\alpha \end{aligned} \qquad (H.5)$$

where the centrifugal maximum $V_{eff}(r_m)$ is given for an ion/dipole system by:

$$V_{eff}(r_m) = \Delta H_0 + (IR/m - q\mu_d)^2/2q^2\alpha \qquad (H.6)$$

(this is derived analagously to Eq. (4.11) for the Langevin case in Chapter 4). The following determination of the minimum sum of states for the coupled dipole rotor is analagous to that presented by Chesnavich *et al.* (1980) wherein the external rotation is also considered to be coupled. From Eq. (4.18) we have:

$$W_c^{\dagger}[\zeta + q\mu_d/r^2 + q^2\alpha/2r^4 - IR/mr^2] =$$

$$\frac{r^2}{4q\mu_d B_d}\left[\zeta + \frac{q\mu_d}{r^2} + \frac{q^2\alpha}{2r^4} - \frac{IR}{mr^2}\right]^2 \quad , \zeta < \frac{q\mu_d}{r^2} + \frac{IR}{mr^2} - \frac{q^2\alpha}{2r^4} \qquad (H.7a)$$

$$W_c^{\dagger}[\zeta + q\mu_d/r^2 + q^2\alpha/2r^4 - IR/mr^2] = \frac{1}{B_d}\left[\zeta + \frac{q^2\alpha}{2r^4} - \frac{IR}{mr^2}\right]$$

$$, \zeta > \frac{q\mu_d}{r^2} + \frac{IR}{mr^2} - \frac{q^2\alpha}{2r^4} \qquad (H.7b)$$

where B_d is the rotational constant of the dipole and we have used the fact that V_0, the barrier to rotation for the dipole, is given by $2q\mu_d/r^2$. Differentiating with respect to r and setting the result to zero, the positions at which $W_c^{\dagger}$ is minimised in Eqs. (H.7a) and (H.7b) are given respectively by:

$$r_{min}^2 = \{c+[c^2+6q^2\alpha\zeta]^{\frac{1}{2}}\}/2\zeta \qquad (H.8a)$$

where $c = q\mu_d - IR/m$, and

$$r_{min}^2 = q^2m\alpha/IR \qquad (H.8b)$$

Substituting Eqs. (H.8a) and (H.8b) into Eqs. (H.7a) and (H.7b) respectively yields:

$$W_{c,min}^{\dagger}[\zeta] = [2c^2/q\mu_d B_d][c+(c^2+6q^2\alpha\zeta)^{\frac{1}{2}}+2q^2\alpha\zeta/c]^2[c+(c^2+6q^2\alpha\zeta)^{\frac{1}{2}}]^{-3} \qquad (H.9a)$$

$$W^{\ddagger}_{c,min}[\varepsilon] = (1/B_d)[\varepsilon - (IR)^2/2q^2\alpha m^2] \qquad (H.9b)$$

At low energies, Eqs. (H.8a) and (H.9a) apply, whereas at higher energies Eqs. (H.8b) and (H.9b) apply. The energy ε_c at which the correct minimum sum of states switches from Eq. (H.9a) to Eq. (H.9b) is obtained when r_{min} of (H.8a) is set equal to that of (H.8b). Solution for ε_c yields:

$$\varepsilon_c = [IR/qm\alpha][\mu_d + IR/2qm] \qquad (H.10)$$

Hence the minimised sum of states for coupled modes is written:

$$W^{\ddagger}_{c,min}[\varepsilon] = [2c^2/q\mu_d B_d]\,[c+(c^2+6q^2\alpha\varepsilon)^{\frac{1}{2}}+2q^2\alpha\varepsilon/c]^2\,[c+(c^2+6q^2\alpha\varepsilon)^{\frac{1}{2}}]^{-3}$$
$$, \ \varepsilon < [IR/qm\alpha][\mu_d+IR/2qm];$$

$$W^{\ddagger}_{c,min}[\varepsilon] = (1/B_d)[\varepsilon - (IR)^2/2q^2\alpha m^2] \quad , \ \varepsilon > [IR/qm\alpha][\mu_d+IR/2qm] \qquad (H.11)$$

Exact variational implementation of Eq. (H.1) then requires substitution of Eqs. (H.11) and (H.5) and the ensuing convolution with non–coupled rotational and vibrational modes of the orbiting transition state. Ensemble averaging of the $k(\epsilon,J)$ so obtained, and multiplication of k_{uni}^{∞} by the equilibrium constant, yields the capture expression of Eq. (4.36).

APPENDIX I

RRKM PARAMETERS FOR CH_3^+/CH_3CN CHEMICAL ACTIVATION REACTION

I. *Reactant Channel.* The parameters for the long-range transition state in the reactant channel are simply those of the separated reactants. CH_3^+ frequencies are those calculated by DeFrees *et al.* (1985). Frequencies for CH_3CN were obtained from the literature (Pillai and Cleveland 1960). Rotational constants were calculated assuming standard bond lengths. The potential of interaction is that between the ion and the dipole (μ) and polarisability (α) of the neutral:

$$V(r) = 410.5 - 6.9492\times10^{26}\alpha/r^4 - 289.21\mu/r^2 \text{ kJ mol}^{-1} \qquad (I.1)$$

where the threshold energy (Deakyne and Meot-Ner 1989) is 410.5kJ mol^{-1}, μ = 3.92 Debye (McClellan 1963), $\alpha = 4.44\times10^{-24}$ cm^3 (Hirschfelder *et al.* 1954). The collision frequency was assumed to be given by the simple Langevin model. At 300K, this yields $\omega = 1.336\times10^5P$, where P is the pressure in Pa. The transition state parameters are included in Table I1. For conversion from k_{uni} to k_{ass}, the equilibrium constant was calculated using the parameters herein for 300K to be 1.39×10^{46} cm^3.

II. *Exit Channel.* In the absence of further knowledge, the frequencies for the tight transition state were taken as those calculated for the molecular ion $CH_3NCCH_3^+$ (Deakyne and Meot-Ner 1989), with the lowest frequencies being adjusted to reproduce the correct branching ratio for exit channels (relative to dissociation back to reactants) in the low-density limit. In an attempt to represent the dynamics of rearrangement in a qualitatively correct way, rotational constants were calculated for an estimated bent geometry such as would be likely to be involved in molecular rearrangement leading to products. The barrier height was taken as 288.7 kJ mol^{-1}. The RRKM parameters are included in Table I1.

III. *Collision Complex.* Frequencies and structure for the $CH_3NCCH_3^+$ ion have been calculated by Deakyne and Meot-Ner (1989). These, and appropriate rotational constants,

are included in Table I2.

Table I1. RRKM parameters for transition states of CH_3^+/CH_3CN chemical activation reaction. Reactant channel (T1); Exit channel (T2). For reactant channel (T1), rotation constant for hindered dipole rotor marked by asterisk.

Vibrations: Degeneracies in parenthesis.

Rotations: Parenthetic quantities are symmetry number and dimension respectively.

Vibrations (cm^{-1}) (T1)	Vibrations (cm^{-1}) (T2)	Rotations: Type	B Values (cm^{-1}) (T2)	B Values (cm^{-1}) (T1)
361 (2)	900 (7)	External inactive	0.230 (1,2)	0.0033 (1,2)
1041 (2)	1089 (2)			
1350 (1)	1135 (2)			
1370 (2)	1415 (1)	External active	0.868 (1,1)	2.51 (3,1)
1400 (1)	1421 (1)			
1454 (2)	1434 (2)			
2267 (1)	1456 (2)			
2965 (1)	2853 (1)	Internal		9.59 (2,2)
2903 (1)	2889 (1)			10.0 (3,1)
3009 (2)	2927 (2)			*0.333 (1,2)
3090 (2)	2982 (2)			
920 (1)				

Table I2. Molecular RRKM parameters for $CH_3NCCH_3^+$ ion.

Vibrations: Degeneracies in parenthesis.

Rotations: Parenthetic quantities are symmetry number and dimension respectively.

Vibrations (cm^{-1})	Rotations	
	Type	B value (cm^{-1})
199 (2)	External inactive	0.116 (1,2)
519 (2)		
587 (1)	External active	2.65 (3,1)
911 (1)		
1089 (2)	Internal	10.6 (3,1)
1135 (2)		
1415 (1)		
1421 (1)		
1434 (2)		
1456 (2)		
2393 (1)		
2853 (1)		
2889 (1)		
2927 (2)		
2982 (2)		

APPENDIX J

RRKM PARAMETERS FOR UNIMOLECULAR DISSOCIATION OF $CH_3CH_2OH_2^+$

The dissociation of $CH_3CH_2OH_2^+$ proceeds via two channels under the present experimental conditions. For reasons discussed above in Chapter 5, the quantity of interest is the total rate of dissociation, obtained by solution of the low-pressure two-dimensional master equation since the experimental data are in the low-pressure regime. The transition state parameters (necessary as part of the input for the RRKM programme) used for the two channels were estimated for the separate products in loose, orbiting transition states. Since the results discussed in Chapter 5 are independent of the precise nature of the parameters used for $k(\epsilon,J)$, by virtue of the total $k_{uni}=\omega k_0$ being dependent only of collisional activation, and reaction thresholds, the transition state parameters are not reproduced here. The threshold energies were calculated from thermodynamics to be 136 kJ mol^{-1} (H_3O^+ channel) and 168 kJ mol^{-1} ($C_2H_5^+$ channel).

Molecular parameters for the $CH_3CH_2OH_2^+$ ion were estimated from standard group frequencies of ethanol (see, e.g., Herzberg 1949). Rotational constants were calcuated assuming standard bond lengths and angles. The collision rate ω was determined from the collision rate coefficient derived in Chapter 5: this was found to vary between 1.13×10^{-9} cm^3 s^{-1} at 750K and 1.23×10^{-9} cm^3 s^{-1} at 1100K. The molecular RRKM parameters are included in Table J1.

Table J1. RRKM parameters for $CH_3CH_2OH_2^+$ unimolecular dissociation in the low pressure limit.

Vibrations: Degeneracies in parentheses.

Rotations: Parenthetic quantities are symmetry number and degeneracy respectively.

Vibrations (cm^{-1})	Rotations	
	Type	B Values (cm^{-1})
1000 (1)	External inactive	0.2644 (1,2)
1200 (1)		
3100 (5)	External active	1.062 (1,1)
1100 (2)		
400 (2)	Internal	24.12 (1,1)
1450 (4)		
1200 (2)		
1150 (5)		
150 (1)		

REFERENCES

Adams, N.G., and Smith, D.,
in "Swarms of Ions and Electrons in Gases", eds. W. Lindinger, T.O. Mark and F. Howorka, Springer-Verlag, Vienna, (1984).

Adams, N.G., and Smith, D.,
Int. J. Mass Spec. Ion Proc. **81**, 273 (1987)

Albritton, D.L., Dotan, I., Lindinger, W., McFarland, M., Tellinghuisen, J. and Fehsenfeld, F.C.,
J. Chem. Phys. **66**, 410 (1977).

Astholz, D.C., Troe, J. and Wieters, W.J.,
J. Chem. Phys. **70**, 5107 (1979).

Bass, L.M., Cates, R.D., Jarrold, N.J., Kirchner, N.J. and Bowers, M.T.,
J. Amer. Chem. Soc. **105**, 7024 (1983).

Bass, L.M., Kemper, P.R., Anicich, V.G. and Bowers, M.T.,
J. Amer. Chem. Soc. **103**, 5283 (1981).

Bates, D.R.,
J. Phys. B. **12**, 4135 (1979).

Beyer, T., and Swinehart, D.F.,
Comm. Assoc. Comput. Mach. **16**, 379 (1973).

Brown, T.C., King, K.D. and Gilbert, R.G.,
Int. J. Chem. Kinet. **19**, 851 (1987).

Bunker D.L. and Patengill, M.,
J. Chem. Phys. **48**, 772, (1968); **64**, 2442 (1976).

Chesnavich, W.J., Bass, L.M., Su, T. and Bowers, M.T.,
J. Chem. Phys. **74**, 2228 (1981).

Chesnavich, W.J. and Bowers, M.T.,
*J.*Amer. *Chem.* Soc. **98**, 8301 (1976).

Chesnavich, W.J. and Bowers, M.T.,
J. Chem. Phys. **66**, 2306 (1977).

Chesnavich, W.J. and Bowers, M.T.,
Prog. Reaction Kinetics **11**, 137 (1982).

Chesnavich, W.J., Su, T. and Bowers, M.T.,
J. Chem. Phys. **72**, 2641 (1980).

Chow, N. and Wilson, D.J.,
J. Phys. Chem. **66**, 342 (1962).

Clary, D.C.,
Mol. Phys. **54**, 605 (1985).

Date, N., Hase, W.L. and Gilbert, R.G.,
J. Phys. Chem. **88**, 5135 (1984).

Deakyne, C. and Meot-Ner, M.,
J. Phys. Chem., in press (1989).

Defrees, D.J., and McLean, A.D.,
J. Chem. Phys. **82**, 333 (1985).

DeFrees, D.J., McLean, A.D. and Herbst, E.,
Astrophys. J. **293**, 236 (1985).

Federer, W., Ramler, H., Villinger H. and Lindinger, W.,
Phys. Rev. Lett. **54**, 540 (1985).

Ferguson, E.E.,
J. Phys. Chem. **90**, 731 (1986).

Ferguson, E.E.,
in "Structure, Reactivity and Thermochemistry of Ions", Eds. P. Ausloos and S.G. Lias, D. Reidel Publishing Company, 1987.

Forst, W.,
"Theory of Unimolecular Reactions", Academic Press, New York, (1973).

Garrett, B.C. and Truhlar, D.G.,
J. Phys. Chem. **83**, 1052 (1979).

Gaynor, B.J., Gilbert, R.G. and King, K.D.,
Chem. Phys. Letters **55**, 40 (1978a).

Gaynor, B.J., Gilbert, R.G. and King, K.D.,
Chem. Phys. Letters **58**, 591 (1978b).

Gilbert, R.G.,
Quantum Chemistry Program Exchange **3**, 64 (1983).

Gilbert, R.G.,
J. Chem. Phys. **80**, 5501 (1984).

Gilbert, R.G. and King, K.D.,
Chem. Phys. **49**, 367 (1980).

Gilbert, R.G., Luther, K. and Troe, J.,
Ber. Bunsenges. Phys. Chem. **87**, 169 (1983).

Gilbert, R.G. and McEwan, M.J.,
Aust. J. Chem. **38**, 231 (1985).

Gilbert, R.G. and Ross, I.G.,
Aust. J. Chem. **24**, 1541 (1971).

Goldstein, H.,
"Classical Mechanics", Addison-Wesley, Reading, MA, 1980 (2^{nd} edition).

Greenhill, P.G. and Gilbert, R.G.,
J. Phys. Chem. **90**, 3104 (1986).

Greenhill, P.G., O'Grady, B.V. and Gilbert, R.G.,
Aust. J. Chem. **39**, 1929 (1986).

Hase, W.L.,
in "Dynamics of Molecular Collisions" Vol. 2,
ed. W.H. Miller, Plenum, New York, (1976).

Herbst, E.,
J. Chem. Phys. **70**, 2201 (1979).

Herbst, E.,
J. Chem. Phys. **82**, 4017 (1985).

Herbst, E.,
in "Interstellar Processes", Eds. D.J. Hollenbach and H.A. Thronsen, D. Reidel Publishing Company, 1987.

Herbst, E.,
private communication (1988).

Herzberg, G.,
"Molecular Spectra and Molecular Structure II, Infrared and Raman Spectra of Polyatomic Molecules", D. Van Nostrand, New York, (1949).

Hinshelwood, C.N.,
Proc. Royal Soc. (A) **113**, 230 (1927).

Hirschfelder, J.O., Curtiss, C.F. and Bird, R.B.,
"Molecular Theory of Gases and Liquids", Wiley, New York, (1954).

Hoare, M.,
J. Chem. Phys. **38**, 1630 (1963).

Huntress, W.T., Pinizzotto, R.F. and Laudenslager, J.B.,
J. Amer. Chem. Soc. **95**, 4107 (1973).

Jarrold, M.F., Kirchner, N.J., Lin, S. and Bowers, M.T.,
J. Phys. Chem. **90**, 78 (1986).

Just, Th. and Troe, J.,
J. Phys. Chem. **84**, 3068 (1980).

Kassel, L.S.,
J. Phys. Chem., **32**, 225 (1928).

Keck, J. and Carrier, G.,
*J. Chem. Phys.***43**, 2284 (1965).

Kemper, P.R., Bass, L.M. and Bowers, M.T.,
J. Phys. Chem. **89**, 1105 (1985).

King, K.D., Golden, D.M., Spokes, G.N. and Benson, S.W.,
Int. J. Chem. Kinet. **3**, 411 (1971).

King K.D., Nguyen, T.T. and Gilbert, R.G.,
Chem. Phys. **61**, 221 (1981).

Knight, J.S., Freeman, C.G. and McEwan, M.J.,
J. Amer. Chem. Soc. **108**, 1404 (1986).

Kohlmaier, G.H. and Rabinovitch, B.S.,
J. Chem. Phys. **38**, 1692 (1963).

Langevin, P.M.,
Ann. Chem. Phys. 5, 245 (1905).

Larson, C.W., Stewart, P.H. and Golden, D.M.,
Int. J. Chem. Kinet. 20, 27 (1988).

Lias, S.G., Liebman, J.F., and Levin, R.D.,
J. Phys. Chem. Ref. Data **13**, (1984).

Lim, K.F. and Gilbert, R.G.,
J. Chem. Phys. 84, 6129 (1986).

Lin, S.L. and Bardsley, J.N.,
J. Chem. Phys. 66, 435 (1977).

Lindemann, F.A.,
Trans. Faraday Soc. **17**, 598 (1922).

Marcus, R.A.,
J. Chem. Phys. 20, 359 (1952).

Marcus, R.A.,
J. Chem. Phys. 43, 2658 (1965).

Marcus, R.A.,
J. Chem. Phys. 45, 4500 (1966).

Marcus, R.A.,
J. Chem. Phys. 52, 1018 (1970).

Marcus, R.A. and Rice, O.K.,
J. Phys. and Colloid Chem. 55, 894 (1951).

Messiah, A.,
"Quantum Mechanics", North Holland, Amsterdam, (1964).

Meot-Ner, M.,
J. Amer. Chem. Soc., submitted (1988).

Meot-Ner, M.,
private communication (1989).

Montroll, E.W. and Shuler, K.E.,
Adv. Chem. Phys., 1, 361 (1958).

McClellan, A.L.,
"Tables of Experimental Dipole Moments", Freeman, San Francisco, (1963).

McEwan, M.J.,
private communication (1988).

McEwan, M.J., Denison, A.B., Huntress, W.T., Anicich, V.G.
Snodgrass, J. and Bowers, M. T.,
J. Phys. Chem., in press (1989).

McFarland, M., Albritton, D.L., Fehsenfeld, F.C., Ferguson, E.E. and Schmeltekopf, A.L.,
J. Chem. Phys. 59, 6610 (1973).

McQuarrie, D.A.,
"Statistical Mechanics", Harper and Rowe, New York, (1973).

Nikitin, E.E.,
"Theory of Thermally Induced Gas-Phase Reactions", Indiana University Press, New York, (1966).

Nobes, R.H. and Radom, L.,
Chem. Phys. **74**, 163 (1983).

Olmstead, W.N. and Brauman, J.I.,
J. Amer. Chem. Soc. **99**, 4219 (1977).

Penner, A.P., and Forst, W.,
Chem. Phys. **11**, 243 (1975).

Penner, A.P., and Forst, W.,
Chem. Phys. **13**, 51 (1976).

Pillai, M.G.K., and Cleveland, F.F.,
J. Molec. Spect. **5**, 212 (1960).

Pritchard, H.O.,
"Quantum Theory of Unimolecular Reactions", Cambridge University Press, Cambridge, (1984).

Quack, M., and Troe, J.,
Ber. Bunsenges. Phys. Chem. **78**, 240 (1974).

Quack, M., and Troe, J.,
Ber. Bunsenges. Phys. Chem. **81**, 329 (1977).

Rice, O.K., and Ramsperger, H.C.,
J. Amer. Chem. Soc. **49**, 1617 (1927).

Ritger, P. and Rose, N.,
"Differential Equations with Applications", McGraw-Hill, New York, (1968).

Robinson, P.J. and Holbrook, K.A.,
"Unimolecular Reactions", Wiley, London, (1972).

Rosenstock, H.M., Draxl, K., Steiner, B.W. and Herron, J.T.,
J. Phys. Chem. Ref. Data **6**, Supplement 1 (1977)

Sakimoto, K.,
Chem. Phys. **68**, 155 (1982).

Saxer, A., Richter, R., Villinger, H., Futrell, J.H. and Lindinger, W.,
J. Chem. Phys. **87**, 2105 (1987).

Schiff, H.I., and Bohme, D.K.,
Astrophys. J. **232**, 740 (1979)

Schranz, H.W., and Nordholm, S.,
Chem. Phys. **74**, 365 (1983).

Schranz, H.W., and Nordholm, S.,
Chem. Phys. **87**, 163 (1984).

Smith, D., and Adams, N.G.,
Chem. Phys. Lett. **47**, 145 (1977).

Smith, D., and Adams, N.G.,
Chem. Phys. Lett. **54**, 535 (1978).

Smith, D., and Adams, N.G.,
in "Gas Phase Ion Chemistry", Vol. 1,
ed. M.T. Bowers, Academic Press, New York, (1979).

Smith, D., Adams, N.G. and Ferguson, E.E.,
Int. J. Mass Spectrom. Ion Processes **67**, 67 (1985).

Smith, D., and Adams, N.G.,
Adv. in Atomic and Mol. Phys. **24**, 1 (1987).

Smith, S.C., and Gilbert, R.G.,
Int. J. Chem. Kinet. **20**, 307 (1988).

Smith, S.C., and Gilbert, R.G. (1989)
Dept. of Theoretical Chemistry,
University of Sydney,
N.S.W. 2006, Australia.

Smith, S.C., Wilson, P.F., McEwan, P. Sudkeaw, R.G.A.R. Maclagan, M.J.,
Huntress, W.T. and Anicich, V.G.,
J. Phys. Chem., to be submitted (1989).

Snider, N.,
J. Chem. Phys. **42**, 548 (1965).

Su, T. and Chesnavich, W.J.,
J. Chem. Phys. **76**, 5185 (1982).

Su, T., Su, E.C.F. and Bowers, M.T.,
J. Chem. Phys. **69**, 2243 (1978)

Tardy, D.C. and Rabinovitch, B.S.,
Chem. Rev. **77**, 369 (1977).

Troe, J.,
J. Chem. Phys. **66**, 4745 (1977a).

Troe, J.,
J. Chem. Phys. **66**, 4758 (1977b).

Troe, J.,
Ber. Bunsenges. Phys. Chem. **87**, 161 (1983a).

Troe, J.,
J. Chem. Phys. **79**, 6017 (1983b).

Troe, J.,
Chem. Phys. Lett. **122**, 425 (1985).

Troe J.,
Z. Phys. Chem. **154**, 73 (1987a).

Troe, J.,
J. Chem. Phys. **87**, 2273 (1987b).

Truhlar, D.G. and Garrett, B.C.,
Annual Rev. Phys. Chem. **35**, 159 (1984).

Viehland, L.A. and Mason, E.A.,
J. Chem. Phys. **66**, 422 (1977).

Viehland, L.A., Lin, S.L. and Mason, E.A.,
Chem. Phys. **54**, 341 (1981).

Waage, E.V. and Rabinovitch, B.S.,
Chem. Rev. **70**, 377 (1970).

Wardlaw, D.M. and Marcus, R.A.,
Adv. Chem. Phys. **70**, 231 (1987).

Whyte, A.R and Gilbert, R.G.,
Aust. J. Chem., in press (1989).

Whyte, A.R., Lim, K.F., Gilbert, R.G. and Hase, W.L.,
Chem. Phys. Lett. **152**, 377 (1988).

Winnewisser, G., and Herbst, E.,
in "Topics in Current Chemistry" **139**, 119 (1987), Springer-Verlag, Berlin.

Zwolinski, B.J., and Eyring, H.,
J. Amer. Chem. Soc. **69**, 2702 (1947).